INTERNATIONAL JOURNAL OF
IJCOE
COASTAL, OFFSHORE AND ENVIRONMENTAL ENGINEERING

Design, Construction, and Implementation of Water Level Recorder With Communication of Information Approach Using GSM and GPRS
Amir Hossein Moadeli[1], Ayob Khodaprast [2], Omid Ghasemiabnavi[3]

Presentation An Approach Based on Control Systems To Purpose Control Simultaneous Vibrations And Maneuver the Arm Robotic With two Degree of freedom
Amirhossein Ghasemkhani[1], DR. Ayoub Khodaparast[2*]

Enhancing Power Quality of AC-AC Direct Converters using Hybrid Filters
MR mohammad javad almasi, Ayoub khodaparast

Hardware-Accelerated Image Moment Computation for UUV Navigation
Mehrnaz Monajati[1]

Design and Application of Multifunctional Robots for Deep-Sea Exploration and Rescue Operations
Mehrnaz Monajati[1], Morteza Shirmohammadi[2]

A Novel Approach to Image Moment Computation for Sonar Image Registration in Underwater Vehicle Autonomy
Mehrnaz Monajati[1]

www.ijcoe.org

International Journal of Coastal, Offshore and Environmental Engineering (IJCOE) Vol .1/Issue 1/ NOV 2023

Volume 1 | Issue1 | NOV2023
WWW.IJCOE.org
info@ijcoe.org

Special Issue

Marine Instrumentation

Editor-in-Chief: Prof, Hamid S. Bahai

International Journal of Coastal, Offshore & Environmental Engineering
Since 2015
ISSN: 2980-8721 (online)

In The Name of God

Message from the Editor-in-Chief

The IJCOE journal office was established in 2015,and its first issue was published in 2016. TheIJCOE covers a wide range of research in thefields of oceanography & ocean technology, aswell as marine industries & marine engineering.The editorial board of IJCOE consists of nearly130 of the greatest scientists and researchersfrom over 30 countries worldwide, and thejournal's review board comprises 1,000 membersfrom all five continents. The membership andapplication process for joining the editorial andreview boards of this journal is ongoing. IJCOE isa research-academic quarterly journal that haspublication and distribution permissions fromthe Press Organization and permission topublish scientific-research articles from theMinistry of Science, Research, and Technology(MSRT) with an "A" rating. It also holds a "Q1"rating from the ISC institute with an impactfactor (IF) of approximately 0.43 and isconsidered a "core journal" (prestigious andoutstanding journal). IJCOE is an open-accessjournal and allows the download and receipt ofaccepted articles in full text for free. It respectsand adheres to copyright and COPE regulations.The journal's office operates 24/7, providingservices to researchers. In addition to publishinga regular quarterly journal, IJCOE has 16 specialissues on specific topics in preparation. It alsoprovides conditions for publishing specializedbooks, references, and handbooks. Moreover, itis ready to cooperate with the secretariats ofreputable international conferences to publishtheir selected and outstanding articles. IJCOEevaluates, appraises, and publishes books,articles, and the scientific achievements andfindings of esteemed researchers and scientistsworldwide who are innovating and conductingin-depth research in the "important and strategicfield of the maritime technology & Oceanengineering." It welcomes any form of jointcooperation with universities, research institutes,and related research centers at the national,regional, and international levels, and extends ahand for collaboration.

Classification of Editorial Board in IJCOE

- Editor-in-Chief
- Director-in-Chief
- Deputy Editor
- Executive Managers
- English Text Editor
- Technical Editor
- International Editorial Board
- National Editorial Board
- Editorial Board Associate
- Editorial Board Assistant
- Guest Editorial Board
- Advisory Board
- Administrative Coordinator
- Honorary Board Member
- Methodology Advisor

Author Benefits

- Open Access
- Rapid Publication
- Thorough Peer-Review
- No Copyright Constraints
- Coverage by Leading Indexing Services
- Discounts On Article Processing Charges (APC)
- No Space Constraints, No restriction on the maximum length of the papers, number of figures or colors

INTERNATIONAL JOURNAL OF IJCOE COASTAL, OFFSHORE & ENVIRONMENTAL ENGINEERING

Aims of IJCOE

Hydrodynamics

Marine equipment

Structural mechanics

Ocean environmental predictions

Stochastic calculations Experimental

Automatic Control of Marine Systems

Scope of IJCOE

Marine Hazards

Ocean Acoustics

Naval Architecture

Ocean Engineering

Coastal Engineering

Marine Meteorology

Marine Earth Sciences

Underwater Technology

Marine Renewable Energy

Polar & Arctic Engineering

Marine Renewable Energy

Marine Geography & Geodesy

Marine Environmental Engineering

Automatic Control of Marine Systems

Hydro Physics & Physical Oceanography

Type of papers

- Case Studies
- Book Reviews
- Review Article
- Letters to the Editor
- Methodology Papers
- Editorials and Commentaries
- Response or Rejoinder Papers
- Perspective or Opinion Papers
- Conceptual or Theoretical Papers
- Meta-Analysis and Systematic Reviews
- Short Communications or Brief Reports
- Research Articles (Original Research Papers)

Scientific Research Journal

Ministry of Science, Research And Technology (MSRT)

Jurnal Ranking 2023: A

Ministry Of Science, Research And Technology (ISC)

Citation Impact 2022: 0.429

Quartile 2022 : Q1

Core Collection



IJCOE is a Member of



Cantact Us

Office 1 | Research Institute of Meteorology and Atmospheric Science

Address | Tehran, Shahid Kharrazi Highway, Pajoohesh Blvd, Research Institute of Meteorology and Atmospheric Science, Sand and Dust Storm International Research Center (SDS-IRC), No. 13, 1st floor.

Phone | +982144787652

Postal code | 13611-14977

website | www.rimac.ac.ir

Office 2 | Iranian National Institute for Oceanography and Atmospheric Science

Address | Tehran, Dr. Fatemi Gharbi St., Shahid Etemadzade St., No. 3, third floor.

Phone | +982166944873

Postal code | 13389 – 14118

website | www.inio.ac.ir

Email | Info@ijcoe.org

Website | www.ijcoe.org

Follow Us

www.ijcoe.org

INTERNATIONAL JOURNAL OF IJCOE COASTAL, OFFSHORE & ENVIRONMENTAL ENGINEERING

Volume & Issue:

Volume 1, Issue 1, NOV 2023

Special Issue of " Marine Instrumentation "

Number of Articles: 6

Content

Design, Construction, and Implementation of Water Level Recorder With Communication of Information Approach Using GSM and GPRS Amir Hossein Moadeli1, Ayob Khodaprast 2, Omid Ghasemiabnavi3	1
Presentation An Approach Based on Control Systems To Purpose Control Simultaneous Vibrations And Maneuver the Arm Robotic With two Degree of freedom Amirhossein Ghasemkhani1, DR. Ayoub Khodaparast2*	8
Enhancing Power Quality of AC-AC Direct Converters using Hybrid Filters MR mohammad javad almasi, Ayoub khodaparast	20
Hardware-Accelerated Image Moment Computation for UUV Navigation Mehrnaz Monajati1	27
Design and Application of Multifunctional Robots for Deep-Sea Exploration and Rescue Operations Mehrnaz Monajati1, Morteza Shirmohammadi2	34
A Novel Approach to Image Moment Computation for Sonar Image Registration in Underwater Vehicle Autonomy Mehrnaz Monajati1	46

IJCOE
COASTAL, OFFSHORE & ENVIRONMENTAL ENGINEERING

INTERNATIONAL JOURNAL OF
COASTAL, OFFSHORE & ENVIRONMENTAL ENGINEERING

IJCOE Vol.1/ Special Issue No.1/
Marine Instrumentation/ 2023(1-7)

Available online at: www. Ijcoe.org

Design, Construction, and Implementation of Water Level Recorder With Communication of Information Approach Using GSM and GPRS

Amir Hossein Moadeli[1], Ayob Khodaprast [2], Omid Ghasemiabnavi[3]

[1] *PhD student, Department of Telecommunications, Faculty of Electrical Engineering, Shiraz University of Technology, Shiraz, Iran, a.moadeli@sutech.ac.ir*

[2] *Ph.D., Control Department, University Complex of Air Sciences and Technology, Shiraz, Iran, khodaparast@mut-es.ac.ir*

[3] *Master's degree, Department of Electronics Education, Faculty of Engineering, Islamic Azad University of Shiraz, Shiraz, Iran, omidghasemi115@gmail.com*

ARTICLE INFO

Article History:
Received : 23 Jan 2023
Accepted : 08 May 2023

Keywords:
Tide gauge
Tide
Water leveler
Data storage
Data transmission

ABSTRACT

The conventional methods of measuring tides are primarily based totally on direct observation of the water level on a graded-index whose information is examined in certain time intervals, although this work is very tiring and elements which include detrimental climate conditions, wind, rain, heat, darkness, people`s fatigue and negligence in wearing out the obligation have brought on the exceptional of accumulated information to decrease. Therefore, new generation mechanical and electronic devices have been used to lessen the error. In these systems, because of the presence of movable parts and parts that are in direct contact with seawater, wear and tear are inevitable. Therefore, fully electronic systems based on ultrasound and water pressure measurement have attracted various attentions due to the fact that they no longer have an operator and mechanical components are not in contact with water. In those systems, the gathering of tidal records is carried out routinely with non-touch electronic measurement, which has greater accuracy, speed, and simplicity of labor in comparison to conventional systems. This study is a report of the construction process and comparison of the results of the construction of an electronic device for measuring tides with the possibility of real-time transmission of tidal data. The advanced tide gauge device calculates the height of the water surface with the use of ultrasonic waves and measuring water pressure continuously. This system is also equipped with a microcontroller that has the mission of collecting, recording, and dealing with data and dealing with the peripheral parts, including managing information communication and receiving settings. In the constructed system, the water level values measured by pressure sensors and ultrasonic range finder are transmitted to a mobile number and a designed server through SMS and GPRS networks. The constructed tide gauge device was hooked up next to the Bushehr tide gauge and the overall performance and accuracy of the device were evaluated and compared via way of means of reconstructing the Topax/Poseidon satellite data and the Bushehr tide gauge records. By examining the results, it can be concluded that the use of two measurement sensors in the constructed system has been capable of enhancing the accuracy of water level measurement, and the communication of information from two different channels reduces the lack of records. These two factors increase the safety factor of using the device

1. Introduction

The phenomenon of tides, like many different natural phenomena, influences human life. This phenomenon has affected the duplicate of fish and ocean plants. Tides stability the temperature at the planets and additionally desire the climate situations via way of means of growing turbulence inside the oceans. By flood tide, the ships attain the shore without problems whilst the water involves the shore. Because the frequency of this phenomenon is numerous instances the afternoon and night, it will likely be great as a renewable energy source [1]. In the traditional technique of measuring the tide level, which is based on the direct observation of the water level on a graded-index [2], its information is read every ten minutes for at least a month, which is, of course, a very tiring task and factors such as unfavorable weather conditions, wind, rain, heat, In the conventional technique of measuring the tide degree, that is primarily based totally at the direct observation of the water degree on a graded-index [2], its statistics is examined every ten mins for as a minimum a month, that is of route a completely tiring venture and elements consisting of unfavorable climate conditions, wind, rain, warmth darkness, people`s fatigue and negligence in wearing out their duties caused a lower withinside the fine of amassed statistics [3] [4]. Due to the problems of conventional methods, mechanical equipment and an aggregate of mechanical and electronic devices were used. Due to the presence of moving parts and parts that are in direct touch with seawater, these systems' wear and tear is inevitable, and therefore they require regular periodic visits so that they do not lose their precise function [5] - [8].

Therefore, all electronic structures based on ultrasound and water pressure measurement have solved the issues of different strategies because they no longer want an operator and mechanical components in touch with water. In those systems, the gathering of tidal statistics is accomplished robotically with non-touch measurement with unique features, fully electronic, which are more accurate, faster, and easier to work with compared to traditional systems.

2. Methodology

The developed tide gauge system continuously measures the height of the water level using ultrasonic waves and water pressure and is also equipped with a microcontroller, that's chargeable for collecting, recording, and handling facts and handling peripheral parts, such as managing communique of facts and receiving settings.

Due to the evolution and development of the mobile network and the Internet, these two platforms are reasonably priced and have alternatives for information transmission. The values measured by the sensors are transmitted to a mobile number and a designed server through SMS and GPRS networks.

The general diagram of the way the device system works is shown in Figure (1). In general, this system has 5 parts: 1- The structure part, 2- The electricity and energy supply part, 3- The control and telecommunication part, 4- The sensors, and 5- The server. In the following, we will examine each part.

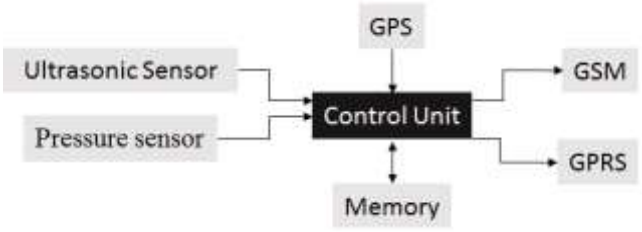


Figure 1: Functional diagram of the constructed tide gauge system

2.1. Structure Sector

A structure was designed and built to install the ultrasonic sensor and hold the solar panel and since the structure must be installed next to the dock or anchorage, its material is chosen from steel and protected with 5 layers of paint and rust so that it has excessive resistance against high humidity and bad weather conditions and does not wear out. The height of this structure is one meter and according to figure (1) this structure has an arm, which is placed at the end of the arm of the altimeter sensor or the ultrasonic sensor of the system. At the time of installation, this arm should be placed on the water surface and create a distance from the edge of the dock so that the water height sensor can measure the water height correctly. Also, the solar panel system is placed on top of this structure with a bolt and nut connection.

To protect the control board and the battery of the system, a metal box with a base that is covered by electrostatic paint is used. Figure (2) it shows an overview of the structure.



Figure 2: overview of the structure

According to Figure (3), a 6-meter aluminum ingot was used to restore the pressure gauge sensor in depth. Due to the position of this element in seawater, a defensive layer in opposition to moss and corrosion because of salt water has been created at the aluminum ingot.



Figure 3: Pressure sensor mounted on an aluminum ingot

2.2. Electricity and energy supply sector

To deliver energy to different parts of the system, direct voltages of 12 V, 5 V, 1.4 V, and 3.3 V are needed. For this purpose, two methods of power supply have been considered for the level recorder system. The first mode is the usage of urban electricity, in this case, switching power sources are used to lessen the city's 220-volt alternating current and convert it into the direct power required by the control board and system sensors. The second mode is the use of solar power systems. This system is installed to enable the use of the system in situations where city electricity is not available or in case of emergency. According to figure (4), it consists of a 30-watt solar panel with mono manufacturing technology, a charge control circuit, and a 12 Volt 9-Amp battery, which is converted to the required voltages of different parts of the system by the battery voltage regulator Acs.



Figure 4: Solar energy system including solar panel, battery charge control, and lead-in wires

2.3. Control and Telecommunications Sector

Microcontrollers or MCUs are small ICs that contain a combination of units and different capabilities and are used to control processes or read sensor values and control operators. Microcontrollers have wide capabilities that vary depending on the type and model. Microcontrollers usually differ from each other in terms of processing power, and the quantity of memory that consists of program memory (Flash memory) and data memory (RAM). Also, input and output ports that allow communication with devices, sensors and operators, and other parts such as timers, and protocols that can be supported

in different categories and series. are positioned differently. The microcontroller for processing system data is from the AVR series of microcontrollers based on the Arduino platform with the technical number Atmega 328. The traits of this microcontroller include 32 kilobytes of memory, low energy consumption, and high speed. [9] - [13].

To save the data of the sensors, the time, and the clock of the measured values, a data logger shield compatible with Arduino was used so that the information could be saved on an SD card. This shield is connected to the microcontroller with the I2c communication protocol, and due to the use of the internal clock, it also provides the possibility of saving the clock. Figure (5) shows the set of control board.

A SIM800L module is used to transmit information in the form of SMS on the global mobile network platform and also to upload it to the server. These modules use the GSM network and provide the ability to send and receive SMS, make calls, and connect to the Internet on the GPRS platform [9] [11] and [14].

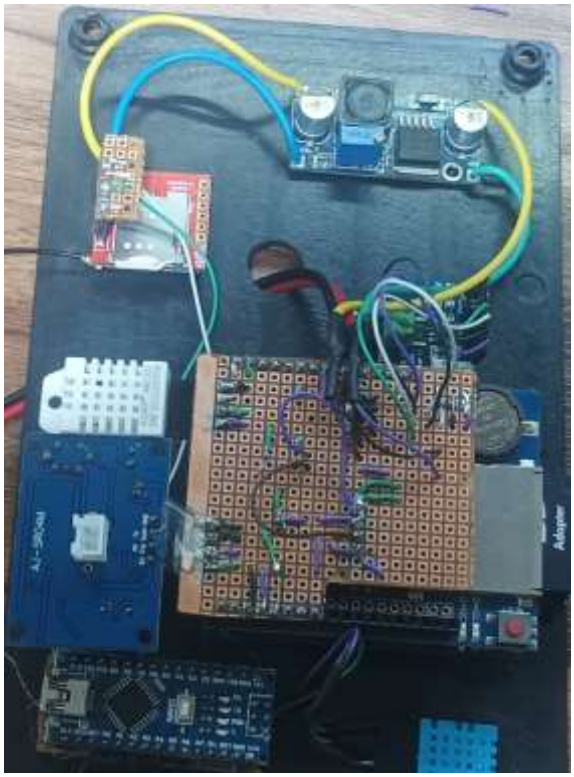


Figure 5: The control board set is placed in the box.

2.4. Sensors

2.4.1. Pressure Sensor

Fluid pressure sensors are used to measure the pressure of liquids such as water, oil, gases, and other fluids. These sensors usually work based on the change in fluid volume in reaction to the pressure. As the fluid volume increases, the pressure also increases, and the sensor can measure this pressure change, and a signal corresponding to the measured pressure is generated on the output, which is used in control systems. These sensors have different models, including diaphragm models, resistance models, etc [15] [17].

The Wika A10 series pressure transmitter (pressure sensor) is made of stainless steel and has a small design. This product also has a digital processing circuit that converts weak signals into standard current signals.

This sensor has many features. The features of this transmitter include small size, lightweight, easy installation and use, and stable performance. This equipment is mainly used in industrial automation equipment and has good compatibility with difficult environmental conditions, which shows the high quality of the sensor [17].

2.4.2. Altimeter

Ultrasonic range finder sensors use high-frequency sound waves that are sent and reflected to the sensor after hitting an object or surface. To use these sensors, after feeding the sensor, the desired control signal must be sent to the sensor so that the sensor can measure the distance. Ultrasonic sensors have two types of analog output and digital output, and to accurately read the distance, the sensor must be placed in a plane perpendicular to the object so that the distance can be measured correctly.

The 04SRF sensor is an electronic range-finding module based on ultrasound, which is used to measure the height of the water surface in this project. This sensor can measure the distance up to 10 meters and the measurement accuracy is millimeters, which is a good option considering the changes in the water level of the Persian Gulf. [18]

2.4.3. Temperature and humidity sensor

Temperature and humidity affect the speed of propagation of waves. With the assistance of a sensor, the temperature and humidity of the environment are measured so that the measurement error of the ultrasonic range finder sensor can be minimized. The DHT-22 temperature and humidity sensor is a good sensor for measuring the temperature and humidity of the environment. This sensor is a digital sensor that communicates with the microcontroller using the I2C communication protocol.

DHT-22 consists of two parts: a capacitive humidity sensor and a resistance temperature sensor. Inside this sensor, a chip is used to convert analog to digital. The humidity measurement range of the sensor is from 0 to 100 percent and it also can measure temperature from -40 degrees to +80 degrees [19] [20].

2.4.4. positioning

Remote sensing measures the Earth's parameters using satellites in the Earth's orbit or airplanes equipped with sensors (without physical contact). The data obtained from this technology provides the possibility of extensive projection and analysis of the parameters of the earth by using data collection through reflected energy from the earth. Remote sensing has a wide range of applications, including recording the water level. Therefore, the use of the GPS global positioning system to receive location information with the help of satellite signals provides information such as geographical longitude and latitude as well as height, which is used to adapt the data measured by range-finder sensors and System pressure is used with satellite data. However, it should be noted that remote sensing systems have far lower accuracy than coastal tide gauges, and comparing the data received from both methods can reduce the measurement error [21].



Figure 6: Port of Bushehr city, the installation site of the level recorder system built next to the level recorder device of the Geographical Organization

3. Results and Discussion

To evaluate the performance of the system, the built tide gauge was installed for 6 months from April 30, 2023, to November 1, 2023, next to the tide gauge of the Geographical Organization located in Bushehr port. Tide-gauge system data is read every 10 minutes and stored in the server. This makes it possible to reveal waves with an interval of 20 minutes or more in tidal modeling based on the principle of sampling. The installation location of the system is shown in Figure (6).

3.1. Tide modeling of satellite data

To examine the performance of the tide gauge, the information from the Topex-Poseidon altimetry satellite has been used. In tide modeling with the assistance of the information acquired from the satellite, it is necessary to perform corrections and processing on the satellite data to see the altimetry information. After observing the altimetry data, a height time series should be made. These series include altitude and time information [22].

One of the problems that sometimes exists in the construction of time series is the reconstruction of lost information. Various methods can be used to solve this problem. One of these methods is the use of the autocorrelation function, which can estimate the statistical correlation between the data and the missing data.

The time series is defined as the following equation (1).

$$r_k = \frac{\sum_{t=1}^{N-K}(x_t - \bar{x})(x_{t+k} - \bar{x})}{\sqrt{\sum_{t=1}^{N}(x_t - \bar{x})^2}} \quad (1)$$

In the above relation, the time series $X_1, X_2, \dots, X_n$ is known. and $r_1, r_2, \dots, r_n$ is the correlation between time series. If it is necessary to calculate X_{n+1} ,the above series can be expanded as $X_1, X_2, \dots, X_n, X_{n+1}$ thatX_{n+1} is unknown.

The remarkable thing about relation (1) is its non-linearity, and to calculate X_{n+1} it is necessary to linearize the relations using the least squares method (2). The relationship (2):

$$F(X) = F(X_0) + \frac{dF}{dX_{(X_0)}}(X - X_0) \quad (2)$$

We can use the value of x_n or $\bar{X} = \frac{1}{N}\sum_{t=1}^{N} X_i$as the initial value of x_{n+1} .

$$F(X) = F(X_0) + \frac{dF}{dX_{(X_0)}}(X - X_0) \quad (3)$$
$$\rightarrow \boldsymbol{dl} = A\delta\boldsymbol{X}$$
$$dX = X - X_0 \rightarrow X = dX + X_0$$
$$A = \frac{dF}{dX_{(X_0)}}$$

This process is repeated until the last answer is calculated. Finally, with the help of Fourier analysis and the least squares method, the

frequencies in the series were calculated and the tide model was extracted. According to Figure (7), the measurements made by the tide gauge are consistent with the data extracted from the satellite, and the difference between the monthly graph of the satellite data and the data measured by the tide gauge can be due to the low accuracy of the obtained data. come from satellites.

3.2. Tides measured by Bushehr tide gauge

To check the tide gauge data more accurately, the tide data measured by the tide gauge of the Geographical Organization located at the Bushehr Customs Wharf was used. Tide information has been compared in daily and monthly intervals. As shown in Table (1) and Figure (8) of the monthly comparison, the measured level is almost identical and has a much smaller error than the satellite data. This matching of data can also be visible in the diagram of Figure (8). But in the daily chart of Figure (9) sometimes the quantity of measurement error is a little higher than in the monthly chart, the cause for this could be the waves of the sea surface, because the weather conditions may cause waves that cause errors in the measurement process. but to study the tides, the average data is studied, which reduces the measurement error.

Table 1: Comparison of the values measured by the tide gauge of the Geographical Organization and the built tide gauge

		April	May	June	August	September	October	November
Maximum Flood Tide	Geographical Organization	2/32	2/42	2/38	2/34	2/28	2/18	2/26
	Tide gauge System	2/33	2/41	2/38	2/33	2/28	2/18	2/27
Mean	Geographical Organization	1/25	1/21	1/24	1/28	1/22	1/21	1/20
	Tide gauge System	1/25	1/21	1/23	1/28	1/23	1/21	1/20
Minimum Ebb	Geographical Organization	0/38	0/29	0/21	0/20	0/22	0/35	0/41
	Tide gauge System	0/37	0/29	0/2	0/2	0/22	0/24	0/41

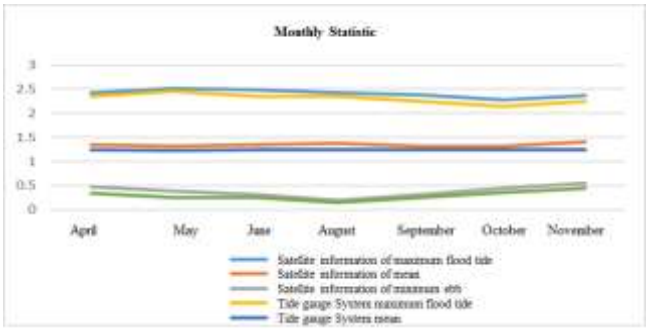


Figure (7): Comparison of monthly tide statistics measured by the constructed tide system and satellite data.

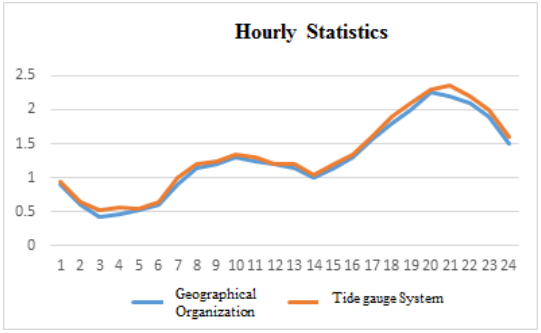


Figure (9): Comparing the hourly error of the level recorder and tide gauge of the Bushehr system

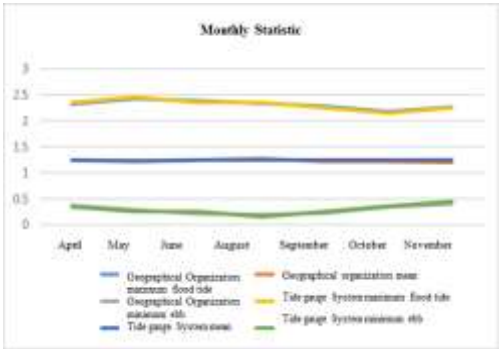


Figure (8): Comparison of the monthly error of level recorder and Tide-gage of Bushehr system

4. Conclusion

Tidal is a very important natural phenomenon that has huge consequences from the life process of organisms to navigation, therefore accurate measurement of this phenomenon could be very vital and allows lots inside the navigation of ships, fishing, etc. According to the results acquired from the assessment of the information measured with the aid of using the tide gauge made with the aid of using the authors of the thing with satellite data and the active tide gauge of the Geographical Organization in Bushehr region, similar to the accuracy of the system and automated

communication, top accuracy within side the tidal measurement is achieved.

Resources

[1] Gregory, J. M., Griffies, S. M., Hughes, C. W., Lowe, J. A., Church, J. A., Fukimori, I., ... & van de Wal, R. S. (2019). Concepts and terminology for sea level: Mean, variability and change, both local and global. *Surveys in Geophysics*, *40*, 1251-1289.

[2] Pugh, D., & Woodworth, P. (2014). Sea-Level Science: Understanding Tides, Surges, Tsunamis and Mean Sea-Level Changes (2014).

[3] Oppenheimer, M., & Hinkel, J. (2019). Sea Level Rise and Implications for Low Lying Islands, Coasts and Communities Supplementary Material.

[4] Kopp, R. E., Kemp, A. C., Bittermann, K., Horton, B. P., Donnelly, J. P., Gehrels, W. R., ... & Rahmstorf, S. (2016). Temperature-driven global sea-level variability in the Common Era. *Proceedings of the National Academy of Sciences*, *113*(11), E1434-E1441.

[5] Meyssignac, B., Piecuch, C. G., Merchant, C. J., Racault, M. F., Palanisamy, H., MacIntosh, C., ... & Brewin, R. (2017). Causes of the regional variability in observed sea level, sea surface temperature and ocean colour over the period 1993–2011. *Integrative Study of the Mean Sea Level and Its Components*, 191-219.

[6] Wöppelmann, G., Pouvreau, N., & Simon, B. (2006). Brest sea level record: a time series construction back to the early eighteenth century. *Ocean Dynamics*, *56*, 487-497.

[7] Palmer, H. R. (1831). XII. Description of a graphical registrer of tides and winds. *Philosophical Transactions of the Royal Society of London*, (121), 209-213.

[8] Woodworth, P. L., & Aarup, T. INTERGOVERNMENTAL OCEANOGRAPHIC COMMISSION. (IOC) of UNESCO, 2002.

[9] Xiaohui, W., & Kewei, L. (2018). The Monitoring and Wireless Transmission System of PM2. 5 in the Scenic. *International Journal of Advanced Network, Monitoring and Controls*, *3*(2), 71-74.

[10] Zulu, C. L., & Dzobo, O. (2023). Real-time power theft monitoring and detection system with double connected data capture system. *Electrical Engineering*, *105*(5), 3065-3083.

[11] Essien, V., Bolu, C. A., Azeta, J., Okokpujie, I. P., Kilanko, O., & Afolalu, S. A. (2021, April). Application of data logger for monitoring indoor and outdoor temperature of buildings: A review. In *IOP Conference Series: Materials Science and Engineering* (Vol. 1107, No. 1, p. 012181). IOP Publishing.

[12] Badhiye, S. S., Chatur, P. N., & Wakode, B. V. (2011). Data logger system: A Survey. *International Journal of Computer Technology and Electronics Engineering (IJCTEE)*, 24-26.

[13] Mahjoubi, A., Fethi Mechlouch, R., & Ben Brahim, A. (2011). A low cost wireless data acquisition system for a remote photovoltaic (PV) water pumping system. *Energies*, *4*(1), 68-89.

[14] Abd Rahman, N. A., Ibrahim, N. H., Lombigit, L., Azman, A., Jaafar, Z., Abdullah, N. A., & Mohamad, G. H. P. (2018). GSM module for wireless radiation monitoring system via SMS. In *IOP conference series: materials science and engineering* (Vol. 298, No. 1, p. 012040). IOP Publishing.

[15] Nikolov, G. T., Nikolova, B. M., & Marinov, M. B. (2005). Data logging system for pressure monitoring. *ELECTRONICS'2005, 21–23 September*, *3*, 81-86.

[16] Sahu, S., Bhuyan, M. R., Rudra, S., Biswas, S., Mohanty, B., & Sahu, P. K. (2015). Design and fabrication of a data logger for atmospheric pressure, temperature and relative humidity for gas-filled detector development. *arXiv preprint arXiv:1507.03575*.

[17] https://assets.rsonline.com/v1698979971/Datasheets/a017ec792c4d81996f6d6a370ef2d4ea.pdf

[18] Aliew, Fuad. "An Approach for Precise Distance Measuring Using Ultrasonic Sensors." Engineering Proceedings 24.1(2022):8.. https://www.mdpi.com/2673-4591/24/1/8

[19] Ahmad, Y. A., Gunawan, T. S., Mansor, H., Hamida, B. A., Hishamudin, A. F., & Arifin, F. (2021, June). On the evaluation of DHT22 temperature sensor for IoT application. In *2021 8th international conference on computer and communication engineering (ICCCE)* (pp. 131-134). IEEE.

[20] Neis, P., Warch, D., & Hoppe, M. (2023). Testing and Evaluation of Low-Cost Sensors for Developing Open Smart Campus Systems Based on IoT. *Sensors*, *23*(20), 8652.

[21] Verma, G., Kumar, M., & Khare, V. (2015). Low power techniques for digital system design. *Indian Journal of Science and Technology*, *8*(17), 1.

[22] Hashemi Farahani, Hassan. "Analysis of tidal conditions and preparation of maps of both amplitude and phase using thesis data, Topex/Poseidon satellite altimeter." Master's degree, Faculty of Engineering, University of Tehran, 2003

INTERNATIONAL JOURNAL OF
COASTAL, OFFSHORE & ENVIRONMENTAL ENGINEERING

IJCOE Vol.1/ Special Issue No.1/
Marine Instrumentation / 2023(8-19)

Available online at: www. Ijcoe.org

Presentation An Approach Based on Control Systems To Purpose Control Simultaneous Vibrations And Maneuver the Arm Robotic With two Degree of freedom

Amirhossein Ghasemkhani[1], DR. Ayoub Khodaparast[2*]

[1] *M.Sc. Graduate in Mechatronics Engineering, Department of Mechanical Engineering; amirhosseinghasemkhani76@gmail.com*
[2*] *Assistant Professor; Malek Ashtar University of Technology; ProfessorAyoubkhodaparast@yahoo.com*

ARTICLE INFO

Article History:
Received :02 Feb 2023
Accepted :27 Apr 2023

Keywords:
Innovation
Hamiltonian
Principles
modeling dynamic
Vibrations Robots
arm robotic

ABSTRACT

In recent times, the field of robotics and its applications have become increasingly attractive for researchers, particularly in the context of industrial control and automation. However, the approach predominant in the design and construction of robots until not too long ago favored solidity over flexibility. The primary rationale behind this inclination was the perceived weakness associated with highly flexible robots. While flexibility is deemed acceptable for certain purposes, the tendency was to prioritize simplicity and control, leading to the widespread adoption of rigid robotic structures. The drawback of this rigid approach became apparent as achieving control in highly rigid robots posed challenges. Such robots were often heavy, voluminous, and possessed a high weight-to-tolerance ratio, resulting in substantial energy consumption. The lack of adaptability and flexibility at joints further compounded these issues. The assumption that rigidity simplifies control was a guiding principle in designing robots. However, the contemporary consensus is that a rigid-centric methodology does not meet all the control needs in robotics. There is a growing recognition of the importance of flexibility and adaptability in robotic joints. This shift in perspective is driven by the understanding that not every joint in a robot needs to be rigid. Accepting flexibility in joints is based on the assumption that simplicity in control can still be achieved without rigid constraints. In the present era, it is acknowledged that a rigid-centric approach does not provide a comprehensive solution for the diverse requirements of robotic control. The acceptance of flexibility and adaptability in robotic systems has gained momentum. This change in attitude is evident in the emphasis on speed and adaptability in flexible robotic systems, leading to increased research efforts in control methodologies that embrace flexibility in the design and operation of robots.
Keywords: arm robotic, System control, Vibrations

1. Introduction

In the ever-evolving landscape of industries and technology, the ubiquity of robots has expanded across diverse sectors, including healthcare, automotive, aerospace, and more. The continual progress in this field has given rise to heightened expectations and demands for enhanced robotic capabilities. Particularly, robotic arms, frequently employed for repetitive tasks, stand to benefit significantly from incremental performance improvements, translating into substantial economic gains. Many contemporary industrial arms, tailored to meet stringent precision and repeatability standards, are characterized by robust yet heavy components. The inherent high inertia of these components necessitates considerable time for movement, resulting in elevated power consumption.

In response to these challenges, the global recognition of flexible jointed arms as a pragmatic problem-solving approach and a viable experimental model has

gained prominence. The incorporation of flexibility into these models is achieved by introducing specific stiffness springs as connection points between flexible arm segments. The flexibility inherent in these springs can be harnessed for rotational or translational movements within the system. In structural flexible systems, each component can be segmented into rigid bodies and elastic springs. Given the absence of constraints on the relative motion of robot components, a discrete coordinate approach proves advantageous for maneuvers involving substantial rotational angles. This hybrid motion comprises rigid (positional) components resulting from connections and flexible arm movements.

The unique model presented here utilizes equations for rigid body motion with point connections in a discrete coordinate system. Notably, none of the defined degrees of freedom correspond to actual deformations of the system. While this coordinate system allows for the modeling of large deformations, significant challenges arise in accurately representing stiffness and damping at connection points, especially beyond their linear behavior.

This article delves into the concurrent control of vibrations and maneuvering in a flexible two-link arm during single-axis maneuvers. It explores the synergistic effects of these two controllers on the arm's oscillatory behavior and targeting accuracy. The control of the flexible component involves the utilization of smart piezoelectric hinges, while arm maneuvering considers actuators applied to the arm connections. Through this exploration, we aim to contribute insights into optimizing the performance of flexible robotic arms in real-world applications

Innovation in Dynamic Modeling and Vibration Control:

This article represents a pioneering advancement in the realm of robotic systems by introducing a revolutionary paradigm shift in dynamic modeling and vibration control. Departing from conventional methodologies, our innovative approach challenges existing norms, introducing novel concepts and equations that redefine precision, adaptability, and efficiency in robotics. A key departure from traditional models is our emphasis on generalized coordinates, redefining their role in specifying particle positions within robotic systems. What distinguishes our research is the introduction of generalized forces associated with each coordinate, extending beyond classical Newtonian mechanics. Addressing the real-world presence of non-conservative forces, such as friction, our comprehensive framework offers insights into the intricate dynamic behaviors of robotic systems.

The integration of Hamiltonian principles plays a central role, providing a holistic representation through the sum of kinetic and potential energy. This innovative integration not only refines the accuracy of equations of motion but also opens avenues for unparalleled control and adaptability in robotic functionalities.

Another noteworthy innovation lies in the dynamic modeling section, where Lagrangian equations are employed to capture both conservative and non-conservative forces. The application of iterative learning methods enhances the understanding and control of the robotic arm's behavior, contributing to the adaptability of the control system for real-world applications.

Acknowledging the complexity of the derived equations and potential computational challenges, the study proposes a practical solution using fuzzy logic for inverse kinematics. This recommendation aims to streamline the implementation process, especially in scenarios where extensive calculations might hinder the operational efficiency of the robot.

In summary, this paper introduces a novel approach to controlling flexible robotic arms, addressing inherent challenges with practical solutions. The synergistic integration of smart materials, advanced control strategies, and fuzzy logic offers a comprehensive and adaptable framework for controlling flexible robotic systems, ushering in a new era of precision and efficiency.

modeling dynamic and Vibrations Robots:

In this article, we delve into dynamic modeling and vibrations of robots through the application of specific motion equations, which will be briefly discussed.

Generalized Coordinates: The position of a particle in space can be defined using three coordinate systems: Cartesian, spherical, and cylindrical. Alternatively, any three suitable parameters can be chosen. If the particle is constrained to move on a fixed plane, only two coordinates are necessary to specify its position. However, if the particle moves along a straight line or a fixed curve, specifying one coordinate becomes sufficient. In the case of a system composed of N particles, N^3 coordinates would be needed to simultaneously determine the positions of all particles.

When constraints are applied to the system, the number of coordinates required to specify the configuration becomes less than N^3. For example, if the system represents a rigid body, only the spatial position of a reference point on the body (e.g., center of mass) and its orientation are essential. Therefore, a minimum of n coordinates is generally required to specify the configuration of a specific system, and these coordinates are termed generalized coordinates.

In the generalized coordinate system, unlike the forces commonly seen in classical Newtonian mechanics, a force associated with each coordinate is defined,

known as the generalized force. This quantity, determined using the work definition, is dimensionally equivalent to work when multiplied by the generalized coordinate. Consequently, if the generalized coordinate has distance dimensions, the quantity becomes force, and if it is angular in nature, the quantity transforms into torque. The Hamiltonian, which is the sum of kinetic and potential energy of the system, is employed to accurately define the equations of motion.

Subsequently, these values are incorporated into the equation known as the Lagrangian equation of motion. The Lagrangian equation is expressed in terms of derivatives of the Lagrangian function concerning generalized coordinates and the time derivatives of the Lagrangian function regarding generalized speeds. In other words, denoting the Lagrangian function as L, the generalized coordinates as qk, and the generalized speeds as q̇k (where the dot denotes the time derivative of the generalized coordinate qk), the Lagrangian equations take the following form:

$$\frac{d}{dt}\frac{L}{q_k} - \frac{L}{q_k} = 0 \quad (1)$$

If the forces within the system are not entirely conservative, indicating the presence of a non-conservative force such as friction, in such instances, the Lagrangian equations on the right-hand side incorporate an additional term, Qk. This term represents the non-conservative generalized force.

$$\frac{d}{dt}\frac{L}{q_k} - \frac{L}{q_k} = Q_k \quad (2)$$

The Lagrangian equations exhibit uniformity across all coordinates, offering a systematic methodology for deriving the differential equations of motion in diverse systems. An alternative means of obtaining Lagrangian equations involves employing the principle of Hamiltonian variations. As previously mentioned, the Hamiltonian function, representing the cumulative kinetic and potential energy of a system, is defined within this approach.

In the context of Hamiltonian variations, an assumption is made about the existence of a potential function, signifying the conservative nature of the considered system. However, when non-conservative forces are present, similar to the Lagrangian equations, the impact of these forces is accounted for independently.

In such instances, the Hamiltonian function becomes the sum of kinetic energy and the work done by all forces, encompassing both conservative and non-conservative elements. This method provides an alternative viewpoint for formulating equations of motion in dynamic systems, placing emphasis on the collective energy and work contributions from all forces.

Hamilton Equations

The Hamiltonian equations consist of n² first-order differential equations, expressed in terms of generalized momentum and its derivatives. The generalized momentum is defined as the derivatives of the Lagrangian function concerning the generalized velocities. Consequently, these equations can be formulated as follows:

$$\frac{H}{p_k} = q_k$$

And,

$$\frac{H}{q_k} = P_k$$

In the given expression, qk denotes the generalized velocity, and the dot above pk (generalized momentum) signifies the time derivative. Upon comparing the Hamiltonian equations with the Lagrangian equations, it becomes evident that the former comprises a higher number of first-order equations. Specifically, in a system with N generalized coordinates, the Hamiltonian equations consist of n² first-order differential equations, while the Lagrangian equations consist of n second-order differential equations. Consequently, working with Hamiltonian equations is generally deemed more straightforward, and they find more frequent use in quantum mechanics and analytical mechanics.

Previous Studies:

A range of studies have explored the control of robotic arms with two degrees of freedom. Vorob'ev (2020) introduced a technique for coordinating the movements of the arms. This article proposes a technique for coordinating the movements of operating links of two-armed robotic systems with six degrees of freedom. The technique is based on introducing relative positioning matrices for the output links of the mechanical arms and solving reverse problems of the relative manipulator positioning. Manipulators with three degrees of freedom are viewed as mechanical arms. The reverse problems of manipulator positioning are solved, whic allow making output manipulator links carry out preset relative movements as solid bodies.

Efafi (2022) further enhanced this by proposing a feedback linearization controller to simultaneously control the main degrees of freedom and reduce vibration. In this paper, 3D dynamic modeling and robust control of a flexible robotic arm are performed with considering nonlinear effects. The simplifying assumptions such as linear vibration or 2D dynamic modeling of the arm significantly affect the accuracy of the arm dynamics. Thus, in this paper, a special

robotic arm is modeled using the 3D Euler–Bernoulli model considering the nonlinear effects of the beam. The Lagrange approach is used to extract the dynamic equations of motion and the coupled states of slow dynamics of the robotic degrees of freedom together with the fast dynamics of beam vibration is considered simultaneously. In order to control the main DOFs of the system and decrease the vibrating response of the system simultaneously, a feedback linearization controller equipped with the input shaping method is proposed through which all of the coupled states of the system can be controlled at the same time. It is shown that the response of the proposed model is closer to a real flexible robotics arm and the designed controller can successfully control all of the rigid and vibrating states of the system.

Lima (2019) addressed the issue of overshoot in a robotic arm with flexible joints, using magnetorheological dampers and a state-dependent Riccati equation for feedback control. In recent years, the evolution of artificial intelligence techniques has widely grown such that it gives new ways to improve human life, not only at work but also living. Nowadays, to the human being, physical human-robot interactions (PHRIs) have been presented very important and present itself as a major challenge for the current engineering. Therefore, this work designs and analyses a two-degree-of-freedom robotic arm with flexible joints driven by a DC motor. Due to the interaction between the robot links and flexible joints, the arm may present overshoots when it is moved such that it becomes difficult to manipulate the arm. Therefore, Magnetorheological dampers (MR damper or MR brake) are attached to the links of the arm in order to control such overshoot and provide a way to adjust the mechanical limitations of the arm. The dynamics of the system will be investigated, showing the appearance of chaotic behavior due to the coupling of the manipulator to the motors. After that, the feedback control is obtained through the state-dependent Riccati equation (SDRE) aiming the control of the positioning of the manipulator and the torque applied on the MR damper. Numerical results showed that the proposed control using hybrid actuators, DC motor, and MR brake was effective to control the position and behavior of the flexible joints of the manipulators.

Gharab (2021) proposed a robust two degrees of freedom PID control system to address the challenges of controlling lightweight single link flexible robots. This system effectively removed actuator friction and link vibrations, and was robust to strain gauge sensor disturbances and payload changes. In this paper, a method to control one degree of freedom lightweight flexible manipulators is investigated. These robots have a single low-frequency and high amplitude vibration mode. They hold actuators with high friction, and sensors which are often strain gauges with offset and high-frequency noise. These problems reduce the motion's performance and the precision of the robot tip positioning. Moreover, since the carried payload changes in the different tasks, that vibration frequency also changes producing underdamped or even unstable time responses of the closed-loop control system. The actuator friction effect is removed by using a robust two degrees of freedom PID control system which feeds back the actuator position. This is called the inner loop. After, an outer loop is closed that removes the link vibrations and is designed based on the combination of the singular perturbation theory and the input-state linearization technique. A new controller is proposed for this outer loop that: (1) removes the strain gauge offset effects, (2) reduces the risk of saturating the actuator due to the high-frequency noise of strain gauges and (3) achieves high robustness to a change in the payload mass. This last feature prompted us to use a fractional-order PD controller. A procedure for tuning this controller is also proposed. Simulated and experimental results are presented that show that its performance overcomes those of PD controllers, which are the controllers usually employed in the input-state linearization of second-order systems.

Lin (2023) presented a vibration control method for a six-axis manipulator, using variational mode decomposition and the Hilbert–Huang transform to analyze and eliminate vibration, and a feedback controller and iterative learning controller to stabilize the system. This paper presents a vibration control method for the vibration suppression of a robotic arm. To understand the causes of the vibration in the six-axis manipulator and then eliminate the vibration through an effective control method, the vibration control structure can be divided into two parts. First, variational mode decomposition (VMD) and the Hilbert–Huang transform (HHT) algorithm are integrated to analyze the vibration signal and extract the vibration characteristics. Second, a smooth trajectory planning method is used to eliminate the residual vibration. Then, a feedback controller and iterative learning controller are used for controlling the vibration to stabilize the system while compensating for the torque of the elastic-joint model and repetitive errors caused by the vibration through the repeated operation of the arm. In addition, to improve the iterative learning control (ILC) performance, the integration of VMD and the HHT is used to distinguish useless information. The ILC is able to learn more quickly and compensate for the error caused by the vibration. The proposed VMD-HHT iterative learning control for the elastic joint (VH-ILC-EJ) method, along with a laboratory-developed six-axis degree-of-freedom (6-DOF) robotic arm, has been numerically and experimentally validated for vibration suppression.

Control System Description:

The control system employs the deviation of frequency from its designated value as a signal to excite the system, ensuring balance in vibrations and maintaining a constant natural frequency. Modern power systems are designed with high capacity for economic reasons. However, the considerable distance for power transmission to arms negatively impacts stability. It is crucial to note that while connecting smaller systems enhances stability against minor disturbances, introducing distortions in one system can affect others within the network.

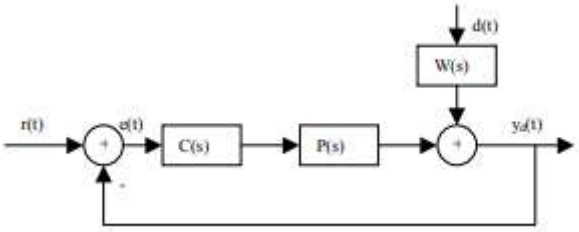


figure 1. Plan Control Feedback

The symbols employed in the aforementioned block diagram are explained as follows:

- *r*: Signal representing the reference entrance.
- *yd*: Output signal.
- *d*: Confusion signal.
- *e*: Signal representing the entrance error tracing.
- *P*: Variable for linear single output.
- *C*: Control time marker for linear single variable.
- *W*: Profile frequency signal for disorder.

In the context of a model based on recurrent fuzzy learning, aimed at overcoming challenges in position control, this study explores the utilization of the combined H2/Hinf controller method to achieve results comparable to a PID controller.

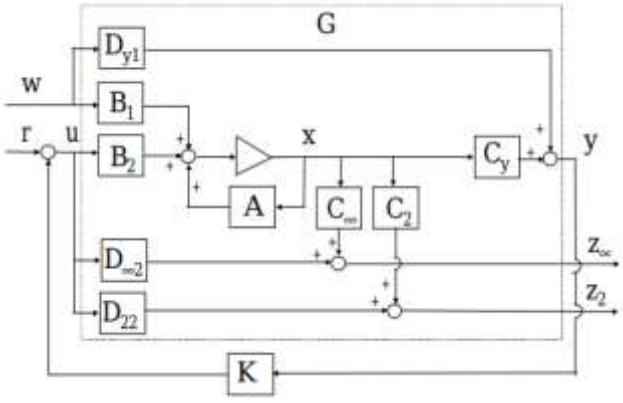


Figure 2. Closed-loop real system for H2/Hinf controller design.

Considering that the identification process and controller design are interconnected rather than independent, a systematic approach based on the iterative learning method is necessary to enhance the performance characteristics of the controlled system. This control method integrates the second-order H2 performance criterion for disturbance rejection with the Hinf performance criterion, aiming to achieve maximum robustness against uncertainty. The desired criterion is attained by tuning various design parameters within this scheme.

In each iteration, the control input undergoes correction based on a portion of the output error from the model. Theoretically, this correction allows the control signal to converge to a value that minimizes the output error of the actual plant. It's important to note that both strategies are developed without prior knowledge of the exact system models and differ in their application areas.

Cinematic Direction

The main goal in designing the dual-link robot is to trace a pre-defined path determined by the end of the second link, commonly known as the gripper. When both the path and the speed of traversal for the gripper are defined, the position of the gripper at any specific moment can be expressed in the global coordinate system. This representation is achieved using the following vector in Equation (20).

$$\boldsymbol{P(t) = u(t)i + v(t)j} \quad (20)$$

The ideal condition for traversing the path described in Equation (20) is predicated on the assumption of rigidity in the components. This implies that if the robot links under consideration lack flexibility, and the correct values of theta(i) are chosen, the robot precisely follows the specified path in Equation (20). However, in the real world, this matter is more complex due to the flexibility of gripper components, leading to oscillations around the desired path. The primary objective of this paper is to mitigate these oscillations, aiming to ensure that the actual gripper path closely conforms to the path outlined in Equation (20).

It's important to note that in this paper, the reduction of oscillations is achieved through the use of piezoelectric and the application of torques by motors. To initiate the analyses, the assumption is made that theta in the flexible state possesses values similar to those in the rigid state [14]. In other words, if theta has comparable values to the rigid state, the flexibility of the links only induces oscillations around the main path. For this purpose, utilizing Equations (2) and considering the assumption of rigidity, the position vectors of the endpoint of the second link are expressed as shown in Equation (21).

$$\begin{cases} \boldsymbol{u(t) = L_1 \cos\theta_1 + L_2 \cos(\theta_1 + \theta_2)} \\ \boldsymbol{v(t) = \ L_1 \sin\theta_1 + L_2 \sin(\theta_1 + \theta_2)} \end{cases} \quad (21)$$

The system of nonlinear equations in Equation (21) can be represented using properties of trigonometric functions, as illustrated in Equation (22).

$$\begin{cases}[u(t) - L_1 \cos\theta_1]^2 + [v(t) - L_1 \sin\theta_1]^2 = L_2^2 \\ [u(t)]^2 + [v(t)]^2 = L_1^2 + L_2^2 + 2L_1L_2 \cos\theta_2\end{cases}$$

(22)

The notable characteristic of equations (22) is that, in contrast to equations (21) where both unknowns were interlinked, these two equations are independent of each other. This implies that they can be solved individually [15]. Recognizing this, the unknowns can be determined by utilizing equations derived from (22). It's important to note that in equations (22), in addition to θ, θ' is also unknown, and this will be further explained. If they are associated with s (in these equations, only θ is present), taking the derivative of equations (22) once will yield Equation (23):

(23)

$$\begin{cases}-L_1\dot{\theta}_1 \sin\theta_1 - L_2(\dot{\theta}_1 + \dot{\theta}_2)\sin(\theta_1 + \theta_2) = \dot{u} \\ L_1\dot{\theta}_1 \cos\theta_1 + L_2(\dot{\theta}_1 + \dot{\theta}_2)\cos(\theta_1 + \theta_2) = \dot{v}\end{cases}$$

It's worth mentioning that the relationship describing the absolute speed of the claw is given by Equation (24):

$$V(t) = \sqrt{(\dot{u})^2 + (\dot{v})^2}$$

(24)

Since the finger is expected to lift a load from one point at time t=0 and carry it to another point at time t=tf, the absolute velocity of the finger at these two instances must be zero. Mathematically, this can be expressed as:

$$\begin{cases}V(0) = 0 \\ V(t_f) = 0\end{cases}$$

(25)

The trajectory of the robot's finger motion has been approximated with a third-degree polynomial.

$$\theta_i(t) = a_0 + a_1 t + a_2 t^2 + a_3 t^3$$

(26)

Differential Equations of the Motion System

The system is influenced by motors generating both single and double torques, leading to the emergence of external forces [9].

$$W = T_1(t)\theta_1 + T_2(t)\theta_2$$

(27)

In this equation, $T1(t)$ and $T2(t)$ denote the torques applied by motors one and two, respectively. In the formulation of the equations of motion, the assumed modes method is utilized, assuming that the lateral displacements of the links in the local coordinates of each link can be expressed as given in equation (28).

$$w_i(x_i, t) = \sum_{j=1}^{n} \phi_{ij}(x_i) q_{ij}(t)$$

In the given equation, the assumption of a cantilever beam with one end supported and the other end having mass leads to the expression for θ as a variable in the problem. Through the use of the assumed modes method, the partial differential equations are converted into ordinary differential equations. Subsequently, by defining the Lagrangian function as L=T−U, where T represents the kinetic energy and U denotes the potential energy, and incorporating the Euler-Lagrange equations alongside equation (28), the differential equations (29) can be derived.

$$\frac{d}{dt}\left(\frac{\partial L}{\partial \dot{\theta}_i}\right) - \frac{\partial L}{\partial \theta_i} = \frac{\partial W}{\partial \theta_i} = T_i(t) \quad i = 1, 2$$

$$\frac{d}{dt}\left(\frac{\partial L}{\partial \dot{q}_{ij}}\right) - \frac{\partial L}{\partial q_{ij}} = \frac{\partial W}{\partial q_{ij}} = 0 \quad i = 1, 2$$

$$j = 1, 2, \dots, n$$

(29)

It appears that the provided text might lack clarity. However, from the context, it seems that the Lagrangian function was derived using the assumed modes method and energy equations. Subsequently, this Lagrangian function was applied to the system equations (29), leading to a set of equations representing the motion of the system (equation (30)). If you have specific questions or if there's a particular aspect you'd like more clarification on, please let me know.

$$M\ddot{z} + v = f$$

(30)

Conditions border

It seems that the given text describes the boundary conditions and the methodology for determining the unknowns in the system. The approach involves introducing four hypothetical forces (F1, F2, F3, and F4) to the mechanism and applying them to establish the initial conditions (q(0)). These forces are assumed to act perpendicular to the respective links and in the positive local coordinate directions. The conditions are established by assuming the mechanism is in a state of static equilibrium under the influence of these hypothetical forces. The resulting displacements are then determined using Castigliano's theorem. If you have specific questions or need further clarification, feel free to ask.

$$M_{cb_1}^{in.} = \sum_{i=1}^{10} M_{1,i}^{in.}$$
$$M_{b_1}^{in.} = \sum_{i=1}^{8} M_{2,i}^{in.} \quad (31)$$

At Relationships Above $in.$ To floor the moment Beginning Move Is. also $M_{cb_1}^{in.}$ torque with came At Intermittent That Piezoelectric Existence has it And $M_{b_1}^{in.}$ To sign to give torque At Intermittent To Work may Process That Lacking Piezoelectric may to be also torques with came At Intermittent From link two That At it Piezoelectric Existence has it And At Intermittent That Lacking Piezoelectric Been particle for direct object may power To order To Description Under sign gave:

$$M_{cb_2}^{in.} = \sum_{i=1}^{5} M_{3,i}^{in.}$$
$$M_{b_2}^{in.} = \sum_{i=1}^{3} M_{4,i}^{in.} \quad (32)$$

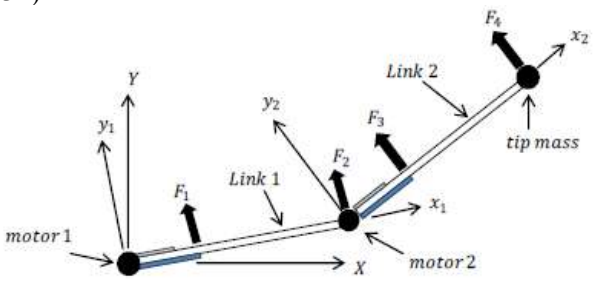


Figure 3 - Virtual Forces Acting on the Manipulator's Two Links

now With Attention To Relation (22), Energy Potential Store done At link particle for direct object may power To Shape Relation (34) wrote:

$$U_i^{sin.} = \frac{1}{2}\int_0^{l_{c_i}} \frac{\left(M_{cb_i}^{in.}\right)^2}{(EI)_{cb_i}} dx_i + \frac{1}{2}\int_{l_{c_i}}^{L_i} \frac{\left(M_{b_i}^{in.}\right)^2}{(EI)_{b_i}} dx_i \quad (34)$$

Pointed may to be That Target From actions loads virtual F_i Find Level Movement arrows, Location actions times Is That it particle for direct object may power With Use From The case Castigliano got brought In this way That Movement δ_i At Location actions Bar Fi from Relation (35) Following may slow [17]:

$$\delta_i = \frac{\partial U}{\partial F_i} \quad (35)$$

It is noteworthy that U represents the potential energy stored in the body, and delta(i) signifies the displacement in the direction of applying the load Fi. Since, in reality, the Fi forces do not exist externally and are only introduced into the problem to determine the displacement of the locations where these virtual loads are applied, their values should be set to zero after differentiation.

Importantly, q(0) remains unknown. To establish a connection between the outcomes derived from equation (34) and these unknown values, the displacement vector in the direction of applying virtual forces is initially expressed in the form of equation (36):

$$\begin{cases} \Delta_i = \delta_i j_1 & i = 1,2 \\ \Delta_j = \delta_j j_2 & j = 3,4 \end{cases} \quad (36)$$

Utilizing the relationship given in Equation (36) in conjunction with the relationship presented in Equation (28), a relationship to describe the shape is formulated, as expressed in Equation (37).

(37)

$$\begin{cases} \delta_1 = \phi_{11}(l_{c_1})q_{11}(0) + \phi_{12}(l_{c_1})q_{12}(0) \\ \delta_2 = \phi_{11}(L_1)q_{11}(0) + \phi_{12}(L_1)q_{12}(0) \end{cases}$$

In the relationships mentioned above, involving $\delta_1 = w_1(l_{c_1}, 0)$ and $\delta_2 = w_1(L_1, 0)$, conditions for computing q11(0) and q12(0) are established. This process is designed to fully prepare the formation. By employing this approach, the unknown q (0) for the two elements can be determined for future reference. A similar procedure is applied to the face, yielding:

$$\delta_3 = -L_1 \sin\theta_{20} + w_1(L_1, 0)\cos\theta_{20} + w_2(l_{c_2}, 0)$$
$$\delta_4 = -L_1 \sin\theta_{20} + w_1(L_1, 0)\cos\theta_{20} + w_2(L_2, 0)$$
$$\begin{cases} \delta_3 + L_1 \sin\theta_{20} - \delta_2 \cos\theta_{20} = \\ \phi_{21}(l_{c_2})q_{21}(0) + \phi_{22}(l_{c_2})q_{22}(0) \\ \delta_4 + L_1 \sin\theta_{20} - \delta_2 \cos\theta_{20} = \\ \phi_{21}(L_2)q_{21}(0) + \phi_{22}(L_2)q_{22}(0) \end{cases} \quad (38)$$

From these two relations, it is also possible to determine q21(0) and q22(0). By considering this order, the unknown q (0) can be fully known. Moreover, it is worth noting that taking q (0) into account, along with the primitive conditions of the robot, to solve the system of differential equations (Equation 31) will lead to further progress.

Presentation of Results:

In this section, the presentation of results will involve creating charts and visual representations. Initially, in Figure 4-3, the presentation of results related to the angles of the robot's links can be observed.

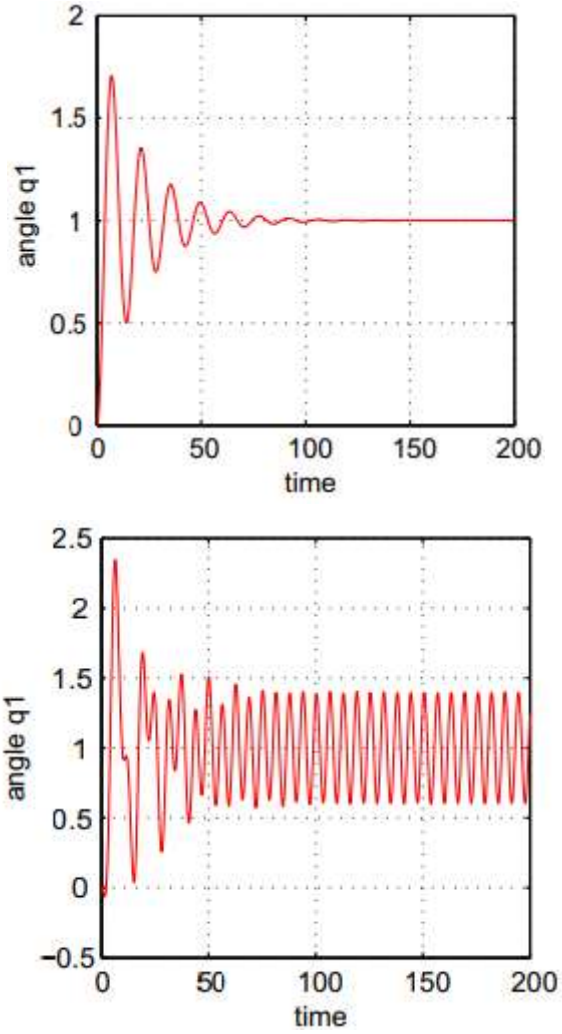


Figure 4: Diagram of the Angle of the First Link (Right side: Uncontrolled, Left side: Controlled)

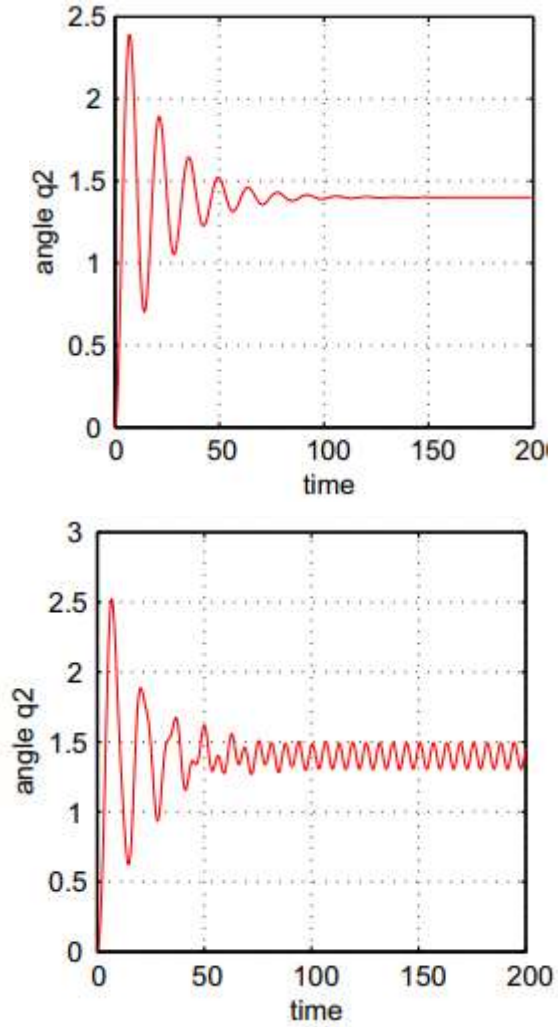


Figure 3: B - Diagram of the Angle of the Second Link (Right side: Uncontrolled, left side: Controlled)

Speed angles connections

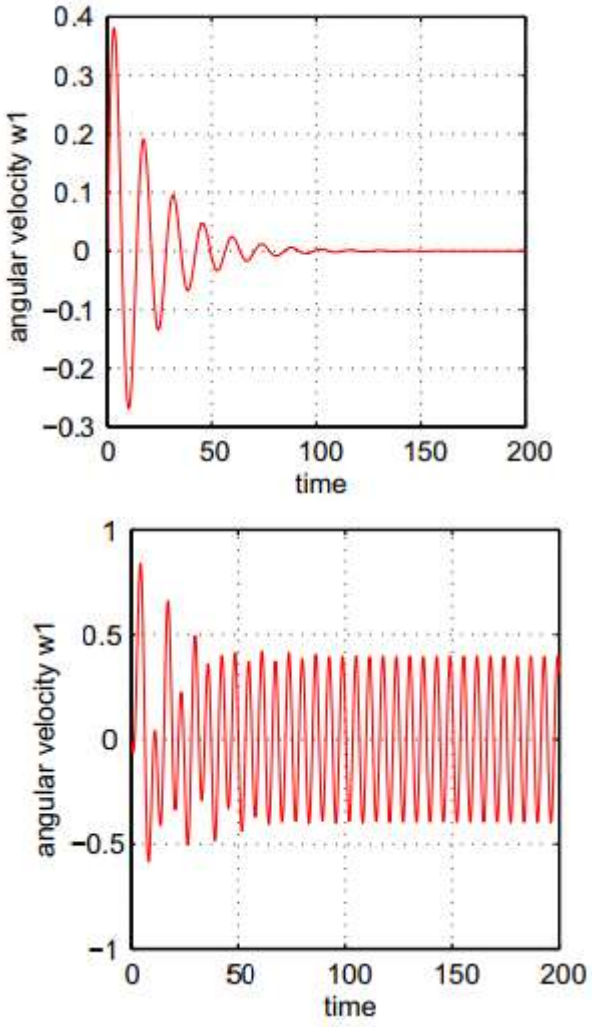


Figure 5: A - Angular Speed of Connection for the First Link (Right side: Non-control, left side: Controlled)

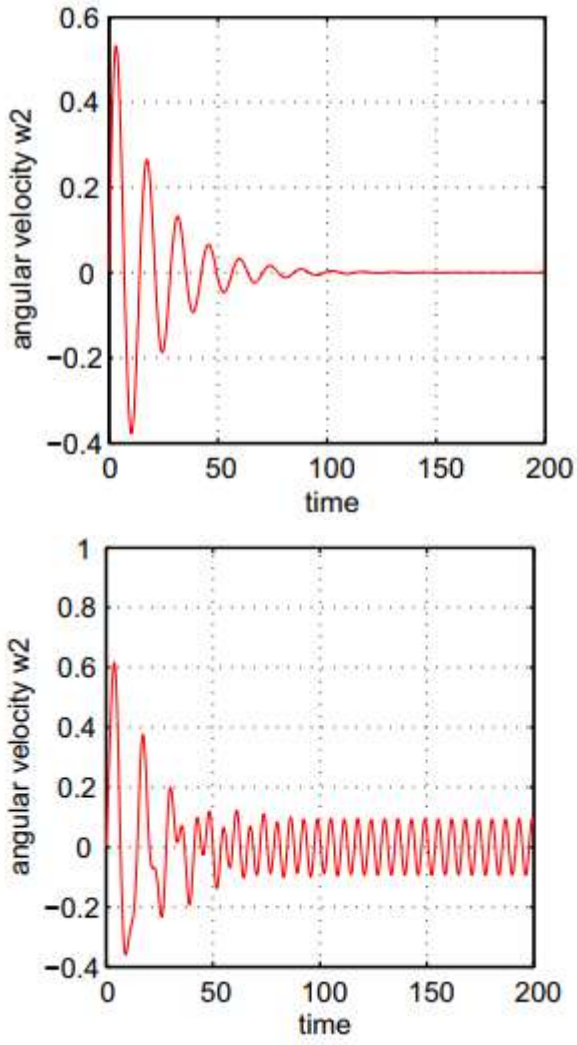


Figure 5: B - Angular Speed of Connection for the Second Link (Right side: Non-control, left side: Controlled)

Theoretical framework

Traditionally, the preference in the design and construction of robots has been for rigid structures rather than flexible ones. The choice was based on the notion that sturdy and inflexible designs would streamline control and improve durability. The perception of flexibility as a possible vulnerability has resulted in the general acceptance of inflexible robotic systems. Nevertheless, with the progress of robotics, namely in the realm of industrial control and automation, there has been a notable change in viewpoint. Researchers increasingly acknowledge the significance of integrating flexibility to enhance adaptability and efficiency in many applications.

The use of inflexible robotic systems poses several difficulties, especially in terms of control and efficiency. Stiff robots often possess a considerable weight and size, rendering them challenging to navigate and leading to increased energy consumption as a consequence of their big mass. Moreover, these robots exhibit a deficiency in flexibility due to the constraints imposed by their rigid joints, which restrict

their capacity to carry out a wide array of jobs. The inflexible characteristics of these robots also impede their ability to quickly adapt to changing settings, resulting in reduced versatility and efficiency while dealing with changeable situations and jobs. Flexible robotic systems have several benefits, beginning with their high energy efficiency. Flexible robots, being typically lighter than rigid robots, need less energy for operation. The decreased weight of these objects also enhances their flexibility and versatility, enabling them to carry out a wider array of duties. Moreover, flexibility might enhance the management of some applications by enabling robots to effectively adapt to disruptions and changes in their surroundings. The enhanced control capacity enhances the efficiency and effectiveness of versatile robots in diverse environments.

Effective control of flexible robots involves advanced methodologies that account for their dynamic nature. State-space representation is a key mathematical model used to describe the robot's dynamics, capturing the relationships between position, velocity, and control inputs. An example equation, $\dot{x} = Ax + Bu$, represents how the robot's state changes over time. Control techniques like PID (Proportional-Integral-Derivative) control, state feedback control, and Model Predictive Control (MPC) are commonly employed. PID control adjusts the control input based on the current error, its integral, and its derivative, offering a balanced approach to error correction. State feedback control uses the full state vector for precise control, with methods like LQR optimizing performance and energy use. Adaptive and learning-based methods, including machine learning, further enhance control by enabling the robot to learn and adapt to its behavior over time. This equation provides a framework for understanding how the robot's state evolves over time based on its current state and the control inputs. Control techniques like PID (Proportional-Integral-Derivative) control are widely used due to their simplicity and effectiveness. The PID control law is given by:

$$u(t) = K_p e(t) + K_i \int e(t)\,dt + K_d \frac{de(t)}{dt} \quad (39)$$

u(t) is the control input at time t, e(t) is the error (difference between desired and actual value) at time t. K_p, K_i, K_d denote the proportional, integral, and derivative gains, respectively.

PID control modulates the control input by considering the present error, its accumulated integral, and its derivative, providing a well-balanced method for error correction.

State feedback control is an advanced approach that utilizes the whole state vector to compute the control input. The control legislation governing state feedback is as follows: u=−Kx

K is the gain matrix that determines how the state variables influence the control input. A specific example of state feedback control is the Linear Quadratic Regulator (LQR), which optimizes control performance by minimizing a cost function that balances performance and energy use. The LQR control law is derived by solving the Riccati equation to find the optimal gain matrix K. Adaptive and learning-based methods, including machine learning, further enhance control by enabling the robot to learn and adapt to its behavior over time. These methods use data-driven approaches to improve control precision and adaptability in dynamic environments.

Result

Upon reviewing the outcomes of inverse kinematics, it reveals both advantages and disadvantages, summarized as follows:

- The equations in this section are intricate, leading to time-consuming calculations.
- The robot necessitates the utilization of direct and inverse kinematic relations to position each foot accurately.
- These non-linear relations, especially for a mobile system with a single leg, are cumbersome. Given that the processor unit must be embedded within the robot and faces processing speed limitations, these relations are better suited for mechanical simulation rather than as a suitable method for controlling the robot independently.
- The presence of an exact solution in these relations implies that the control system built on this foundation is expected to exhibit zero steady-state error and achieve a very short time to reach the steady state.

In practical implementation, the routine steps of this robot should not involve extensive calculations. Hence, fuzzy logic is suggested. In the fuzzy logic approach to inverse kinematics – akin to what insects, including the discussed insect, employ – there is no requirement for an exact solution. Instead, utilizing the differentials of joint vectors and employing fuzzy logic facilitates the implementation of inverse kinematics.

Furthermore, based on the results, it is noted that when exploring the foot space within the robot's width, achieving a better and faster outcome is preferable when the position is closer to the obtained angle.

The field of robotics has undergone significant evolution, particularly in the context of industrial control and automation. Traditionally, robot design has favored rigidity over flexibility due to the perception that flexible robots were inherently weaker. The rationale behind this preference was that rigid structures simplified control, despite the drawbacks of increased weight, volume, and energy consumption. These rigid robots were often characterized by their

high weight-to-tolerance ratios and lack of adaptability at the joints, leading to inefficient energy usage and limited functionality in dynamic environments.

However, the limitations of a rigid-centric approach have become increasingly apparent. Controlling highly rigid robots is complex and often impractical for applications requiring adaptability and precision. Consequently, the contemporary consensus in robotics is shifting towards incorporating flexibility and adaptability into robotic joints. This paradigm shift is driven by the recognition that not all joints need to be rigid to achieve effective control. Flexible joints can provide the necessary simplicity in control without the constraints imposed by rigidity. Modern robotic research emphasizes the benefits of flexible and adaptive systems. These systems are designed to be more efficient, faster, and capable of handling a broader range of tasks. The focus on flexibility has spurred increased research into control methodologies that accommodate and leverage adaptable joints. This shift acknowledges that rigid-centric designs do not adequately address the diverse and evolving requirements of robotic control. By embracing flexibility, researchers aim to create more versatile and efficient robotic systems that can meet the demands of contemporary industrial applications. The results obtained in the work can be validated by comparing our findings with the previous ones given in the recent years. For example, S. Dhifaoui,et al. [19] have discussed that in vibration isolation systems, vibration suppression and platform positioning were both critical. The author also presented, absolute velocity feedback caused difficulties in achieving these goals simultaneously; hence, this paper proposed an H_∞ control strategy based on sensor fusion feedback. Signals from inertial and displacement sensors were combined using complementary filters, allowing effective control of both vibration and position. This method also reduced noise levels in the fusion signals, maximizing system damping and bandwidth to improve performance. The effectiveness of the proposed strategy was demonstrated by comparing it with conventional absolute velocity feedback on a 3-DOF isolator. M. I. Azeez , et al. [20] have aimed to enhance the performance of a nonlinear three-rigid-link maneuver (RLM) in terms of trajectory tracking, disturbance and noise cancellation, and adaptability to joint flexibility. An optimized sliding mode controller with a proportional integral derivative surface (SMC-PID) was employed, optimized using a multi-elite guidance artificial bee colony algorithm (MGABC). The MGABC algorithm was selected for its efficient exploration and exploitation, resulting in optimal controller parameters. The optimized SMC-PID system have showen superior performance by reducing tracking error, eliminating chattering, and demonstrating robustness against disturbances, noise, and variations in payload mass. However, such papers did not succeed to give the novelty presented in the current work.

5. Conclusions

In conclusion, this article marks a significant stride in the field of robotic systems, particularly in dynamic modeling and vibration control. The innovative approach outlined in this study not only challenges traditional methods but also introduces novel concepts and equations that redefine the precision, adaptability, and efficiency of robotic systems. The emphasis on generalized coordinates, with associated forces, provides a fresh perspective, extending beyond classical Newtonian mechanics and addressing real-world challenges such as non-conservative forces. The incorporation of Hamiltonian principles enhances the accuracy of equations of motion, paving the way for unprecedented control and adaptability in robotic functionalities. The application of Lagrangian equations and iterative learning methods in dynamic modeling contributes to a deeper understanding and effective control of robotic arm behavior, making the proposed approach well-suited for practical applications. Furthermore, the suggestion of using fuzzy logic for inverse kinematics presents a practical solution to streamline implementation, especially in scenarios where computational challenges may impact operational efficiency.

References

1. B. Subudhi, AS Morris, Dynamic modeling, simulation and control of a manipulator with flexible links and joints, Robotics and Autonomous Systems, No. 41, pp. 257–270, 2002.

2. SK Tso, TW Yang, WL Xu, ZQ Sun, Vibration control for a flexible-link robot arm with deflection feedback, International Journal of Non-Linear Mechanics, No 38, pp. 51–62, 2003.

3. G. Oke, Y. Istefanopulos, Tip position control of a two-link flexible robot manipulator based on nonlinear deflection feedback, Chaos, Solitons and Fractals, No. 17, pp. 499–504, 2003.

4. MH Korayem, H. Ghariblu, Analysis of wheeled mobile flexible manipulator dynamic motions with maximum load carrying capacities, Journal of Robotics and Autonomous Systems, Vol. 48, No. (2-3), pp. 63-76, 2004.

5. Sharifi, S. Behzadipour, and GR Vossoughi, "Nonlinear model reference adaptive impedance control for human-robot interactions", Control Engineering Practice, vol. 32, pp. 9–27, 2014

6. Korayem, AM Shafei, Motion equations proper for forward dynamic of robotic manipulators with flexible links by using recursive Gibbs-Appell

formulation, Scientia Iranica Transaction B-mechanical engineering, Vol. 16, No. 6, pp. 479-495, 2009.

7. Wang, WK Timoszyk, JE Bobrow, Payload maximization for open chained manipulator: Finding motions for a Puma 762 robot, IEEE Transactions on Robotics and Automation, Vol. 17, No. 2, pp. 218-224, 2001.

8. Vicente Feliu, Emiliano Pereira, Iv´an M.D´ıaz, PedroRoncero, Feedforward control of multimode single-link flexible manipulators based on an optimal mechanical design, Robotics and Autonomous Systems, Vol. 54, pp. 651–666, 2006.

9. Shiller, Time-energy optimal control of articulated systems with geometric path constraints, IEEE Int. Conf. on Robotics and Automation, Vol. 4, pp. 2680-2685, 1994.

10. Mirzaee E, Eghtesad M, Fazelzadeh SA (2010) Maneuver control and active vibration suppression of a two-link flexible arm using a hybrid variable structure/lyapunov control design. Acta Astronautics 15: 1218-1232.

11. Choi SB, Cheong CC, Kim SH (1995) Control of flexible structures by distributed piezoelectric actuator and sensor. J Intel Mat Syst Str 6: 430-435.

12. Fleming AJ (2009) A MHz bandwidth dual-amplifier for driving piezoelectric actuators and other highly capacitive loads. Review of Scientific Instruments.

13. Budynas RG, Nisbett JK (2011) Shigley's mechanical engineering design. McGraw-Hill.

14. Vorob'ev, E.I. (2020). A Technique for Configuring the Relative Program Movements of Robotic Systems with Two Arms. Journal of Machinery Manufacture and Reliability, 49, 273 - 279.

15. Efafi, M., Hosseini, S.A., & Tourajizadeh, H. (2022). Robust Control and Vibration Reduction of a 3D Nonlinear Flexible Robotic Arm. *Iranian Journal of Science and Technology, Transactions of Mechanical Engineering, 46*, 1157-1173.

16. Lima, J.J., Balthazar, J.M., Rocha, R.T., Janzen, F.C., Bernardini, D., Litak, G., Bassinello, D.G., & Tusset, Â.M. (2019). On Positioning and Vibration Control Application to Robotic Manipulators with a Nonideal Load Carrying. *Shock and Vibration*.

17. Gharab, S., Benftima, S., & Batlle, V.F. (2021). Fractional Control of a Lightweight Single Link Flexible Robot Robust to Strain Gauge Sensor Disturbances and Payload Changes. Actuators.

18. Lin, J., Huang, H., & Lin, C. (2023). Iterative Learning Control for Vibration Suppression of a Robotic Arm. Applied Sciences.

19. S. Dhifaoui, C. Houaidia, and L. A. Saidane, "Computing paradigms for smart farming in the era of drones: a systematic review," Annals of Telecommunications, vol. 79, no. 1, pp. 35-59, 2024/02/01 2024, doi: 10.1007/s12243-023-00997-0.

20. M. I. Azeez, A. M. M. Abdelhaleem, S. Elnaggar, K. A. F. Moustafa, and K. R. Atia, "Optimized sliding mode controller for trajectory tracking of flexible joints three-link manipulator with noise in input and output," Scientific Reports, vol. 13, no. 1, p. 12518, 2023/08/02 2023, doi: 10.1038/s41598-023-38855-7.

INTERNATIONAL JOURNAL OF
COASTAL, OFFSHORE & ENVIRONMENTAL ENGINEERING

IJCOE Vol.1/ Special Issue No.1/
Marine Instrumentation/ 2023(20-26)

Available online at: www. Ijcoe.org

Enhancing Power Quality of AC-AC Direct Converters using Hybrid Filters

[1] *MR mohammad javad almasi kopaie Instructor; mjasanat@gmail.com*
[2*] *DR Ayoub khodaparast Assistant Professor Ayoubkhodaparast@yahoo.com*

ARTICLE INFO

Article History:
Received : 28 Feb 2023
Accepted : 03 Jun 2023

AC-AC converters, hybrid filters, power quality, harmonic distortion

ABSTRACT

This study explores enhancing power quality in AC-AC direct converters using hybrid filters. AC-AC direct converters, crucial in motor drives and renewable energy systems, often face power quality issues like harmonic distortion and voltage fluctuations. Hybrid filters, which combine passive and active filtering techniques, offer an effective solution. The research examines the historical evolution of matrix converters, highlighting advancements that inform current AC-AC direct converter technology. Control strategies, specifically Space Vector Modulation (SVM) and Pulse-Width Modulation (PWM), are investigated to optimize hybrid filter performance. The study finds that implementing hybrid filters in AC-AC direct converters significantly improves power quality and system stability. These insights contribute to better application and understanding of hybrid filters in enhancing AC-AC direct converter performance.

1. Introduction

The topic of electric power quality, or power quality, has garnered significant attention from both operators and consumers of electrical networks in recent years [1]. It is estimated that the damages resulting from power quality disturbances amount to around $100 billion annually in the United States alone. Therefore, investing in mitigating these disturbances is significantly less than the incurred damages. Undoubtedly, the quality of electric power generation is better today than in the past. Additionally, transmission and distribution networks have become more extensive and rely on newer and more reliable technologies [2]. So, why has the issue of power quality become more important nowadays, receiving serious attention and extensive research?

This issue can be examined from two perspectives. First, technological advancements have led to various nonlinear loads with non-sinusoidal waveform characteristics being dispersed throughout the network [2]. The presence of these loads deviates the waveform from its normal sinusoidal state, leading to power quality disturbances. On the other hand, many loads today are controlled by sensitive electronic and microprocessor-based systems. These systems are sensitive to the various disturbances present in the network and their performance can easily be compromised [3]. These disturbances can lead to significant damages. Therefore, investment and study for improving power quality and preventing the aforementioned damages have received considerable attention today. Consequently, it is necessary to assess and control power quality in power system networks, determine power quality parameters at certain points in the network, and, on the other hand, supplementary electricity tariff regulations oblige subscribers to comply with reducing power quality pollution caused by them. Consumers of electrical power show a significant inclination towards using devices with new technologies [4]. These devices, which enhance the quality and speed of industrial production sectors and improve the standard of living for household consumers, have created two fundamental problems for both producers and purchasers of electrical power [5]. On one hand, these types of loads are highly sensitive to voltage disturbances due to their specific designs. On the other hand, the power electronic circuits used in these devices inject harmonic currents into the distribution network. Current harmonics reduce the lifespan of network components and, upon passing through the network impedance, generate voltage disturbances. Power quality disturbances can be broadly categorized into two main types: 1) voltage disturbances imposed on the load by the network, such as voltage sags and swells, and 2) current disturbances introduced by the load to the network, such as current harmonics.

With the rapid development of the industrial economy, the installation and operation of a multitude of nonlinear loads significantly deteriorate the power

quality of the network. Increased usage of power electronic devices exacerbates the situation further. Low power factor and high harmonics in the network decrease system efficiency, resulting in consumers being unable to receive quality electricity that meets their needs. Harmonic standards like IEEE 519 exist to specify acceptable levels of harmonics. Conventional dynamic VAR compensation solutions, including inverter-based static compensators, have been available in the market for over 20 years, but these technologies are often too costly. Unfortunately, large capacitor banks are typically used on the DC side as energy storage elements in the form of a DC voltage source, leading to very high installation and maintenance costs, which are not acceptable for large-scale industrial applications. As a result, the market penetration of conventional active power filters is very limited.

AC-AC converters, or frequency converters, are a category of power electronic converters used for exchanging energy between two systems with different frequencies or two systems with the same frequency but asynchronous operation. Various applications of these converters include AC drives, HVDC lines, output converters of micro-turbines, external power sources for aircraft, and propulsion systems for modern ships. Different structures of AC-AC converters have been proposed, each with its own advantages and disadvantages. Generally, characteristics such as low weight and volume, high-quality input and output waveforms, high efficiency, high reliability, and ultimately, competitive cost are major requirements for these converters. In a general classification, AC-AC converters can be divided into two types: "direct" and "indirect" [6].

Indirect AC-AC converters involve an intermediate DC circuit and are therefore referred to as DC-AC-AC converters. The quantity of the DC circuit can be either voltage or current. Nowadays, indirect converters with a voltage intermediate circuit are among the most common and widely used AC-AC converters. However, some major drawbacks, such as relatively large size and low efficiency, persist in these converters. Additionally, the electrolytic capacitors used in these converters tend to lose their reliability significantly over time, ultimately compromising the overall performance of the converter. Efforts have been made to replace these capacitors with non-electrolytic capacitors with smaller volumes and longer lifespans, but the results obtained have generally not been confirmed and have not become industrialized.

2. Literature review

In a study conducted by Purwanto et al. [7], the investigation focused on a direct three-phase matrix converter with space vector modulation for driving induction motors [7]. Three-phase induction motors are extensively used in industries and electric vehicles due to their robust and simple construction, relatively low cost with high reliability, and low maintenance expenses. Adjusting the rotational speed of an induction motor can be achieved by controlling the input voltage and frequency. Typically, three-phase inverters are used to change the input voltage and frequency, requiring the conversion of DC voltage to three-phase AC voltage. However, this method has drawbacks, including the non-sinusoidal waveform of the output voltage, which can lead to high harmonics. Harmonics increase losses, which can reduce system efficiency and destabilize power systems. A direct matrix converter with space vector modulation (SVM) offers several advantages that can address these issues and achieve stable performance in driving three-phase induction motors [8].

In another research by Bedoud et al (2018), a dual-fed induction generator was investigated using a matrix converter [9]. With the advancements in power electronics devices, particular attention has been given to a new generation of power converters, namely AC to AC matrix converters. These converters offer direct AC/AC conversion, bidirectional power flow, and nearly sinusoidal input and output waveforms. In this article, the performance of a variable-speed wind turbine based on a dual-fed induction generator powered by a matrix converter is presented. The focus is on maximum power point tracking method to extract maximum power from wind. The entire system is represented in a synchronous d-q reference frame. The control scheme has been tested, and its performance has been evaluated through simulation results. The simulation results obtained using MATLAB/Simulink software demonstrate the effectiveness and validity of the intended control.

3. Methodology

An induction motor is a type of alternating current (AC) motor, specifically an asynchronous AC motor, in which the required power for its moving part is supplied through electromagnetic induction. Induction motors are the most widely used motors in industrial motion control systems as well as household appliances. Their simple and robust design, low cost, low maintenance, and easy and complete connection to an AC power source are fundamental advantages of AC induction motors. Various types of AC induction motors are available in the market, suitable for various applications. Although the design of AC induction motors is simpler than that of DC motors, controlling speed and torque in different types of AC induction motors requires a deeper understanding in their design and manufacturing. An electric motor converts electrical energy into mechanical energy in its rotor. Various methods exist to supply the required power to the rotor. In a DC motor, the armature power is directly supplied by a direct current source, while in an induction motor, this power is induced electromagnetically in the rotor through the stator. Due to their striking similarity to transformers, induction motors are also referred to as rotary transformers, as

their stator closely resembles the primary winding and their rotor resembles the secondary winding of a transformer. Induction motors, especially three-phase induction motors, are widely used in the industry. High power, simple structure, absence of brushes (which require extensive maintenance), and the high controllability of induction motors for speed control are among the reasons for their use. The biggest difference between an AC induction motor and a synchronous AC motor is that in a synchronous motor, the rotor power is directly supplied from an external source. This current in the rotor will also produce its own magnetic field, and due to the interaction of the stator and rotor magnetic fields, the rotor will move in the direction of the stator's rotating field. On the other hand, for inducing current in the rotor, a speed difference between the rotor's rotation speed and the rotating field speed is necessary. Otherwise, the rotating field will not be able to move the rotor, and the rotor's conductors will not cut the magnetic field produced by the stator, resulting in no induced voltage in the rotor. This speed difference between the rotating field speed and the rotor movement speed is called "slip". Slip is a dimensionless quantity. Since the speed difference is a condition and necessity for the operation of induction motors, they are called asynchronous motors.

AC/AC converters have gained a special position in power electronics in recent decades [10]. These converters can be used in power regulators, induction motor drives, and converters related to wind turbines, among other applications. These converters have the capability of bidirectional power transfer, in addition to being unidirectional. With the advancement of technology, high-power switches, commutation strategies, modulation techniques, and corresponding switching techniques, these converters are continuously improving in terms of power conversion quality, efficiency enhancement, and reduction of losses and costs. Structurally, AC/AC converters are classified into two main categories [11]:

A) Structure (AC/DC/AC): Converters with DC energy storage interface, including voltage source inverters (VSI) and current source inverters (CSI). For example, a VSR/VSI inverter, as shown in Figure (1), consists of a rectifier stage and an inverter stage. These two stages are coupled to each other through a large and expensive energy storage element such as a capacitor and an inductor.

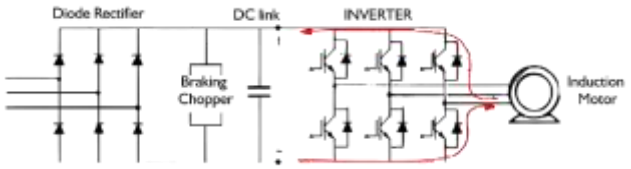


Figure (1), Frequency Converter with AC-DC-AC Structure

VSR/VSI converters have a DC voltage link and a parallel capacitor element, while CSR/CSI converters have a DC current interface and a series inductor element. In addition to these interface elements, these converters are equipped with additional filtering elements to remove harmonics and commutation strategy equipment, etc. Therefore, power factor correction in these converters is significant, and solutions such as using resonant interfaces and high-frequency techniques are recommended.

B) Direct AC/AC: Converters without a DC interface and energy storage, including cycloconverters and matrix converters, which have both direct and indirect structures. Cycloconverters and matrix converters belong to the second category of AC/AC converters, which lack a DC interface and energy storage elements (ZES). Cycloconverters come in two types: three-phase and single-phase, at different power levels, often used in three-phase configurations for high-power and low-frequency applications (Figure 2). In these converters, the output frequency is a fraction of the input frequency [12].

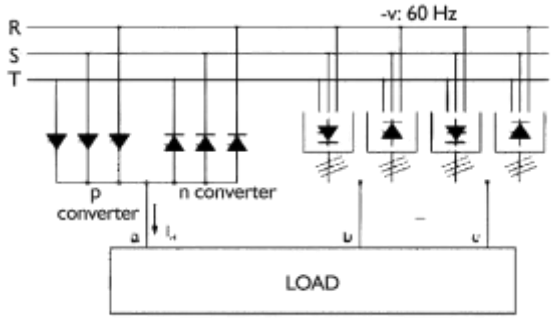


Figure (2), Three-Phase Cycloconverter

The history of matrix converters dates back to 1976 when Gyagy and Pully first introduced the concept as a theoretical and innovative approach to optimize the fundamental operation of cycloconverters. Their goal was to achieve an output voltage with an unlimited frequency and enable direct conversion using controllable bidirectional switches. However, the initial matrix converters faced challenges, including the presence of significant undesired harmonics in the output voltage and input current, which couldn't be easily eliminated by filters [13].

In 1980, Venturini and Al Sina addressed these challenges by proposing a new modulation technique utilizing Pulse Width Modulation (PWM). Despite this advancement, practical applications of matrix converters remained limited at that time due to issues with current commutation and the complexity of control algorithms [14]. Continued research efforts have focused on analyzing mathematical relationships and studying converters at lower frequencies. With the development of suitable modulation techniques and power converter circuits structured as matrices of controllable bidirectional switches, researchers were able to introduce matrix converters with a direct method [15].

Later, in 1983, Rodriguez presented a different control technique based on a virtual DC link. In this method, each output line's switching is performed using PWM

during input lines with minimum values, known as indirect matrix conversion. This evolution marked significant progress in the practical application and control of matrix converters.

The structure of the matrix converter is similar to that of a buck converter. Examining the evolutionary trend of the buck converter helps us understand the performance of matrix converters. Figure 3 illustrates a buck converter where the switch (Sw) is periodically connected to the positive and negative terminals of the DC input voltage source (Vin).

The methodology encompasses the design and evaluation of hybrid filters integrated into AC-AC converters to enhance power quality. Firstly, the design parameters for the hybrid filters are established, including cutoff frequencies and filter orders, crucial for defining their operational range and complexity. Control strategies, namely Pulse-Width Modulation (PWM) and Space Vector Modulation (SVM), are implemented with specific parameters such as modulation index and switching frequency, influencing the converters' output waveform and overall system performance. Converter ratings, including voltage and current specifications, are also considered to ensure compatibility with practical applications.

Following the design phase, the hybrid filter system is evaluated using established performance metrics. Total Harmonic Distortion (THD), voltage stability, and power factor are among the key criteria utilized to assess the effectiveness of the filters in mitigating harmonic distortion and enhancing system stability. The evaluation process involves rigorous testing under various operating conditions, including different load scenarios and harmonic levels. Results are analyzed to determine the extent of power quality improvement achieved through the integration of hybrid filters into the AC-AC converters. This methodology ensures a systematic approach to designing, implementing, and evaluating hybrid filter systems, facilitating reproducibility and comparison with other studies in the field.

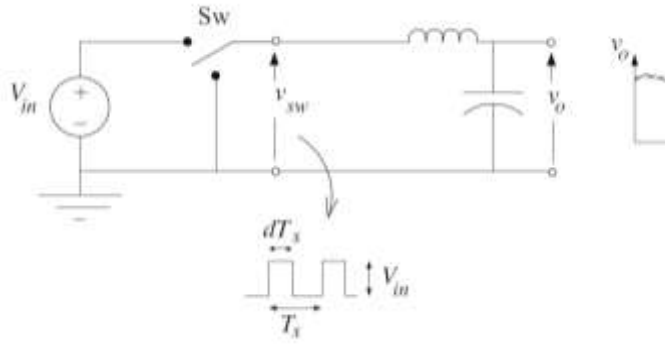


Figure 3, Buck Converter

The DC component of Vsw is obtained using the average waveform over one switching cycle Ts:

$$Vsw = \frac{1}{Ts}\int_0^{Ts} Vsw\, dt = dVin \quad (1)$$

Therefore, by adjusting the duty cycle (d), it is possible to generate a desired DC component from the switching voltage (Vsw). The frequency components (f=1/Ts) and their harmonics present in Vsw can be significantly reduced by an LC filter. The important point is that the desired DC component can only be produced when the output voltage is less than the source voltage (Vin) [2].

The conversion of output voltage from a three-phase sinusoidal to a DC rectifier provides valuable assistance in analyzing converters. Figure 4 illustrates a three-phase diode rectifier and the output voltage.

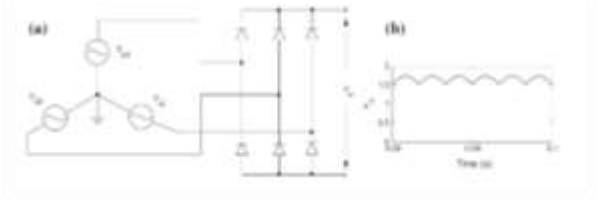


Figure 4 illustrates a three-phase diode rectifier and the output voltage.

The input voltages are as follows:

$$Vsa = \sin 2\pi 50T, \quad (2)$$

$$Vsb = \sin(2\pi 50t - 120), \quad (3)$$

$$Vsc = \sin(2\pi 50t - 240), \quad (4)$$

By replacing three diodes connected to each output terminal with a Single Pole-Triple Throw (SPTT) switch, it is possible to fully control it.

The study employs MATLAB/Simulink to simulate the integration of hybrid filters into AC-AC direct converters, ensuring a detailed analysis of their impact on power quality. The system is modeled to reflect real-world configurations, incorporating both the AC-AC converter and the hybrid filter components. Control strategies, specifically Space Vector Modulation (SVM) and Pulse-Width Modulation (PWM), are implemented within the simulation to optimize the converter's performance. Key parameters such as input voltage, load conditions, and switching frequencies are carefully selected to represent typical operating conditions.

Various test scenarios are simulated to evaluate the hybrid filter's effectiveness under different conditions, including varying loads and harmonic levels. The performance is assessed using metrics like Total Harmonic Distortion (THD), voltage stability, and power factor. The results show significant improvements in power quality, demonstrating the hybrid filter's capability to mitigate harmonic distortion and enhance system stability. This transparent and detailed simulation methodology ensures the study's findings are credible and reproducible, providing a solid foundation for future research and practical applications.

In any engineering study, particularly those involving power electronics, simulation plays a vital role in validating theoretical designs and predicting their real-

world performance. Without specifying the use of software tools, the study lacks a crucial layer of verification that would otherwise strengthen its claims about the effectiveness of hybrid filters in improving power quality. Simulation helps in identifying potential issues, optimizing the design, and ensuring that the proposed solution can achieve the desired outcomes under various operating conditions.

Clarifying whether software tools were used, and providing details about the simulation process, would significantly enhance the study's credibility. Information such as the type of software used (e.g., MATLAB/Simulink, PSpice), the parameters and scenarios tested, and the results obtained from these simulations would provide a more comprehensive understanding of the methodology. This transparency allows other researchers to replicate the study, verify the results, and build upon the findings. It also demonstrates a rigorous approach to design validation, ensuring that the proposed integration of hybrid filters is not only theoretically sound but also practically feasible.

4. Results and discussion

The switches will be turned on for a duration of *d*0*Ts* =*T*0. During this period, all output phases will be connected to one input phase, resulting in zero line voltages. To minimize switching losses, the state before this stage should be considered, ensuring that the least amount of change in the switch states occurs. Therefore, we have:

$V_0(A,B,C) = v(b,a,b) \Rightarrow A = b, B = a, C = b$

5

So, to reduce switching losses during this period, the switching should be performed as follows:

$V_0(A,B,C) = V_0(b,b,b)$

6

Therefore, during this period, switches S2, S5, and S8 are turned on, while the rest of the switches are off.

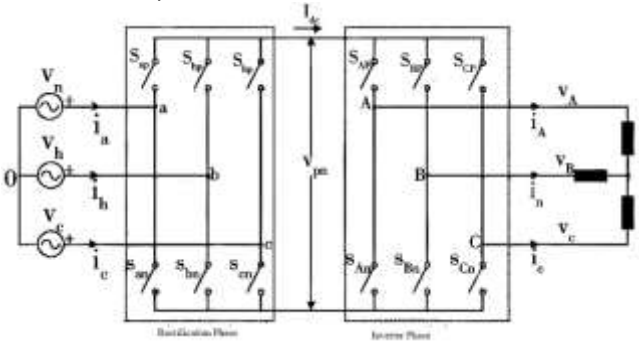


Figure (5), equivalent circuit of the matrix converter used in the control method.

The times are considered symmetrical to reduce the harmonics present in the output voltage. The steps performed were for a scenario where the output voltage vector was in the first sector and the input current vector was in the third sector [16]. For this scenario, the gate signals of the switches are as follows.

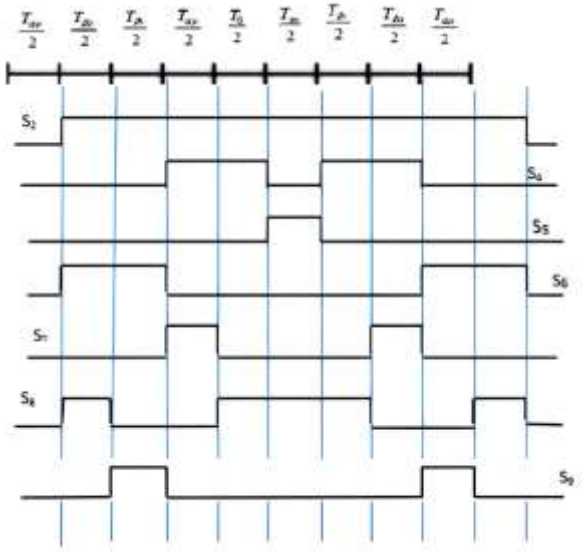


Figure (6), gate signals for the scenario where the output voltage vector was in sector one and the input current vector was in sector three.

Furthermore, the study elucidates the utilization of matrix converters in various industrial applications, such as wind turbine systems and dual-fed induction generators. By employing advanced modulation techniques and control algorithms, matrix converters demonstrate remarkable potential in enhancing power system efficiency and stability. The analysis of gate signals and switching schemes underscores the importance of optimized control strategies to mitigate harmonics and minimize switching losses. Overall, the research provides valuable insights into the evolution, optimization, and practical applications of matrix converters in power electronics. It underscores the importance of advanced modulation techniques and control algorithms in improving efficiency, stability, and performance, paving the way for their wider adoption in diverse industrial and renewable energy systems. The investigation into matrix converters showcases their capability to address challenges associated with traditional power conversion methods, such as harmonics, switching losses, and control complexity. By leveraging vector space modulation and advanced control techniques, matrix converters offer efficient and reliable solutions for power conversion tasks in various industrial sectors.

If software simulation was not conducted in this study, the primary reason could be the focus on validating the proposed design through an experimental setup to ensure real-world applicability. Experimental setups provide direct and tangible results, reflecting actual operational conditions that simulations might not fully capture. This approach can offer more reliable data on how the hybrid filters perform when integrated into AC-AC direct converters, accounting for practical variables such as noise, temperature variations, and other environmental factors that simulations often idealize or overlook.

Despite the strengths of experimental validation, it is important to recognize the limitations of not including software simulations. Simulations offer a controlled environment to test a wide range of scenarios, which can help in identifying potential issues and optimizing the system before physical implementation. The absence of simulations might mean some performance aspects are not thoroughly explored. To mitigate this limitation, future work could incorporate both simulation and experimental phases, providing a more robust and comprehensive evaluation. By explaining these considerations, the study can justify its methodological choices and outline a path for further research enhancements.

5. Conclusions

In this study, we explored the enhancement of power quality in AC-AC direct converters through the integration of hybrid filters. These filters, combining passive and active filtering techniques, offer a promising solution to address power quality issues such as harmonic distortion and voltage fluctuations. Our investigation delved into the historical evolution of matrix converters, providing valuable insights into the development of AC-AC direct converter technology. Through the implementation of sophisticated control strategies including Space Vector Modulation (SVM) and Pulse-Width Modulation (PWM), we aimed to optimize the performance of hybrid filters.

While our study offers valuable insights into the potential of hybrid filters to improve power quality, there are areas for further enhancement. The methodology section lacked clarity on specific design parameters and values, hindering a comprehensive assessment of the proposed hybrid filter integration. Future research should focus on providing detailed design parameters to facilitate a more robust evaluation of the filters' effectiveness. Additionally, incorporating both software simulations and experimental validation would offer a more comprehensive understanding of the hybrid filter performance under various operating conditions.

Overall, this research contributes to advancing the understanding and application of hybrid filters for enhancing the power quality of AC-AC direct converters. By addressing the limitations highlighted and further refining the methodology, future studies can build upon these findings to develop more efficient and reliable power quality enhancement solutions for diverse applications.

References

[1] J. Chen, X. Zhang, and C. Wen, "Harmonics attenuation and power factor correction of a more electric aircraft power grid using active power filter," *IEEE Transactions on Industrial Electronics,* vol. 63, no. 12, pp. 7310-7319, 2016.

[2] D. J. Hogan, F. J. Gonzalez-Espin, J. G. Hayes, G. Lightbody, and R. Foley, "An adaptive digital-control scheme for improved active power filtering under distorted grid conditions," *IEEE Transactions on Industrial Electronics,* vol. 65, no. 2, pp. 988-999, 2017.

[3] P. P. Biswas, P. N. Suganthan, and G. A. Amaratunga, "Minimizing harmonic distortion in power system with optimal design of hybrid active power filter using differential evolution," *Applied Soft Computing,* vol. 61, pp. 486-496, 2017.

[4] B. Sahoo, M. M. Alhaider, and P. K. Rout, "Power quality and stability improvement of microgrid through shunt active filter control application: An overview," *Renewable Energy Focus,* vol. 44, pp. 139-173, 2023.

[5] C. A. Slongo, "Low-voltage direct current distribution grids: main AC/DC converter, power quality, and protections analysis," Université de Bordeaux, 2023.

[6] W. U. Tareen, S. Mekhilef, M. Seyedmahmoudian, and B. Horan, "Active power filter (APF) for mitigation of power quality issues in grid integration of wind and photovoltaic energy conversion system," *Renewable and Sustainable Energy Reviews,* vol. 70, pp. 635-655, 2017/04/01/ 2017, doi: 10.1016/j.rser.2016.11.091.

[7] E. Purwanto, F. D. Murdianto, D. Wahyu Herlambang, G. Basuki, and M. P. Jati, "Three-Phase Direct Matrix Converter with Space Vector Modulation for Induction Motor Drive," in *2019 2nd International Conference on Applied Information Technology and Innovation (ICAITI)*, 2019/09// 2019, pp. 11-16, doi: 10.1109/ICAITI48442.2019.8982139. [Online]. Available: https://ieeexplore.ieee.org/abstract/document/8982139

[8] N. F. Guerrero-Rodríguez, A. B. Rey-Boué, L. C. Herrero-de Lucas, and F. Martinez-Rodrigo, "Control and synchronization algorithms for a grid-connected photovoltaic system under harmonic distortions, frequency variations and unbalances," *Renewable Energy,* vol. 80, pp. 380-395, 2015.

[9] K. Bedoud, A. Rhif, T. Bahi, and H. Merabet, "Study of a double fed induction generator using matrix converter: Case of wind energy conversion system," *International Journal of Hydrogen Energy,* vol. 43, no. 25, pp. 11432-11441, 2018/06/21/ 2018, doi: 10.1016/j.ijhydene.2017.07.010.

[10] P. Dey and S. Mekhilef, "Current harmonics compensation with three-phase four-wire shunt

hybrid active power filter based on modified D–Q theory," *IET Power Electronics,* vol. 8, no. 11, pp. 2265-2280, 2015.

[11] N. Hamouda, K. E. Hemsas, H. Benalla, and A. Boutaghane, "An advanced control approach for current harmonic cancellation using shunt active power filter," *International Journal of Industrial Electronics and Drives,* vol. 2, no. 1, pp. 35-42, 2015.

[12] Q. Xu, F. Ma, A. Luo, Z. He, and H. Xiao, "Analysis and Control of M3C-Based UPQC for Power Quality Improvement in Medium/High-Voltage Power Grid," *IEEE Transactions on Power Electronics,* vol. 31, no. 12, pp. 8182-8194, 2016/12// 2016, doi: 10.1109/TPEL.2016.2520586.

[13] C. Cheng and H. Nian, "Low-complexity model predictive stator current control of DFIG under harmonic grid voltages," *IEEE Transactions on Energy Conversion,* vol. 32, no. 3, pp. 1072-1080, 2017.

[14] I. Bouloumpasis, P. Vovos, K. Georgakas, and N. A. Vovos, "Current harmonics compensation in microgrids exploiting the power electronics interfaces of renewable energy sources," *Energies,* vol. 8, no. 4, pp. 2295-2311, 2015.

[15] Y. Fang, J. Fei, and K. Ma, "Model reference adaptive sliding mode control using RBF neural network for active power filter," *International Journal of Electrical Power & Energy Systems,* vol. 73, pp. 249-258, 2015.

[16] A. Chebabhi, M. Fellah, A. Kessal, and M. F. Benkhoris, "Comparative study of reference currents and DC bus voltage control for Three-Phase Four-Wire Four-Leg SAPF to compensate harmonics and reactive power with 3D SVM," *ISA transactions,* vol. 57, pp. 360-372, 2015.

INTERNATIONAL JOURNAL OF
COASTAL, OFFSHORE & ENVIRONMENTAL ENGINEERING

IJCOE Vol.1/ Special Issue No.1/
Marine Instrumentation/ / 2023(27-33)

Available online at: www. Ijcoe.org

Hardware-Accelerated Image Moment Computation for UUV Navigation

Mehrnaz Monajati[1]

[1] *Assistant professor, Department of Electrical and Computer Engineering, Graduate University of Advanced Technology, Kerman, Iran;* m.monajati@kgut.ac.ir

ARTICLE INFO

Article History:
Received: 05 Mar2023
Accepted :10 Jun 2023

Keywords:
Unmanned Underwater Vehicles (UUVs)
Image moment
Pipeline
Systolic array
Real time

ABSTRACT

Image moments are pivotal in the control of Unmanned Underwater Vehicles (UUVs), empowering them to extract valuable insights from onboard camera images, identify objects, navigate autonomously, and adapt to evolving environmental conditions. Integrating image moment analysis into UUV control systems amplifies their effectiveness in exploration, research, surveillance, and various underwater applications. However, the computational demands of moment calculation algorithms pose challenges for real-time implementation, particularly with higher moment orders. In this study, we propose a novel structure based on systolic arrays, leveraging pipeline technique, to compute moments up to the 14th order of grayscale images in real time. Implemented in 45nm CMOS technology, our design demonstrates impressive performance, with each cell capable of computing the 14th order moment of a 1024×1024 image at a remarkable rate of 954 fps. Moreover, our design boasts low power consumption, registering at only 3.254 mW, demonstrating its potential for enhancing UUV control systems for diverse underwater applications.

1. Introduction

Unmanned Underwater Vehicles (UUVs) are autonomous robotic vessels designed for underwater operations without direct human control [1]. Equipped with sensors and propulsion systems, they navigate underwater environments, collect data, and perform tasks across various fields including oceanographic research, underwater mapping, marine biology, defense, infrastructure inspection, and search and rescue operations. UUVs offer a versatile platform for exploration, research, security, and industrial applications, contributing to our understanding and utilization of the world's oceans [2].

Image moments are indispensable tools in the realm of UUVs, playing a pivotal role in various aspects of their operation [3]. These moments are integral to extracting meaningful information from onboard camera images, enabling UUVs to recognize objects, navigate autonomously, and adapt to changing environmental conditions. The incorporation of image moment analysis into UUV control systems significantly enhances their capabilities for exploration, research, surveillance, and various underwater applications [3].

In feature extraction, image moments serve as essential mathematical descriptors derived from pixel intensities, providing valuable insights into an image's shape, size, orientation, and object distribution [4]. This feature extraction process is particularly crucial for UUV navigation, where visibility is often limited, making it imperative to extract pertinent features from onboard camera imagery for effective navigation and obstacle avoidance.

Furthermore, image moments facilitate object recognition and tracking, empowering UUVs to identify and monitor objects of interest in their surroundings [5]. This capability is essential for tasks such as detecting underwater structures, monitoring marine life, and identifying potential hazards. By accurately recognizing and tracking objects, UUVs can autonomously navigate through complex underwater environments while adeptly avoiding obstacles. Additionally, image moments contribute significantly to localization and mapping efforts. Through the analysis of moments extracted from successive images, UUVs can estimate their position and orientation relative to known landmarks or predefined maps. This information is crucial for ensuring precise navigation and achieving mission objectives, especially in environments where GPS signals may be unreliable or inaccessible [6].

Real-time implementation of image moments is crucial for UUVs because it enables swift decision-making, autonomous navigation, and obstacle avoidance in underwater environments [6]. By analyzing visual data in real-time, UUVs can recognize objects, track their movements, and adjust their course accordingly, ensuring efficient and safe operation. Additionally, real-time processing enhances mission efficiency by enabling prompt responses to changing conditions and optimizing task execution. This capability not only enhances the autonomy and reliability of UUVs but also contributes to their overall safety and effectiveness in diverse underwater applications [7].

An approach for swiftly computing Krawtchouk moments in grayscale images, alongside rapid calculation techniques for binary images is presented in [8]. By decomposing 8-bit/pixel grayscale input images into corresponding bitplanes represented by image blocks, lower-order bitplanes exhibit a resemblance to a half-intensity image. Consequently, only the moments of higher-order bitplanes are computed, with the least significant bitplanes replaced by half-intensity images to significantly accelerate moment computation while maintaining an acceptable error margin between original and reconstructed images. Experimental findings confirm the effectiveness of substituting the lower 5 bitplanes with half-intensity images, resulting in minimal error in reconstructed images and notable acceleration in moment computation. Additionally, it demonstrates rapid performance, achieving real-time operation under typical conditions in pattern recognition scenarios requiring a moderate number of moment calculations in small-sized images.

In [9], researchers introduce an algorithm for computing discrete image moments based on first-order moments, achieved through a simple mathematical deduction, enabling the utilization of a fast algorithm for their calculation. Unlike conventional methods relying on moment kernel polynomials' properties, this approach allows for the computation of any discrete image moments, offering advantages such as a straightforward computation structure, no need for multiplication operations, independence from image intensity distribution, and applicability to all discrete image moment families. Additionally, they present a discrete image moment computation structure based on a systolic array, leveraging its characteristics for implementation using very large-scale integration (VLSI) technology.

In [10], the Hu Moment concept serves as a detection algorithm implemented on an FPGA system through hardware description language. This algorithm effectively recognizes target shapes within test images. The implementation involves utilizing two finite state machines to compute Hu Moments and the NLM filter. The findings demonstrate that the hardware implementation significantly outperforms software in the computation of image moments, showcasing the efficiency of FPGA-based processing for such tasks.

In [11], the hardware implementation of a Shape Recognition Algorithm based on Invariant Moments is outlined, aiming for optimized execution speed and resource utilization. Manual optimization, combined with pragma commands, results in the most efficient version in the third implementation, fully utilizing available resources. The study underscores the importance of specific optimizations for improved performance, as High-Level Synthesis (HLS) and programmable logic alone do not guarantee efficiency. Results indicate significant time efficiency gains using HLS tools and certain optimization methods compared to software implementation, with manual optimization being particularly effective. However, a trade-off between performance and chip utilization in FPGA technology persists, as demonstrated by compromises between processing speed and the ability to handle multiple matrices simultaneously across different implementations.

In this article, we introduce two novel structures designed for real-time computation of two-dimensional moments up to the 14th order (q=0,1,2,...,7, p=0,1,2,...,7) for grayscale images. These structures utilize a systolic parallel array employing pipelining techniques and a compressor. Computation is performed in floating-point format and implemented using 45nm CMOS technology.

2. Image Moments

Image moments are mathematical descriptors used in image processing and computer vision to characterize various properties of an image, such as its shape, size, orientation, and intensity distribution. These moments provide valuable information for tasks such as object recognition, tracking, and analysis. The formula for computing image moments depends on the specific moment being calculated. However, the general formula for computing moments of an image function is given by Eq. 1:

$$M_{pq} = \sum_{x=1}^{m} \sum_{y=1}^{n} x^p y^q f(x,y) \qquad x \le m, y \le n \qquad (1)$$

where M_{pq} represents the (p,q)-th moment, and the integration is performed over the entire region R. This equation captures the essence of moment computation, wherein pixel intensities f(x,y) are multiplied by the spatial coordinates x^p and y^q, and then integrated over the region of interest.

Image moments find widespread utility across diverse domains, serving as essential mathematical descriptors used in image processing and computer vision [12]. They characterize various properties of an image, including its shape, size, orientation, and intensity distribution. These moments play a crucial role in numerous applications, such as object recognition, shape analysis, image registration, segmentation, and texture analysis. They facilitate tasks like object recognition and classification by extracting discriminative features capturing an object's centroid,

orientation, and size. Additionally, moments aid in shape analysis, enabling comparisons between shapes and facilitating tasks like template matching and shape similarity measurement. In image registration, moments are instrumental in aligning and matching images from different sources, while in segmentation, they contribute to partitioning images into meaningful regions based on their moment properties [13]. Furthermore, image moments play a crucial role in texture analysis, capturing statistical properties of image textures for tasks such as texture classification and discrimination [14]. Overall, image moments serve as foundational elements in image analysis and computer vision, empowering a broad spectrum of applications across various fields.

Low-order moments are utilized for extracting features and determining the center of gravity, position, and orientation of an object within an image [15]. On the other hand, higher-order moments capture additional intricate features of the image and are commonly employed in pattern recognition and image reproduction tasks. However, directly computing the moments according to Eq. 1 necessitates $m \times n \times (p+q+2)$ addition operations, where m and n denote the dimensions of the image. This poses significant challenges when dealing with a large number of calculation operations, including $m \times n$ multiplication operations, particularly in scenarios requiring real-time moment computation.

In [16], orthogonal moments are computed using recurrence relations for Legendre and discrete Chebyshev polynomials, aiming to achieve both speed and accuracy in computation. The study emphasizes minimizing errors in moments approximation to maintain their discriminative capability in classification tasks. Numerical experiments across six texture image databases reveal that moments computed via recursion formulas outperform those derived from closed-form representations. Additionally, moments extracted from the Gray-Level Co-occurrence Matrix (GLCM) demonstrate high classification accuracy, especially with a higher number of moments. The study also highlights the potential of weighted moments to enhance classification results. [17] presents a parallel algorithm effectively implemented to compute 2D and 3D Legendre moments for gray-level images and objects. This algorithm is assessed on multicore CPUs and GPUs, with experimental results closely aligning with theoretical-to-optimal speedup ratios for multicore CPUs and demonstrating significant acceleration for GPUs. Furthermore, [10] presents a hardware-based shape detection algorithm utilizing Hu's moments and a non-local means filter on an FPGA system. The paper outlines the algorithm's design stages, emphasizing speed and parallelism in signal processing, and showcases its effectiveness in recognizing target shapes within test images.

3. Systolic Array

The Systolic Array serves as a versatile solution for translating high-level computations into hardware structures. Its fundamental design involves processing data from memory in a sequential manner, with each cell performing computations before passing the data to the next cell in the array. Noteworthy advantages of the systolic system include its modularity, regular and streamlined data flow, rapid response time, and the ability to utilize uniform and simplistic cells [4].

According to Eq (1), the calculation of image moments involves repeated multiplication operations for each pixel of the image, followed by the summation of these calculated expressions. In real-time processing, it's essential to initiate the computation for each pixel as it emerges from the camera and continue until the arrival of the next pixel. Once the entire image has been captured, the processing concludes. If the camera output is in Raster Scan format, the expression $x^p y^q f(x, y)$ needs to be computed for individual pixels in the first row of the image. Subsequently, as each subsequent row is captured, the operation is repeated for that row. Given this process, employing a systolic array is well-suited for implementing the moment calculation algorithm, with numerous existing structures relying on this architecture [18],[19].

In this study, we utilize the systolic structure depicted in Figure 1. This structure comprises n+1 pipeline stages. The symbol "+" denotes the unit of calculation for the adder unit, while "P" signifies the unit for exponentiation and multiplication. The final adder combines the output of the preceding adder with the previously stored value. Each combination of "+" and "P" forms a moment processor element (MPE). Figure 2 illustrates the structure of MPE cell. The control unit receives data f(x, y) from the camera and transmits f(x, y) along with y and x values relevant to each cell. For brevity, the schematic of the control unit is omitted. In this configuration, all units operate simultaneously on the rising edge of the clock pulse. The x^p computing unit, also known as an exponentiation unit (EXP), is responsible for raising a given input value x to the power of P. This unit is essential in various computational tasks where exponentiation operations are required, such as in polynomial evaluations, signal processing, and numerical simulations. The unit typically consists of arithmetic and logic circuits designed to efficiently compute exponentiation operations with high accuracy and low latency.

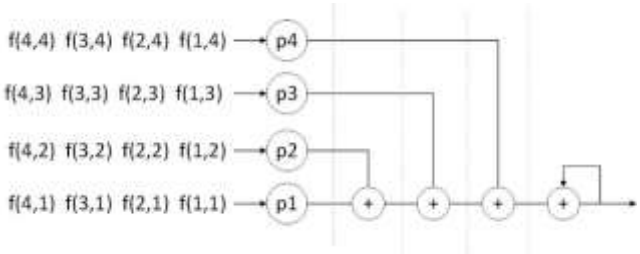


Figure 1. The systolic array structure for implementing the image moment calculation algorithm utilizes four processors.

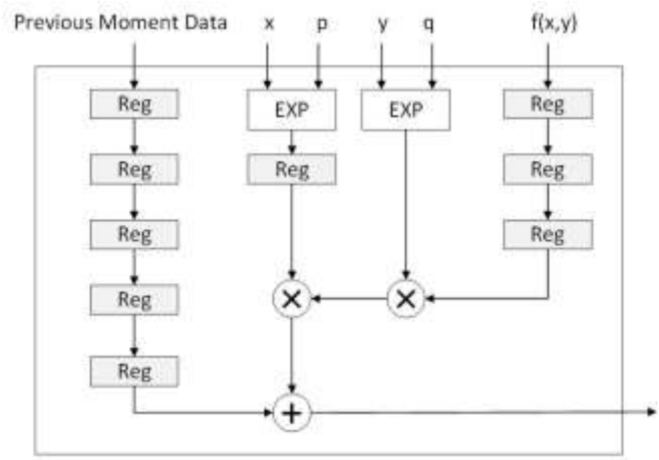


Figure 2. Moment processor element (MPE).

When multiple MPEs are connected sequentially, they form a systolic array of cells, each responsible for processing specific portions of the image data. In Figure 3, we observe a structural arrangement composed of four cells. In this setup, MPE1 initially processes pixels associated with the kth column of the image. Following this, MPE2, MPE3, and MPE4 consecutively handle calculations for the subsequent columns. Upon completing computations for these four columns, the result from MPE4 is fed back to MPE1, initiating a continuous processing cycle. Subsequently, pixels from the next set of four columns are directed to MPE1 through MPE4, thus repeating this sequence iteratively for all columns in the image. This feedback loop ensures seamless and efficient processing of the entire image dataset through the systolic array structure.

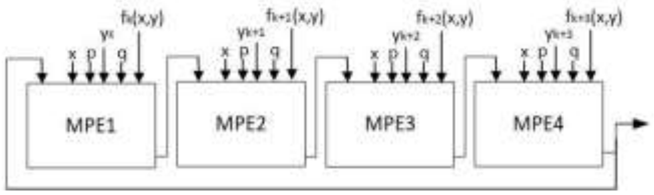


Figure 3. Structure of a Systolic Array Consisting of Four Cells for Image Moment Computation.

3.1 Computatonal units

Choosing the number format is crucial in designing the moment calculation structure, as it dictates the bit width of computing units and transmission lines. A 164-bit number is necessary to represent the maximum value of the 14th-order moment in binary format. However, employing binary numbers for moment calculation up to the 14th order would require 164-bit arithmetic units, increasing complexity, power consumption, and gate count. To mitigate this, floating-point number formats are utilized. In this research, the maximum moment order calculated is 5.8688×10^{48}. Using 8 bits for the exponent and 10 bits for the mantissa ensures sufficient range and precision. The decimal equivalent of the maximum number represented by this number of bits is equal to 1.16×10^{77}, which exceeds the maximum value of M77.

Since the calculation of moments involves only positive numbers, the sign bit is omitted. Furthermore, to enhance accuracy, the normalized mode of floating-point numbers is utilized. The maximum relative rounding error in calculating moments up to the 14th order using this format is 3.27%, which is acceptable for practical applications.

3.1.1 Adder

In this design, a Carry Select Adder (CSA) is constructed using a combination of multiplexers (muxes) and full adders (FAs). The CSA architecture facilitates efficient addition of two multi-bit binary numbers by distributing the carry bits across multiple stages, reducing the critical path delay and enhancing performance [20]. The design commences with the computation of the least significant bit (LSB) sum (Sum[0]) and carry-out (C-out) using a single full adder. Subsequently, the next bit of the sum (Sum[1]) is computed alongside the carry-in (C-in) from the previous stage, once again employing a single full adder. To compute the next two bits of the sum (Sum[3:2]), a pair of serial full adders are utilized in conjunction with a 4:2 multiplexer, allowing for efficient carry propagation and selection. Similarly, the subsequent three bits of the sum (Sum[6:4]) are computed using a combination of 6:3 multiplexers and three serial full adders.

This architecture enables parallel computation of multiple bits of the sum while efficiently managing carry propagation. By distributing the addition process across multiple stages and utilizing serial adders where necessary, the design achieves reduced critical path delay and optimal performance. Additionally, to efficiently add two 18-bit floating-point numbers, the process involves comparing the numbers and adjusting the smaller number's mantissa based on the difference in their exponents. This addition operation requires a 10-bit adder, such as the ten-bit Carry Select Adder (CSA) utilized in this study. Ensuring optimal performance entails balancing the input paths to the CSA to maintain uniform delay across all layers. The design of a high-speed and low-power ten-bit CSA adder, crucial for achieving fast and energy-efficient computation, is illustrated in Figure 4. The CSA offers several advantages, including high-speed addition, low power consumption, compact hardware utilization, scalability to larger bit widths, and minimized critical path delay, making it a preferred choice for arithmetic units in various computing systems.

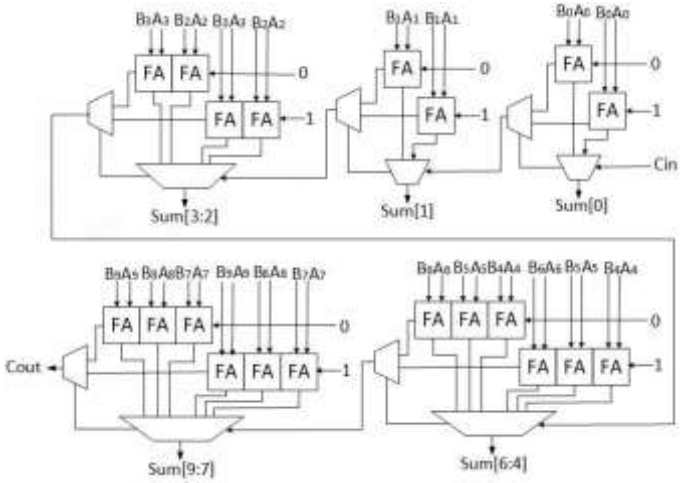


Figure 4. Ten bit CSA.

3.1.2 Multiplier

In this study, the 10*10 Dadda multiplier is employed as the multiplier unit, acknowledged for its superior speed compared to similar types. Leveraging a modified Booth encoding technique, the Dadda multiplier facilitates efficient and rapid multiplication operations by reducing the number of partial products, thereby enhancing computational performance. Operating in stages, each stage of the Dadda multiplier comprises a specific number of rows of partial products. The height of each stage is determined by working backward from the final stage, typically consisting of two rows of partial products. The design incorporates a strategy to reduce the number of partial products, utilizing two layers of full adders. Each full adder input carries a Cin, representing the Cout of the previous full adder. By utilizing several full adders, a logical circuit is created to add multiple-bit numbers, with each carry bit "rippling" to the next full adder. This architecture necessitates employing the Ripple Carry Adder (RCA) procedure. Data is transmitted to adders, with the carry of each stage added to the next two data inputs in the same stage. Ultimately, the ripple carry adder process is executed at the final stage, yielding product terms p1 to p8, as illustrated in Figure 5.

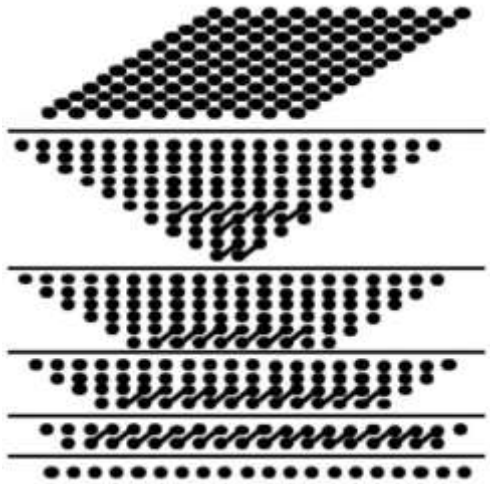


Figure 5. Dot diagram illustrating the 10×10 Dadda multiplication process.

3.1.3 Exponentiation Unit

To compute the powers of x^p and y^q, p and q clock cycles are required, respectively. However, as the order of moments increases, the processing time becomes extended. Figure 6 illustrates a more efficient structure for this operation. The proposed design comprises three pipeline stages, allowing the computation of the power of a number within three clock cycles. Notably, this time remains constant regardless of the value of p. This scheme supports calculations up to x^7. Based on the power value, the multiplexer selects and outputs the desired value.

The use of floating-point units for processing numbers leads to higher power consumption compared to binary number formats. Complex adder and multiplier units are required for binary formats, such as the 164-bit CSA which demands multiple layers of adders. In contrast, the hardware complexity of comparators and 10-bit shifters is significantly lower. Designing Dadda multipliers presents even greater complexity than CSA architectures.

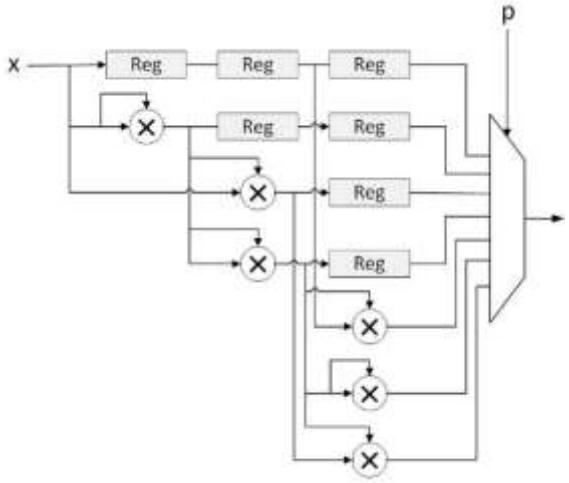


Figure 6. Pipeine exponentiation unit computing x^p.

4. Simulation Results

The physical attributes of the moment computation structure were analyzed by synthesizing them with the Nangate 45nm open cell library using the Synopsys Design Compiler. Power consumption was estimated using the Synopsys power analysis tool, based on a VCD file generated from post-synthesis simulations with 100,000 random inputs. All comparisons were conducted post-synthesis for all designs at the block level, following the practices of ASIC designers who thoroughly assess building blocks for potential integration into future chips.

Table 1 compares different architectures, including the proposed approach, based on speed, power consumption, and area. The proposed approach exhibits significantly higher speeds in gigabits per second (618.243 Gbit/s) and frames per second (954.012 frames/s) compared to existing architectures, marking an improvement of approximately 571% and 1024%, respectively. Additionally, it demonstrates substantially lower power consumption (3.254 mW), showcasing a reduction of around 98.7% compared to other methods. However, it occupies a slightly larger area (0.734 mm²) than some of the other structures, representing a minor increase.

Table 1. Comparative analysis of performance metrics for various structures.

Architecture	[21]	[22]	[16]	Proposed
Max Moment Order	16	10	18	14
Transistor count	43894	143253	639804	543251
Speed (Gbit/s)	86.481	32.215	92.285	618.243
Speed (frame/s)	45.277	25.568	84.237	954.012
Power (mw)	254.863	185.657	19.586	3.254
Area (mm^2)	0.218	0.521	0.657	0.734

The combined utilization of systolic array, parallelization process, pipeline, and the implementation of fast multiplier and adder units in the proposed method has significantly enhanced its efficiency compared to other methods. By optimizing the performance of each block within the structure, such as employing the "Dada Multiplier", CSA adder, and a specially designed power supply unit, the operational speed of the entire system has been notably increased. This enhancement underscores the effectiveness of the proposed methodology in achieving superior performance metrics across various parameters.

Based on Figure 7, the proposed structure exhibits a notable decrease in delay, ranging from approximately 47% to 84% compared to [21], [22], and [16], indicating significantly improved efficiency across various moment orders.

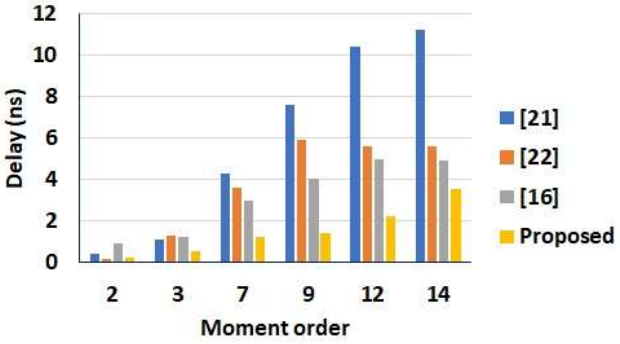


Figure 7. Comparison of delay for various moment orders in different structures.

5. Conclusion

In this article, we introduced a novel structure utilizing systolic arrays and pipelines for the computation of high-order two-dimensional moments in grayscale images. Our proposed structure demonstrates remarkable efficiency, with each cell capable of computing the 14th order moment of a 1024×1024 image at an impressive rate of 954 frames per second (fps). Notably, our design achieves low power consumption, registering at only 3.254 mW. Leveraging these promising outcomes, future enhancements could focus on augmenting computational speeds by scaling up the number of computing cells, thereby further optimizing performance.

7. References

[1] Yuh, J. Design and control of autonomous underwater robots: A survey. *Autonomous Robots, 8*, 7-24. (2000)

[2] Terracciano, D. S., Bazzarello, L., Caiti, A., Costanzi, R., & Manzari, V. Marine robots for underwater surveillance. *Current Robotics Reports, 1*, 159-167. (2020)

[3] Liu, J., Gao, J., An, X., & Yan, W. (2019). *Autonomous Landing of an Unmanned Underwater Vehicle using Hybrid Visual Servoing Control with Image Moments and Quaternions.* Paper presented at the OCEANS 2019-Marseille.

[4] Eustice, R. M., Pizarro, O., & Singh, H. Visually augmented navigation for autonomous underwater vehicles. *IEEE Journal of oceanic Engineering, 33*(2), 103-122. (2008)

[5] Forouher, D., Hartmann, J., Klüssendorff, J. H., et al. (2012). *HANSE—A Low-Cost Autonomous Underwater Vehicle.* Paper presented at the Autonomous Mobile Systems 2012: 22. Fachgespräch Stuttgart, 26. bis 28. September 2012.

[6] Humais, M. A. Tools for Detection Tracking and Autonomous Operations by Unmanned Aerial Vehicles. (2020)

[7] Eren, F. (2015). *Pose detection and control of unmanned underwater vehicles (UUVs) utilizing an optical detector array.* University of New Hampshire.

[8] Karampasis, N. D., Spiliotis, I. M., & Boutalis, Y. S. Real-time Computation of Krawtchouk Moments on Gray Images Using Block Representation. *SN Computer Science, 2*, 1-15. (2021)

[9] Hua, X., Hong, H., Liu, J., & Shi, Y. A novel unified method for the fast computation of discrete image moments on grayscale images. *Journal of Real-Time Image Processing, 17*, 1239-1253. (2020)

[10] Raffaitin, C., Romero, J.-S., Romero, J.-S., & Procel, L.-M. (2019). *Hardware implementation of a shape recognition algorithm based on invariant moments.* Paper presented at the Proceedings of the 32nd Symposium on Integrated Circuits and Systems Design.

[11] Stančić, S. M., Popović-Božović, J. S., & Ponjavić, M. M. (2017). *Hls efficiency in the case of image moments algorithm*

implementation. Paper presented at the 2017 25th Telecommunication Forum (TELFOR).

[12] Hjouji, A., El-Mekkaoui, J., Jourhmane, M., & Bouikhalene, B. New set of non-separable orthogonal invariant moments for image recognition. *Journal of Mathematical Imaging and Vision, 62*, 606-624. (2020)

[13] Manjunath, K., Prabhu, G., & Siddalingaswamy, P. A quantitative validation of segmented colon in virtual colonoscopy using image moments. *Biomedical Journal, 43*(1), 74-82. (2020)

[14] Majumdar, I., Chatterji, B., & Kar, A. (2020). *A moment based feature extraction for texture image retrieval.* Paper presented at the Information, Photonics and Communication: Proceedings of Second National Conference, IPC 2019.

[15] Shao, X., Liu, N., Wang, Z., Zhang, W., & Yang, W. Neuroadaptive integral robust control of visual quadrotor for tracking a moving object. *Mechanical Systems and Signal Processing, 136*, 106513. (2020)

[16] Di Ruberto, C., Putzu, L., & Rodriguez, G. Fast and accurate computation of orthogonal moments for texture analysis. *Pattern Recognition, 83*, 498-510. (2018)

[17] Salah, A., Hosny, K. M., & Abdeltif, A. M. (2023). A Generic Multicore CPU Parallel Implementation for Fractional Order Digital Image Moments *Recent Advances in Computer Vision Applications Using Parallel Processing* (pp. 1-12): Springer.

[18] Wang, B., Ma, S., Zhu, G., Yi, X., & Xu, R. A novel systolic array processor with dynamic dataflows. *Integration, 85*, 42-47. (2022)

[19] Zhang, J., & Pan, C. (2020). *New algorithm and its systolic implementation for digital correlation by using first-order moment.* Paper presented at the MIPPR 2019: Parallel Processing of Images and Optimization Techniques; and Medical Imaging.

[20] Monajati, M. Underwater Image Enhancement Using FPGA-Based Gaussian Filters with Approximation Techniques. *International Journal Of Coastal, Offshore And Environmental Engineering (ijcoe), 8*(4), 49-58. (2023)

[21] Roma, N., & Sousa, L. (2000). *In the development and evaluation of specialized processors for computing high-order 2-D image moments in real-time.* Paper presented at the Proceedings Fifth IEEE International Workshop on Computer Architectures for Machine Perception.

[22] Iwashita, A., Komuro, T., & Ishikawa, M. An image-moment sensor with variable-length pipeline structure. *IEICE transactions on electronics, 90*(10), 1876-1883. (2007)

INTERNATIONAL JOURNAL OF
COASTAL, OFFSHORE & ENVIRONMENTAL ENGINEERING

IJCOE Vol.1/ Special Issue No.1/
Marine Instrumentation/ 2023 (34-45)

Available online at: www. Ijcoe.org

Design and Application of Multifunctional Robots for Deep-Sea Exploration and Rescue Operations

Mehrnaz Monajati[1], Morteza Shirmohammadi[2]

[1]*Faculty of Electrical and Computer Engineering, Graduate University of Advanced Technology, Kerman, Iran,* m.monajati@kgut.ac.ir
[2]*Department of Civil Engineering – Structure, Islamic Azad University of West Tehran Branch, Tehran, Iran,* nventorcentury21@gmail.com

ARTICLE INFO

Article History:
Received: 24 Mar 2023
Accepted :25 Jul 2023

Keywords:
Robotic Structure
Mechanical Design
Exploration Robots
Deep Seas and Wells
Multiple Operations

ABSTRACT

Despite ongoing advancements in science and technology, human casualties persist in deep-sea and subterranean environments due to hazardous conditions, limited accessibility, and insufficient safety measures. These risks are exacerbated by the lack of effective innovations in project execution and emergency response. The extreme depths of oceans and drilled wells often render direct human intervention impractical, especially for rescue, inspection, and maintenance tasks. This research presents the design and evaluation of a multifunctional robotic system capable of operating in high-risk environments where human access is restricted or unsafe. The robot is engineered to perform a wide range of tasks, including exploration beneath ocean ice, seabed data collection, geological and geotechnical analysis, rescue operations, sampling in toxic zones, and interventions in corrosive or contaminated conditions. Experimental results from three pilot projects—spanning water and wastewater systems, oil and gas wells, and underwater environments—demonstrated robot success rates ranging from 80% to 90%. The robot completed welding, cutting, and sampling operations within 1.5 to 2 hours, outperforming traditional methods in terms of safety, speed, and operational efficiency. These findings confirm the robot's reliability in environments characterized by high pressure, toxic exposure, and limited human accessibility. By replacing manual intervention with autonomous systems, this research highlights the transformative potential of robotics in bridging the gap between scientific theory and industrial practice. The proposed design contributes to safer, more efficient workflows and lays the foundation for future innovations in extreme-environment robotics.

1. Introduction

Deep wells—including water, gas, and abandoned wells—pose significant operational and safety challenges due to their extreme depths, limited accessibility and the presence of hazardous gases. These conditions often render conventional maintenance and equipment replacement impractical, as , as human access to the bottom of such wells is frequently impossible. In response to these constraints, researchers and engineers worldwide have proposed innovative solutions tailored to regional needs.

One promising approach involves the development and deployment of exploration robots designed for subsurface and rescue operations. These robotic systems are engineered to perform tasks traditionally carried out by human specialists, enabling remote intervention without exposing workers to life-threatening environments [4].

Parallel to terrestrial applications, the exploration of deep-sea environments presents similarly formidable challenges. Over 90% of marine biodiversity remains undiscovered and unclassified, and the deployment of sufficient oceanic sensors to monitor global phenomena with adequate temporal and spatial resolution remains a daunting task [10]. While underwater robotics has significantly advanced marine research, the vastness of the ocean and the limitations of individual robotic units constrain operational

efficiency. These robots, however, are uniquely capable of withstanding the extreme pressures of deep-sea environments, making them indispensable for tasks such as exploration, sampling, reconnaissance, and target search [11].

Recent studies have outlined a forward-looking trajectory for deep-sea robotics, emphasizing the potential integration of space-derived technologies across three key domains: biomimetic structural and energy systems, artificial intelligence (AI), and the miniaturization of life-detection sensors[12]. These interdisciplinary approaches aim to enhance the operational capabilities of underwater robots in extreme environments. In parallel, the rapid advancement of AI has prompted growing interest in its application to social robotics, particularly in contexts where human caregiving is insufficient [32]. However, scholars have also noted the inherent unpredictability of technological evolution, which often challenges the accuracy of long-term projections and invites critical reflection on the development paths of emerging innovations [33].

2. Problem Definition

Robotic systems have become essential tools for remote exploration and intervention in hazardous environments, particularly in deep-sea and subterranean settings. The robot discussed in this study is designed for a wide range of applications, including laboratory applications, , including laboratory research, welding and cutting operations on submerged objects, geological surveying, fault detection, and soil classification through sampling, photography, and videography. It is also capable of operating in high-risk wells—such as those lacking oxygen or containing explosive, toxic, or flammable gases—where human access is unsafe or impractical. Additional use cases include the retrieval of trapped humans or animals from collapsed wells and underwater locations, and the remote repairs of underground and submarine equipment [1].

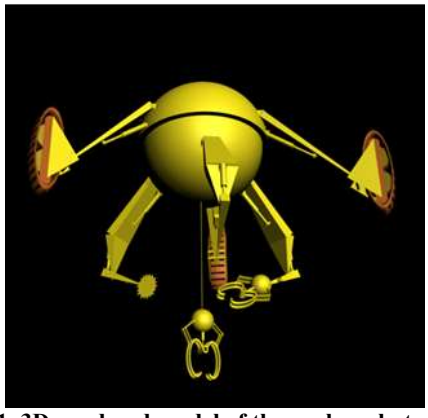


Figure. 1. 3D-rendered model of the probe robot, designed using 3ds Max software, showcasing its articulated arms and mechanical structure for deep-environment operations.

In deep sea and underground environments, equipment such as pipes structural components are often subject to damage from corrosion, erosion, cracking, and mechanical stress caused by tectonic activity or the cumulative weight of installed systems. These failures can lead to costly delays, safety hazards, and operational inefficiencies. Timely and reliable repair or replacement of such components is critical to minimizing project costs and protecting human lives [1].

The digital revolution has accelerated the development and deployment of robotic technologies, making them integral to both economic and scientific advancement. Robots now play a pivotal role in remote operations across domains such as space exploration, marine research, and industrial automation [25].



Figure 2. Deep-sea mobile robot equipped for exploration and maintenance tasks [25]

This particular robotic system is also designed for aquatic rescue missions, capable of retrieving both conscious and unconscious individuals without endangering the rescuer. Statistical data on water-related accident indicate that many fatalities occur during rescue attempts by untrained individuals. Consequently, recent research has emphasized the development of marine robotic systems to perform tasks that exceed human physical limits or pose significant safety risks [13].

Operationally, the robot is that the user or guide first places the robot at the top of the well (for operations inside the wells) or on platforms and marine vessels (for operations in deep waters), then using a “remote control device, guides it to the bottom of the well and the accident site or the ocean floor and performs the desired operation in the relevant project” [1, 9].

Operationally, the robot is deployed either at the mouth of a well or from marine platforms and vessels. It is then guided via remote control to the target site—whether within a well or on the ocean floor—where it performs the designated task in accordance with the project’s objectives [1], [9].



Figure 3. View of the probe robot model, featuring articulated arms and mechanical components for deep-environment operations.

3. Significance of Robotic Systems

The integration of advanced tools and robotic systems is increasingly vital across a range of industries, including civil engineering, water and wastewater management, marine operations, military applications, petrochemical processing, oil and gas extraction, nuclear facilities, and aerospace engineering. In these domains, replacing human intervention with robotic systems—particularly in research, laboratory work, welding, cutting, and rescue operations—offers significant advantages in terms of safety, efficiency, and precision. This is especially critical in high-risk environments such as deep-sea and well-based operations, where human access is limited or hazardous [5, 9].

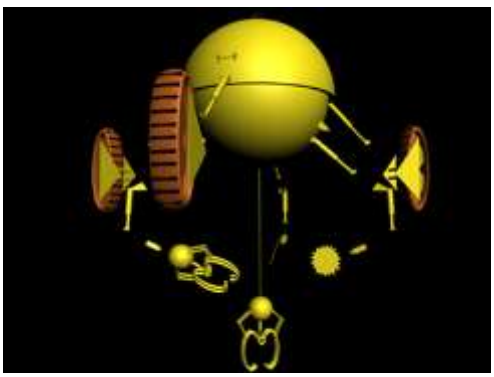


Figure 4. 3D MAX-rendered view of the probe robot, highlighting its symmetrical structure and mechanical components for advanced operational tasks.

4. Classification of Robots by Autonomy

Robotic autonomy determined by the system's ability to operate independently, which depends on the integration of sensors, computational hardware, and control algorithms. Based on their operational capabilities, robots can be classified into three categories:

- Non-autonomous: Fully dependent on human control.
- Semi-autonomous: Capable of performing certain tasks independently but still require human oversight.
- Fully autonomous: Operate independently across a range of tasks without human intervention [7].

The level of autonomy directly influences the complexity of the system design and the scope of its applications.

5. Robot Navigation and Movement Strategies

Path planning in unknown environments presents significant engineering challenges. methods of spatial exploration are often inefficient or impractical in dynamic marine settings. To address this, hybrid search algorithms have been proposed to enable efficient and adaptive pathfinding for underwater robots engaged in target search missions [26].

Underwater robots are increasingly deployed to perform complex tasks in environments that are inaccessible or dangerous for humans. . These include scientific exploration, industrial operations, and military missions. The robot's propulsion system plays a critical role in determining its maneuverability, endurance, and stealth concealment [27].

Structurally, underwater vehicles are categorized as:

- Remotely operated vehicles (ROVs : Tethered systems controlled from the surface.
- Autonomous underwater vehicles (AUVs): Untethered systems capable of independent operation [39, 40].

Functionally, they are further divided into: :

- Investigation robots: Used for observation, measurement, and sample collection.
- Operation robots: Designed for tasks such as underwater welding, pipe manipulation, construction, and underwater cutting, etc.) [39, 41].

Exploration of the Arctic seafloor remains remains a major challenge due to persistent ice cover, which limits the effectiveness of of oceanographic tools [14].

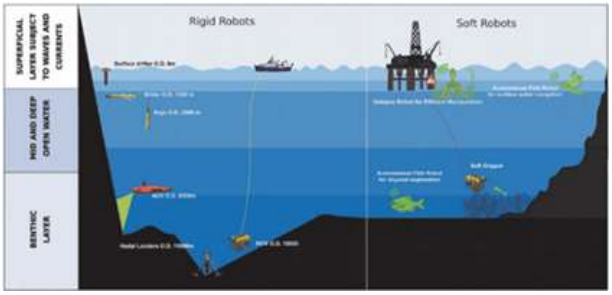


Figure 5. Overview of marine depth zones and the operational range of rigid and soft robots across ocean layers, from surface to hadal depths [14]

Only a few robot ic systems worldwide are capable of reaching depths of 6,000 meters, typically for seabed mapping and industrial surveys. These systems must follow predefined paths and be continuously

monitored, which restricts their flexibility and coverage [14, 31].

The Underwater Vehicle-Manipulator System (UVMS) has seen growing adoption for marine resource exploration. However, underwater environments pose substantial challenges for controll, navigating, and communication. These difficulties have driven ongoing technological innovation and made UVMS development a focal point of marine robotics research [20]. Recent advances in autonomy, sensor integration and robotic design have enabled deep-sea exploration capabilities that may one day be extended to extraterrestrial oceans, such as those on icy moons [12].

6. Robotic Welding and Cutting Applications

Welding robots are particularly, promising for use in steel structure construction. Manual methods methods face limitations in precision, efficiency, and safety, making the development of automated welding systems increasingly urgent. Robotic welding offers high-speed, consistent performance, contributing to industrial modernization[15-18].

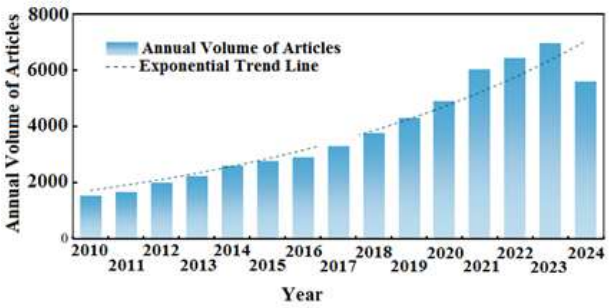


Figure 6. Annual publication volume of research articles on welding robots from 2010 to 2024, showing an overall exponential growth trend [19].

Moreover, traditional welding process often result in high energy consumption and the release of harmful emissions, including fumes and toxic gases. Robotic systems can mitigate these issues by precisely controlling welding parameters, optimizing paths, and employing advanced techniques. This not only improves environmental sustainability but also enhances worker safety [19].

7. Environmental and Structural Considerations

Deep-sea robots are typically enclosed in pressure-resistant structures, including metallic housings and pressure-compensation systems, to protect sensitive electronics and mechanical components from extreme underwater pressures [35]–[38].

Simultaneously, marine pollution poses a growing threat. An estimated 70% of marine litter sinks to the seabed, with p lastics compose over 60% of this debris. These materials degrade slowly and can enter the global carbon cycle, ultimately impacting human health. Effective investigation and retrieval of this litter are essential to prevent irreversible environmental damage [42, 43].

To address this, underwater robots are increasingly being used for large-scale, upward transport tasks such as sampling marine organisms and collecting submerged waste. These labor-intensive operations benefit significantly from robotic assistance, which can reduce human exposure and improve operational efficiency [42, 44].

8. Design Requirements

To ensure safe and effective operation in aquatic and subterranean environments, the robot must meet several critical design criteria:

- Waterproofing and Environmental Safety: All electrical components are housed within a sealed body, minimizing the number of moving parts to reduce potential points of water ingress. Mechanical joints between the body and moving components must be engineered to prevent leakage. Additionally, any materials in direct contact with water must be non-polluting and environmentally safe [8].



Figure 7. 3D MAX-rendered model of the probe robot, featuring symmetrical arms and mechanical joints for precision tasks in hazardous environments.

- Functional Versatility: The robot is designed to perform a wide range of tasks, including soil layer analysis, mechanical sampling data transmission from deep wells or underwater locations, and the welding or cutting of damaged metallic components. It also supports the transport of objects from the ocean floor to the surface. These capabilities require integration of diverse technologies and performance mechanisms to support field workers and advance project objectives. [1, 9].

9. Research on Deep-Well Robotics

Deep wells are generally categorized into two types based on their internal structure:

Wells with rods or pipes: These typically contain structural elements for water supply, oil and gas extraction, or sewage transfer.

Wells without rods or pipes: These are more common in industries such as oil and gas, petrochemicals, and wastewater management. With diameters typically

ranging from 40 or 50 cm, such wells lack internal infrastructure, making manual intervention impractical or unsafe. Robotic systems offer a viable solution for inspection, maintenance, and operational tasks in these environments [1], [3], [9].

The concept of telepresence—the remote operation of devices as extensions of human capability—was first introduced in 1942 through science fiction literature. The story depicted an engineer controlling robotic tools remotely, a vision that has since influenced technological innovation and public imagination regarding human-machine interaction [22, 23].

One notable advancement inspired by this vision is the All-Round Six-Limbed Robotic Extraterrestrial Exploration (ATHLETE) platform, developed for planetary exploration. ATHLETE features six limbs with seven degrees of freedom, enabling both locomotion over rugged terrain and manipulation of tools. Each wheel contains an interface for instruments such as drills, clamps, and anchors, allowing the robot to interact dynamically with its environment [28]–[30].

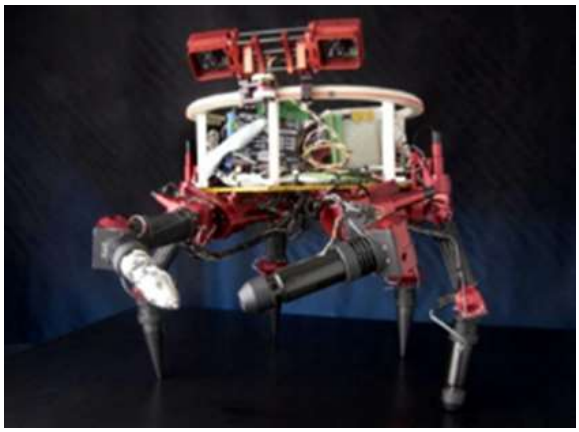


Figure 8. The Lemur robot, designed for space assembly, utilizes wrist-mounted tools to perform tasks such as drilling, bolt manipulation, and visual documentation [28]

10. Robot Mechanisms and Capabilities

Robotic systems designed for deep wells and underwater environments must possess a wide range of capabilities to perform complex and hazardous tasks. These include:

- Research and exploration: direct inspection of well interiors and seabed equipmentfor scientific and operational analysis.
- Maintenance and Repair: cutting and welding of damaged components located at the bottom of wells or the ocean floor, including inaccessible or angular positions.
- Object Retrieval: Extraction and transport of submerged objects to the surface, even from confined or irregular spaces.
- Infrastructure operations: Servicing of underground water and sewage pipelines, seabed conduits, and ocean-floor fiber optic cables.
- Hazardous Environment Deployment: Operation within oil and gas well containing flammable or toxins substances, as well as high-radiation zones such as heavy water ponds in nuclear power plants. In these contexts, robotic intervention is essential to minimize human exposure and risk [6], [9].

These robots are engineered to function `in environments where the electromagnetic spectrum technologies enable long-range imaging and high bandwidth communication. Despite the challenges posed by marine and extraterrestrial conditions, robotic systems have demonstrated cost- effective, high precision performance in these domains [45].

11. Marine Robotic Technologies

Recent analyses have identified key classes of robotic components used in marine sampling operations [46]:

- Manipulator claws:
  - Parallel fingers: Provide stable grip for flat or uniform objects.
  - Opposed/ intermeshed fingers: Offer enhanced dexterity for irregular shapes.
  - Grabber claw: Suitable for firm grasping of larger specimens.
  - Cage claw: Designed to enclose and secure delicate or mobile samples. details on each class are provided in Figure (9).

- Sampling gears:
  - Suction samplers: Ideal for collecting fine particles or small organisms.
  - Scoops and scoop-nets: Used for sediment and biological sampling.
  - Corers: Extract cylindrical samples from seabed layers.
  - Traps: Capture mobile marine organisms.
  - Water bottles: Collect water samples at specific depths.

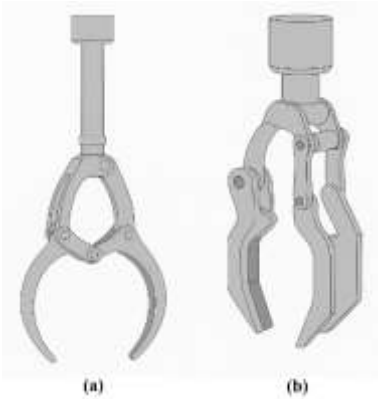


Figure 9. (a) Examples of parallel, intermeshed, and grab claw grippers, shown from left to right. (b) Cage-type gripper used in the ROV Liropus 2000 [46–48].

Details on each class of sampling gear are illustrated in Figure 10. Additionally, round-shaped manipulator fingers, typically configured with two jaws and three to

four fingers are specifically designed to gently enclose spherical or cylindrical specimens. This configuration is particularly effective for retrieving delicate samples or entire organisms without inflicting damage, making it well-suited for biological and ecological studies in sensitive marine environments [46].

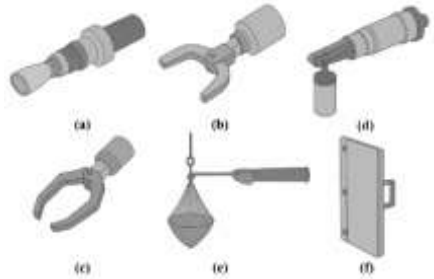


Figure 10. ROV collection tools used in marine sampling: (a) suction sampler, (b) scoop and net, (d) corer, (e) trap, and (f) Niskin bottle. Sources: (a–e) [46, 49, 50], Schmidt Ocean Institute; (f) [46, 21].

12. Research Hypotheses and Case Motivation

Deep oil wells similar subterranean structures are often inaccessible due to their extreme depth and narrow openings, rendering direct humans intervention impractical or impossible.. This limitation has prompted the development of robotic systems capable of performing complex operations remotely from the surface [1], [9].

The impetus for this research originated from a tragic incident in Iran involving an abandoned well.

Due to inadequate safety measures and poor oversight in sealing the well opening, a child fell into the narrow shaft. Rescue efforts were severely hindered by the confined dimensions of the well, highlighting the urgent need for a robotic solution capable of navigating and operating within such constrained environments.



Figure 11. Bottom view of the probe robot, modeled in 3ds Max, showing its mechanical limbs and structural layout for ground-level operations.

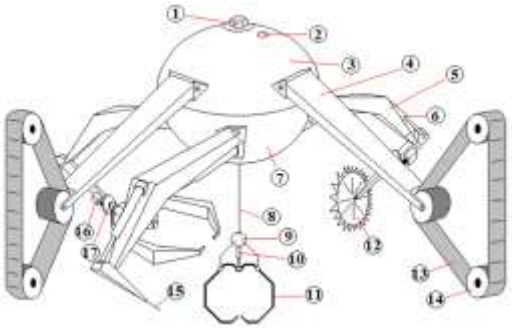
13. Materials and Methods

The initial design of this robot was completed in 2005 and officially registered in 2006 [2]. It was developed to perform complex operations in deep wells and underwater environments, including welding, cutting, sampling, and object retrieval. The system is remotely operated via radio control by a technician positioned above the well or offshore platform. Once deployed to the target site, the robot begins executing its assigned tasks [9].

Structurally, the robot consists of three large base units and three stainless steel arms, each equipped with pneumatic jacks and gears. The arms are capable of 360-degree rotation and are fitted with advanced tools for shearing, welding, lifting, and manipulating objects at various angles. The robot is designed to function in confined spaces and can retrieve heavy items from deep locations. It also includes CCTV cameras and a control interface for real-time monitoring and guidance.

The system incorporates 11 pneumatic jacks for vertical and rotational movement, 13 motorized reels powered by high- and low-power DC motors, and two half-spherical enclosures—one fixed and one rotatable—housing the robot's arms and lifting mechanisms. The motors are engineered to be waterproof, heat-resistant, corrosion-proof, and shock-resistant, ensuring durability in harsh environments. Additional features include imaging devices such as direct and indirect camcorders, a microscopic camera, and high-adhesion belts that allow the robot to grip various well surfaces, including metal, plastic, concrete, and stone.

The robot's mechanical and electrical components are distributed across upper and lower metal enclosures, connected by screws, nuts, and cable entry points. Figures 12 through 16 provide detailed schematics of the robot's design and layout.



Front view of the robot showing key structural and functional components, including the metal enclosures, pneumatic jacks, articulated arms, welding and cutting systems, and accessories for balance, mobility, and cable management. Components labeled 1–17 correspond to mechanical and electrical features integrated for deep-environment operations.

To model the robot's joint dynamics, Lagrangian mechanics is applied. The torque at each joint is calculated using:

$$\tau i = \frac{d}{dt}\left(\frac{\partial L}{\partial qi}\right) - \frac{\partial L}{\partial qi} \quad (1)$$

where L = K - P, with K representing kinetic energy and P potential energy. The variable q_i denotes the joint angle or displacement, and τ_i is the torque applied to joint i

.

For gripping operations, the total force exerted by the robot's gripper is modeled as:

$$F_{grip} = \sum_{i=1}^{n} Ti \,.\sin(\theta) \quad (3)$$

Here, $Ti$is the torque at joint i, θi is the angle of that joint to the main axis. This equation accounts for the effective torque components that contribute to linear gripping force at the fingertips.

A gripper consists of several mechanical fingers, each with several joints. Each joint generates a torques (e.g. by a motor or actuator). These torques, when transmitted through the joints to the fingertip, create a linear force. Depending on their angle, that grips the object. The above formula calculates the sum of all effective components of the torque in gripping the object. Since only the component of the torque that is in the direction of gripping the object is effective, it must be multiplied.

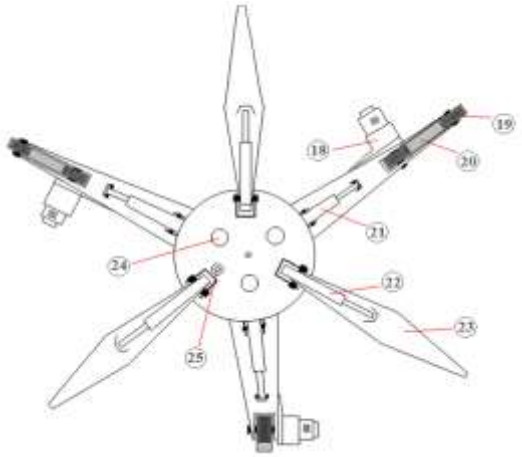


Figure 13. Bottom view of the robot showing key accessories, including wheel chain alternator, pneumatic jacks, rubber mobility components, lighting mounts, and CCTV installation point. Components 18–25 illustrate the mechanical and sensory systems supporting vertical movement and environmental monitoring.

The robot's vertical movement via chain drive is governed by:

$$\nu = \frac{r.\tau}{I+m.r2} \quad (4)$$

where ν is the velocity, r the radius of the chain wheel, τ the motor torque, I the moment of inertia, and m the total mass of the robot. This formula helps determine the optimal motor specifications and wheel-chain configurations for vertical mobility.

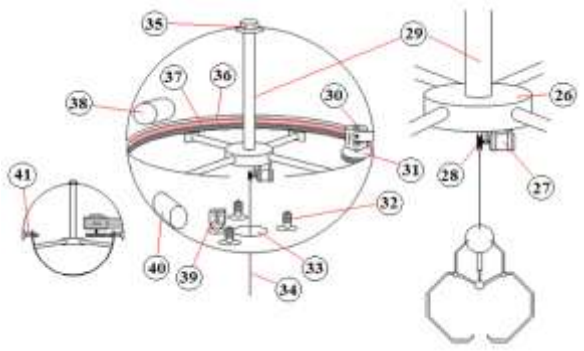


Figure 14. Internal view of the robot showing mechanical and electrical components, including alternators, pneumatic jacks, wiring systems, support structures, and integrated CCTV for operational monitoring. Accessories labeled 26–41 illustrate the robot's internal architecture and functional layout.

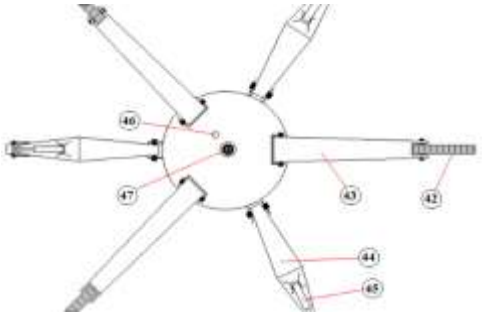


Figure 15. Upper view of the robot showing structural and functional components, including rubber bands, arm bases, pneumatic jacks, wire entry points, and fastening elements connecting the upper and lower enclosures.

For cutting operations, the required torque is calculated using:

$$\tau_{cut} = F_{cut}.\, r_{blade} \quad (5)$$

This equation relates the cutting force (F_{cut}) to the blade radius (r_{blade}), allowing engineers to select motors capable of delivering sufficient torque for material penetration.



Figure 16. Perspective view of the robot featuring cable-free mechanical grippers, designed for precision handling and autonomous operation in constrained environments.

The robot's dual-chamber design enhances its operational flexibility. The upper chamber remains fixed, while the lower chamber rotates freely, enabling full-range manipulation of tools and equipment. Arms mounted on the lower chamber are equipped with multifunctional tools for metal removal, welding (oxygen/gas), and milling. Finite element analysis confirms that flexible joints outperform rigid ones in underwater conditions, offering greater range of motion and improved maneuverability. The control module, equipped with advanced sensors and a CPU, manages the dynamic behavior of these joints, ensuring precise and responsive operation [34].

14. Applications of the Robot

The robot is engineered to perform a wide range of operations in extreme and hazardous environments, making it suitable for deployment across various industrial and scientific domains. One of its core capabilities is executing welding and cutting tasks in deep wells and corrosive settings, including environments contaminated with toxic chemicals, microbial agents, or explosive gases. This includes applications in water and wastewater systems, oil and gas extraction, petrochemical facilities, and marine infrastructure [9].

Its mechanical design enables precise manipulation and movement of objects in all directions and orientations, even within confined or irregular spaces. This flexibility supports geological exploration, soil mechanics research, and the classification of subsurface layers through sampling, surveying, and marking [9].

The robot is equipped with CCTV cameras capable of capturing high-resolution images and video in environments containing suffocating gases, acidic compounds, and other hazardous substances. This visual capability is essential for inspection, documentation, and remote decision-making in inaccessible or life-threatening conditions [9].

In rescue scenarios, the robot can identify and retrieve injured individuals from deep wells or submerged locations, minimizing human exposure to danger. Its operational range is robust across temperature extremes, functioning reliably in gaseous environments from –30°C to +30°C, and in liquid environments from –15°C to +45°C [9].

The system is also adaptable for use in vacuum or gas-free environments, making it suitable for space research and extraterrestrial exploration. Its modular architecture allows for self-repair and reconfiguration, enabling the robot to restore damaged components and rearm itself autonomously [9].

Constructed from lightweight and durable materials—including compact aluminum, stainless steel with zinc coatings, and corrosion-resistant nano-polymers—the robot maintains structural integrity under mechanical stress and chemical exposure. Its design includes a rotatable semicircular chamber and a base platform capable of 360-degree horizontal rotation deep underground. The arms themselves are engineered to rotate freely in all directions, allowing full spatial coverage during operations [9].

Additionally, the robot demonstrates a high degree of waterproofing and resistance to corrosion in acidic environments, with optimal performance in pH ranges between 5 and 7. This ensures long-term reliability in chemically aggressive settings and supports sustained deployment in industrial and research applications [9].

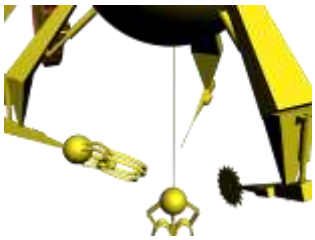


Figure 17. Front view of the robot rendered in 3ds Max, highlighting its mechanical accessories and structural layout for operational deployment.



Figure 18. Front view of the robot rendered in 3ds Max, illustrating its structural components and integrated accessories for advanced operational functionality.

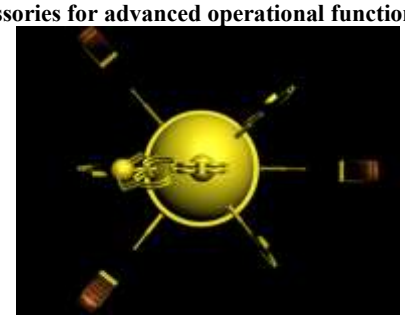


Figure 19. Upper view of the robot rendered in 3ds Max, showcasing its structural components and accessory layout designed for advanced mechanical operations.

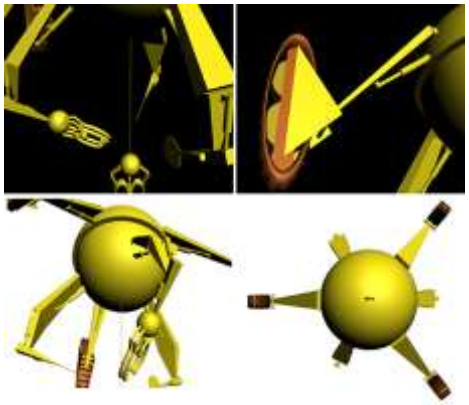


Figure 20. Demonstration of the probe robot's welding and cutting operations across all angles, rendered in 3ds Max to showcase its full-range articulation and multifunctional tool deployment.

15. Results and Discussion

The performance of the proposed robotic system was evaluated across three distinct project domains: water and wastewater, oil and gas operations, exploring deep underground and seabed exploration. Tables 1 and 2 summarize the results of these tests, highlighting operational efficiency, execution time , and comparative advantages over traditional human-led methods. [9].

Table 1 presents the success rates and contextual challenges associated with each test scenario. In experimental and workshop settings, the robot achieved an 80% success rate, demonstrating its ability to operate in deep, inaccessible locations. In geological sampling missions conducted on the seafloor, the robot reached a 90% success rate, significantly mitigating the risks typically faced by human divers, such as exposure to toxic substances and physical hazards. In high-pressure fluid environments, the robot maintained an 85% success rate, outperforming human capabilities in conditions prone to marine animal interference and physiological stress [9].

Table 2 outlines the operational merits of using the robot in real-world scenarios. In a 25-meter-deep water well in Tehran, the robot completed welding and cutting tasks in 1.5 hours, eliminating the need for manual labor and reducing capital expenditure. In a dry well of similar depth, the robot conducted soil mechanics and geological investigations over a two-hour period, avoiding reliance on outdated tools and minimizing operational losses. In a corrosive and toxic underwater environment, the robot performed welding and cutting tasks within 1.5 hours, removing the necessity for divers and specialized equipment [9].

Table 1. Report No. (A): Robot Efficiency and Human Limitations

Row	Project success rate	Type of Test	Disadvantages Without Robots
1	% 80	Experimental and Workshop	Inaccessibility of deep, impassable areas
2	% 90	Seafloor geological sampling	High-risk environments in wells and seas
3	% 85	High-pressure, viscous fluid operations	Marine animal threats, , physical strain, vital sign compromise

Table 2. Report No. (B): Operational Merits of Robots

Row	Merits of Robotic Operation	Duration	Location	Type of the Operation
1	No labor or large capital needed	1.5 hrs	25m deep water well (Tehran)	Welding and cutting
2	Avoids outdated tools and losses	2 hrs	25m deep dry well (Tehran)	Soil samplings and geological analysis
3	No need for divers or underwater gear	1.5 hrs	6m deep pool (Tehran)	Welding and cutting in corrosive/toxic conditions

These results collectively demonstrate the robot's versatility, reliability, and efficiency across diverse and hazardous environments. The system not only reduces human risk but also streamlines operational workflows, offering a scalable solution for industrial and research applications. The comparative analysis underscores the robot's superiority in terms of safety, precision, and adaptability, validating its role as a viable alternative to human intervention in high-risk scenarios.

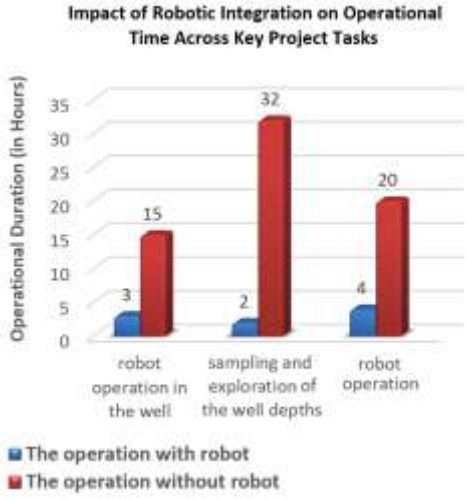


Figure 21. Comparative analysis of operational time and efficiency fluctuations between robotic and human-led methods across various projects, demonstrating the enhanced performance and time savings achieved through robotic implementation [9].

16. Conclusion

This research has demonstrated the effectiveness and continuity of operational methods involving robotic systems compared to traditional mechanisms. The integration of advanced robotics into industrial applications—particularly in water and wastewater management, oil and gas exploration, and deep-sea or underground operations—marks a significant leap forward in both technological innovation and practical execution.

The adoption of such technologies not only enhances economic efficiency by reducing labor costs and operational risks, but also fosters a robust scientific foundation for future advancements. Robots enable access to environments that are hazardous or inaccessible to humans, thereby accelerating data collection, improving precision, and minimizing human exposure to danger.

Moreover, the deployment of robotic systems bridges the gap between theoretical research and real-world application. It catalyzes the development of new inventions, supports interdisciplinary collaboration, and transforms abstract scientific concepts into tangible solutions. As industries continue to evolve, the role of robotics will be pivotal in shaping a future where knowledge, safety, and efficiency converge seamlessly.

14. Acknowledgements

I would like to express my deepest gratitude to all the researchers whose sources were used in this article.

Statements and Declarations

Conflicts of interest

The authors declare no conflict of interest regarding the authorship or publication of this article.

Funding

The authors declare that no funds, grants, or other support were received during the preparation of this manuscript.

Data availability

The datasets generated and analyzed during the present study were collected in Iran and are available from the lead author upon request.

Author contributions

The entire research process was done by myself as the responsible author: Data curation; Investigation in Civil Engineering-Structure; and mechanic and mechatronic Formal analysis; Writing – original draft; Supervision, Validation; Writing – review and editing.

References

[1] Shirmohammadi, M. (2015). Robots Replacing Workers in Wells, Daneshmand Magazine (Science section) Persian weekly of Canada - Vancouver, Vol 10, Issue.478, 45. www.Daneshmand.Ca

[2] Rajabi, A. (2016). Iranian Inventor Makes Robot for digging deep wells, Iran Daily News (International Newspaper), Science and Technology, News ID: 82031456, No.5325, 8. https://newspaper.irandaily.ir/5325

[3] Matinfar. F. (2009). I do not want Edison, I want support, The Morning Newspaper (Vatan Emrooz Today) Newspaper of the Economic, Culture, Science, politics, ISSN: 2008-2886, Vol. 1, No.142, 10. http://www.vatanemrooz.ir/142

[4] Aryani. A.N. (2008). Iranian youth Reap the Rewards of the Worth Championships, Monthly Journal Scientific, Educational, (Pars Oil Company Magazine), Specialist-Scientific-Educational, Sixth Years, No.61, 30-31. http://www.magiran.com/naftepars.ir/61

[5] Aqazadeh, M. (2013). Iranians have great potential for inventions, Iran News, Domestic Newspaper, ISSN: 1024-6053, issue 478, Vol. XVIII, No.5134, 3. https://irannewsdaily.com/5134

[6] Jalili, M. (2013). I wish that the students would be more confident, (Hamshahri Newspaper), ISSN: 1735-6237, No.5875, 3. https://www.hamshahrionline.ir/service/provinces/kordestan/5875

[7] Jong-Hoon, K. (2011). Sensor-based autonomous pipeline monitoring robotic system, Louisiana State University and Agricultural and Mechanical College, (LSU Digital Commons), 16-18. https://repository.lsu.edu/gradschool_dissertations/2566

[8] Sangbae, K., & Sami, H. J. (2014). Development of Pipe-Crawling Robot for Pipeline Network Discovery, (Kuwait – MIT Center for Natural Resources and the Environment), Project Code No.2012-5505-01, 21-60. https://pure.kfas.org.kw/ar/projects

[9] M. Shirmohammadi, Robots replacing workers in wells with drill rods or tubes with welding, cutting and research capabilities, Journal of Science and Engineering Elites, Article Code: 17-12610695, ISSN 2538-581X, Volume 5, No 5 (2020) 86-100. https://elitesjournal.ir/editor_file/Az997

[10] Xu. N. W., & Dabiri, J O. (2022). Roger Revelle Commemorative Lecture (Bio-Inspired Ocean Exploration, Vol .35, No.2, 35. http://doi:10.5670/oceanog.2022.214

[11] Zhou, Liu, Z. J. & et al. (2022). A Survey of Underwater Multi-Robot Systems, IEEE/CAA Journal of Automatica Sinica, VOL. 9, NO. 1, 1. http://doi.10.1109/JAS.2021.1004269

[12] Aguzzi, J. Flogel, S. Marini, S. & et al. (2022). Developing technological synergies between deep-sea and space research, Elem Sci Anth, 10: 1, 2. https://doi.org/10.1525/elementa.2021.00064

[13] Bonfitto, A. Amati, N. (2018). Mechanical Construction and Propulsion Analysis of a Rescue Underwater Robot in the case of Drowning Persons, MDPI Applied Sciences, 1. http://doi:10.3390/app8050693

[14] Aracri, S. Serchi, F. G. & et al. (2021). Soft Robots for Ocean Exploration and Offshore Operations: A Perspective, Soft Robotics, Volume 8, Number 6 625-627. http://doi: 10.1089/soro.2020.0011

[15] Zhang, G. Yun, T. J. & et al. (2020). A study on seam tracking in robotic GMA welding process, Material Today Proceedings, 1771–1777, 22. http://doi:10.1016/j.matpr.2020.03.010

[16] Sharma, A. Sharma, K. & et al. (2020). Effect of welding parameters on automated robotic arc welding process. Materials Today: Proceedings, Vol 26. 2363–2367. http://doi:10.1016/j.matpr.2020.02.507

[17] Muhammad, J. Altun, H. & et al. (2017). welding seam profiling techniques based on active vision sensing for intelligent robotic welding. Int. J. Adv. Manuf. Technol., Vol 88, 127–145. http://doi:10.1007/s00170-016-8707-0

[18] Rout, A. Deepak, B. B. V. L. & Biswal, B. B. (2019). Advances in weld seam tracking techniques for robotic welding: A review. Robot. Robotics and Computer-Integrated Manufacturing Vol 56, 12–37. https://doi.org/10.1016/j.rcim.2018.08.003

[19] Han, B. Xiaolu, C. & et al. (2024). Research Review and Future Directions of Key Technologies for Welding Robots in the Construction Industry, MDPI, Buildings, 1-3. https://doi.org/10.3390/buildings14082261

[20] Sun, L. Wang, Y. Hui, X. & et al. (2024). Underwater Robots and Key Technologies for Operation Control, Cyborg and bionic Systems (A Science Partner Journal), 1. https://doi.org/10.34133/cbsystems.0089

[21] General Oceanics. (2021). Water Sampling: Water Sampling Bottles: ROV Niskin Bottles: Rov Niskin Water Sampler, 5L. https://www.generaloceanics.com

[22] Mirmalek, Z. & Raineault, N. A. (1942). Remote science at sea with remotely operated vehicles, Robotics and AI, 2. https://doi.org/10.3389/frobt.2024.1454923

[23] Heinlein, R. A. MacDonald, A. Waldo. (1942). Astounding Sci. Fiction 29, 9–53. https://archive.org/details/Astounding

[24] Kunz, C. Murphy, C. & et al. (2008). Deep Sea Underwater Robotic Exploration in the Ice-Covered Arctic Ocean with AUVs, The University of Rhode Island, Intelligent Robot Sand Systems, IROS. IEEE/RSJ International Conference, 3654-3660. http://dx.doi.org/10.1109/IROS.2008.4651097

[25] Vaishnavi, V. Shwetha. S. (2023). A Review on Robotics in Marine and Space Exploration, International Journal of Research Publication and Reviews, ISSN 2582-7421, Vol 4, No 4, 3552-3553. https://ijrpr.com/uploads/V4ISSUE4/IJRPR11901

[26] Liu, J. (2022). Research on the development and path exploration of autonomous underwater robots, EDP Sciences, ITM Web of Conferences 47, 01029, CCCAR2022, 1. https://doi.org/10.1051/itmconf/20224701029

[27] Zeng, X. Xia, M. Luo, Z. & et al. (2022). Design and Control of an Underwater Robot Based on Hybrid Propulsion of Quadrotor and Bionic Undulating Fin, journal of Marine Science and engineering MDPI, 10, 1327, 1. https://doi.org/10.3390/jmse10091327

[28] Nayar, H. Ali, K. Aubrey, A. & et al. (2012). Jet Propulsion Laboratory, California Institute of Technology, Space Robotics Technologies for Deep Well Operations, (OTC 22989-PP), the Offshore Technology Conference held in Houston, Texas, USA, 7. http://doi:10.4043/22989-MS

[29] Wilcox, B. (2009). ATHLETE: A Cargo and Habitat Transporter for the Moon, California Institute of Technology, IEEE Aerospace Conference, (Big Sky, MT). http://doi:10.1109/AERO.2009.4839568

[30] Wilcox, B. H. Litwin, T. Biesiadecki, J. & et al. (2007). Athlete: A Cargo Handling and Manipulation Robot for the Moon, Journal of Field Robotics, 24 (5), 421- 434. http://doi:10.1002/rob.20193

[31] Barker, L. D. L. Jakuba, M. V. & et al. (2020). Scientific Challenges and Present Capabilities in Underwater Robotic Vehicle Design and Navigation for Oceanographic Exploration Under-Ice, (Remote Sensing), MDPI, 12, 5. http://doi:10.3390/rs12162588

[32] Cooney, M. Staffa, M. (2025). Robotics, Special Issue on Social Robots for Human Well-Being, MDPI, 14, 37, 1. https://doi.org/10.3390/robotics14040037

[33] Matthew, J. D. (2022). Dennis, Social robots and digital well‐being: how to design future artificial agents, Mind & Society 21 (1), 39. https://doi.org/10.1007/s11299-021-00281-5

[34] Wang, J. L. Song, J. L. Liu, A. R. & et al. (2024). Design and architecture of a slender and flexible underwater robot, Intelligent Service Robotics, 1. https://doi.org/10.1007/s11370-024-00539-0

[35] Li, G. Wong, T. W. Shih, B. & et al. (2023). Bioinspired soft robots for deep-sea exploration, Nature Communications, 14 (1):7097, 1. https://doi.org/10.1038/s41467-023-42882-3

[36] de-Leon, P. S. Phillips, B. & et al. (2018). Deep-sea hydrothermal vents as natural egg-case incubators at the Galapagos Rift, Scientific Reports. 8,1788. http://doi:10.1038/s41598-018-20046-4

[37] Yoerger, D. Govindarajan, A. & et. al. (2021). A hybrid underwater robot for multidisciplinary investigation of the ocean twilight zone, Science Robotics 6(55): eabe1901. http://doi:10.1126/scirobotics.abe1901

[38] Błachut, J. Smith, P. (2008). Buckling of multi-segment underwater pressure hull. Ocean Engineering. Vo 35, No 2, 247–260. https://doi.org/10.1016/j.oceaneng.2007.08.003

[39] Cui, Z. Li, L. Wang, Y. & et al. (2023). Review of research and control technology of underwater bionic robots, Intelligent Marine Technology and Systems Vol 1, No 7, 2. https://doi.org/10.1007/s44295-023-00010-3

[40] Wynn, R. B. Huvenne, V. A. I. & et al, (2014). Autonomous Underwater Vehicles (AUVs): their past, present and future contributions to the advancement of marine geoscience. Marine Geology 352, 451–468.

[41] Vu, M. T. Jeong, S. K. Choi, H. S. & et al. (2018). Study on down-cutting ladder trencher of an underwater construction robot for seabed application. Applied Ocean Research, 71, 90–104.

[42] Wang, T. Joo, H. J. Song, S. & et al. (2023). A versatile jellyfish-like robotic platform for effective underwater propulsion and manipulation, Applied Sciences and Engineering, Science Advances 9(15): eadg0292, 1. http://doi: 10.1126/sciadv. adg0292

[43] Madricardo, F. Ghezzo, M. Nesto, N. & et al. (2020). how to deal with seafloor marine litter: An overview of the state-of-the-art and future perspectives. Frontiers. Marine. Science. 7, 505134.

[44] Gruber, D. F. Wood, R. J. (2020). Advances and future outlooks in soft robotics for minimally in- vasive marine biology. Science Robotics. 7(66), eabm6807.

[45] Jacobstein, N. Bellingham, J. Yang, G. Z. (2017). Robotics for space and marine sciences, Space and Marine Robots, Science. Robotics. 2(7), eaan5594, 1. http://doi: 10.1126/scirobotics. aan5594

[46] Mazzeo, A. Aguzzi, J. Calisti, M. & et al. (2022). Marine Robotics for Deep-Sea Specimen Collection: A Systematic Review of Underwater Grippers, Sensors

(MDPI), 22(2), 648, 1-7. https://doi.org/10.3390/s22020648

[47] Instituto Español de Oceanografía (2021). (IEO) Liropus 2000. Available online. http://www.ba.ieo.es/es/presentacion/equipamiento

[48] Instituto Español de Oceanografía. (2021). First Video Volcano El Hierro from ROV Liropus 2000: 1 November 2011, Timestamp: 00:00:51, YouTube. Available online. https://www.youtube.com/watch

[49] Schmidt Ocean Institute ROV Dive 416. (2021). Ashmore Reef Location Six, Dive 2-Part B, Timestamp: 01:25:39—YouTube. Available online. https://www.youtube.com/watch

[50] Schmidt Ocean Institute ROV SuBastian Dive 350. (2021). Cloates Canyon, Australia-FK200308, Timestamp: 00:40:13—YouTube. Available online. https://www.youtube.com/watch

INTERNATIONAL JOURNAL OF
COASTAL, OFFSHORE & ENVIRONMENTAL ENGINEERING

IJCOE Vol.1/ Special Issue No.1/
Marine Instrumentation/ 2023 (46-54)

Available online at: www. Ijcoe.org

A Novel Approach to Image Moment Computation for Sonar Image Registration in Underwater Vehicle Autonomy

Mehrnaz Monajati[1]

[1] *Assistant professor, Faculty of Electrical and Computer Engineering, Graduate University of Advanced Technology, Kerman, Iran;* m.monajati@kgut.ac.ir

ARTICLE INFO

Article History:
Received : 20 Apr 2023
Accepted : 08 Aug 2023

Keywords:
Sonar image registration
Image Moment
Parallel processing
Autonomous underwater vehicles
Real-time image processing

ABSTRACT

Sonar image registration poses significant challenges due to the unique characteristics of sonar imagery and the stringent requirements of real-time underwater applications. Compared to optical images, sonar images exhibit lower resolution, higher noise levels, and a lack of distinct features, which complicates traditional detection and registration methods. Furthermore, the computational complexity increases rapidly with higher-order moments and larger image sizes, limiting the responsiveness of autonomous underwater vehicles (AUVs). Addressing these challenges requires innovative hardware architectures and parallel processing techniques. Building upon our previous work, which introduced a systolic array and pipelined structure for high-order moment computation in grayscale images, this paper presents the Parallel Comparator-Based Structure (PCS) to accelerate moment calculation for sonar image registration. PCS achieves fixed-latency computation by strategically relocating adders outside processing cells and integrating power cores, comparator-assisted compressors, and floating-point adder units. The proposed architecture enables all processing elements to operate in parallel while ensuring numerical consistency and scalability. Post-synthesis simulations and comparative analysis demonstrate that PCS delivers substantial speed improvements, high maximum moment order computation, and deterministic low-latency performance, making it a highly effective solution for real-time sonar image processing in AUVs. The results highlight the potential of PCS to advance autonomous underwater perception and navigation tasks, offering a robust, high-throughput, and scalable approach for future marine robotics applications.

1. Introduction

The development of new technologies, the refinement of sensor capabilities, and the continuous evolution of research in marine robotics have catalyzed the emergence of various underwater autonomous applications, including the manipulation and inspection of underwater structures and oil pipelines [1]. Despite notable strides, the realization of truly autonomous functionalities in underwater robotics remains somewhat constrained. These autonomous capabilities still heavily depend on precise environmental models and pre-programmed operations for their execution [2]. As a result, significant challenges persist in achieving robust and adaptive autonomy, particularly in complex and dynamic underwater environments where environmental conditions are often unpredictable.

Within the realm of underwater robotics, image moments assume a pivotal role in facilitating tasks such as manipulation and inspection of underwater structures and oil pipelines. Serving as mathematical descriptors, image moments encapsulate critical properties of an image, including its centroid, area, and orientation. These descriptors furnish invaluable insights into the shape, size, and orientation of objects within the underwater milieu, thus proving indispensable for autonomous applications [3]. In contrast to conventional geometric features, which may be highly sensitive to noise or distortions, image moments offer more compact yet descriptive representations that can be exploited to improve robustness in perception and decision-making.

In manipulation tasks, image moments play a fundamental role in accurately detecting and localizing

objects of interest, such as underwater structures or components of oil pipelines. Through the meticulous analysis of captured image moments, robotic systems can precisely ascertain the position and orientation of these objects, thereby facilitating effective manipulation maneuvers.

In manipulation tasks, image moments play a fundamental role in accurately detecting and localizing objects of interest, such as underwater structures or components of oil pipelines. Through the meticulous analysis of captured image moments, robotic systems can precisely ascertain the position and orientation of these objects, thereby facilitating effective manipulation maneuvers. This becomes particularly crucial in conditions where traditional visual cues are unreliable due to turbidity, occlusion, or light attenuation, which are common challenges in underwater environments. By leveraging image moments derived from sonar data, robotic platforms can establish more reliable estimations of object features, ultimately improving dexterity and operational safety.

Similarly, in inspection tasks, image moments serve as vital tools in identifying anomalies or damages on underwater structures or pipelines. By comparing the moments of captured images with reference models or predefined criteria, robotic systems can discern deviations or irregularities, signaling potential areas of concern warranting further inspection or maintenance [4]. Such functionality is highly valuable in industries like offshore energy production, where the early detection of defects can prevent costly failures and mitigate environmental risks. Moreover, moments-based approaches can support the classification of structural features, enabling more efficient prioritization of inspection tasks and reducing reliance on human intervention in hazardous underwater settings.

Furthermore, in the context of underwater applications, particularly in the inspection of structures and pipelines, the importance of image moments for accurate sonar image registration cannot be overstated [5]. Sonar imaging remains a primary sensing modality for underwater robotics, largely due to its ability to operate effectively in visually degraded conditions where optical imaging proves insufficient. However, sonar images are often characterized by significant levels of noise, speckle artifacts, and distortions that complicate feature extraction and alignment. In this regard, image moments provide an efficient mathematical mechanism for summarizing key image properties, thereby enabling more robust image registration processes.

Consequently, the development of innovative methods for computing image moments tailored for sonar images holds promise for enhancing the accuracy and robustness of image registration processes. Improved registration not only ensures precise spatial alignment between successive sonar frames but also strengthens the consistency of environmental mapping, object recognition, and localization. Such advancements are poised to augment the capabilities of autonomous underwater vehicles (AUVs), particularly in tasks necessitating precise image alignment, object detection, and navigation in cluttered or unstructured environments. By addressing the inherent limitations of conventional image moment computation techniques, novel approaches to sonar image processing have the potential to substantially broaden the scope of autonomous underwater missions and elevate the overall reliability of underwater vehicle autonomy.

The remainder of this paper is organized as follows. Section 2 provides an in-depth discussion of sonar image registration, highlighting its challenges in underwater environments and reviewing existing hardware and algorithmic approaches. Section 3 introduces the proposed PCS for efficient image moment computation, describing its architectural design and performance characteristics. Section 4 details the shift register optimization method that enables effective parallelization while reducing latency and power consumption. Section 5 presents the simulation results, comparing PCS with existing architectures in terms of speed, power, and area utilization. Finally, Section 6 concludes the paper by summarizing the key findings, emphasizing the broader implications of PCS, and outlining potential directions for future research.

2. Sonar Image Registeration

In contrast to optical images, which boast intricate textures, sonar images are generally simpler and cannot rely on robust point feature detectors [6]. raditional feature extraction and matching algorithms, such as Scale-Invariant Feature Transform (SIFT) and Speeded Up Robust Features (SURF), are designed to exploit gradient and texture variations in optical images. However, in sonar imagery, these approaches often fail due to high levels of noise, poor contrast, and limited texture content [7]. Consequently, their instability renders them unsuitable for sonar image analysis in the context of underwater robotics.

Despite these limitations, sonar images tend to exhibit well-defined geometric structures and prominent boundaries, making them highly amenable to shape-based methods. A common approach for sonar image registration is the utilization of image moments—particularly Hu's invariant moments—due to their ability to encapsulate shape descriptors in a compact and mathematically robust manner [8]. By leveraging such geometric representations, sonar image registration can achieve reliable alignment even in conditions where traditional texture- or keypoint-based methods break down.

All vehicle perceptions are translated into computational units known as local view cells, which

act as abstract representations of the perceived environment. To derive stable and reliable geometric features from sonar images, a preprocessing pipeline is typically applied. This pipeline includes Gaussian filtering to reduce noise while preserving large-scale features, and median filtering to mitigate speckle noise characteristic of sonar data. Following this enhancement stage, thresholding techniques are employed to convert the sonar image into binary format. From this binarized representation, image contours are extracted by identifying regions of strong gradient response, thereby isolating the relevant shapes that will serve as inputs for moment computation.The moment of a shape, denoted as M_{pq}, is calculated by summing the weighted intensities of its pixels.

The mathematical formulation of a geometric moment of order (p,q), denoted as M_{pq}, is given by:

$$M_{pq} = \sum_{x=1}^{m} \sum_{y=1}^{n} x^p y^q f(x,y) \qquad x \le m, y \le n \qquad (1)$$

Where, f(x, y) is the intensity function, typically represented in binary form after preprocessing. These raw moments form the foundation for computing normalized and invariant moments. In particular, the seven Hu invariant moments, first introduced in 1962, provide descriptors that are invariant to translation, rotation, and scaling. Their robustness makes them especially well-suited for sonar image analysis, where sensor orientation, vehicle movement, and environmental variability are frequent.

The significance of computational speed in this context cannot be overstated. Given that many underwater applications—including navigation, pipeline inspection, and structural monitoring—require real-time processing, the rapid calculation of image moments is essential [9]. The ability to compute Hu moments quickly during sonar image registration directly impacts an autonomous underwater vehicle's (AUV) capacity to localize itself, update its map, and respond dynamically to environmental changes. Faster moment computation not only supports timely decision-making but also ensures that the vehicle can react to unexpected obstacles or alterations in mission objectives. Consequently, the performance of sonar-based navigation and inspection systems is intrinsically tied to the efficiency of the underlying moment calculation algorithms.

Several hardware and architectural innovations have been proposed to accelerate the process of moment computation. Raffaitin et al. developed a hardware-based shape recognition framework employing the Non-Local Means (NLM) filter and Hu's moments, specifically optimized for FPGA implementation [10]. Their work involved modifying the NLM filter to simplify its deployment on FPGA and employing finite state machines for computing both the NLM filter and Hu's moments. The results highlighted the superior speed of hardware-based solutions compared to software implementations, demonstrating their suitability for real-time sonar processing in robotic systems.

In another notable contribution, Watanabe et al. introduced a parallel extraction architecture aimed at handling multiple object features simultaneously [11]. Their FPGA-based implementation was validated for correctness and demonstrated exceptional performance in high-frame-rate scenarios. This parallel approach was particularly effective in extracting abundant information from sonar imagery in real time, making it valuable for applications demanding both high speed and accuracy.

Iwashita et al. further advanced this domain by presenting the design of an image-moment sensor capable of real-time statistical computation [12]. They proposed a variable-length pipeline architecture for moment calculation, implemented in a 128×128 pixel sensor array. By sharing processing elements, the design minimized circuit area while maintaining high throughput. Their experimental results confirmed the feasibility of compact, cost-effective, and high-speed moment computation sensors. Such dedicated hardware platforms hold promise not only for underwater robotics but also for factory automation, human interfaces, and other domains requiring real-time image feature extraction.

Building on this foundation, we have recently introduced a novel structure leveraging systolic arrays and pipelined architectures for the computation of higher-order two-dimensional moments in grayscale images [13]. Each moment processor element (MPE) comprises adder, exponentiation, and multiplication units, arranged in a modular fashion. Input data, represented as f(x,y), is provided to the control unit, which then distributes pixel values along with their corresponding x and y coordinates to the MPEs. When multiple MPEs are connected in sequence, they form a systolic array capable of parallelized processing of distinct portions of the image. This configuration not only enhances computational throughput but also reduces latency, thereby enabling high-speed image registration.

Figure 1 illustrates a representative structure consisting of three interconnected MPE cells. Each cell is responsible for a subset of the overall computation, and together they collaboratively generate higher-order moments. This architecture demonstrates the feasibility of accelerating sonar image registration through parallel hardware structures, laying the groundwork for further innovations in underwater vehicle autonomy.

2.1 Limitations of Hu-Based Sonar Registration

While Hu's invariant moments have been widely adopted for sonar image registration due to their simplicity and robustness against basic geometric transformations, several limitations constrain their effectiveness in practical underwater scenarios.

1. Sensitivity to Noise and Clutter:
   Sonar images often contain substantial noise, including speckle artifacts and false reflections from the seafloor or surrounding debris. Hu moments, being global descriptors, aggregate pixel information across the entire shape, making them susceptible to even minor noise perturbations. This sensitivity can lead to unstable descriptors and poor registration accuracy in cluttered underwater environments.
2. Loss of Local Detail:
   Hu moments capture global shape characteristics but fail to preserve localized geometric information. In environments where multiple objects overlap or when partial occlusions occur, this lack of local feature discrimination can result in misregistration or ambiguous alignments.
3. High Computational Overhead for Large Images:
   Although Hu moments are compact once computed, their calculation—particularly for higher-order moments—can be computationally intensive. For large sonar images or real-time applications, this overhead may limit the speed of registration, ultimately reducing the responsiveness of AUV systems.
4. Limited Discriminative Power in Complex Scenarios:
   In cases where multiple objects exhibit similar global shapes (e.g., cylindrical pipes, structural beams, or marine growth encrustations), Hu moments alone may not provide sufficient discriminative capability. This limitation can hinder object recognition and accurate registration when multiple candidate matches exist.

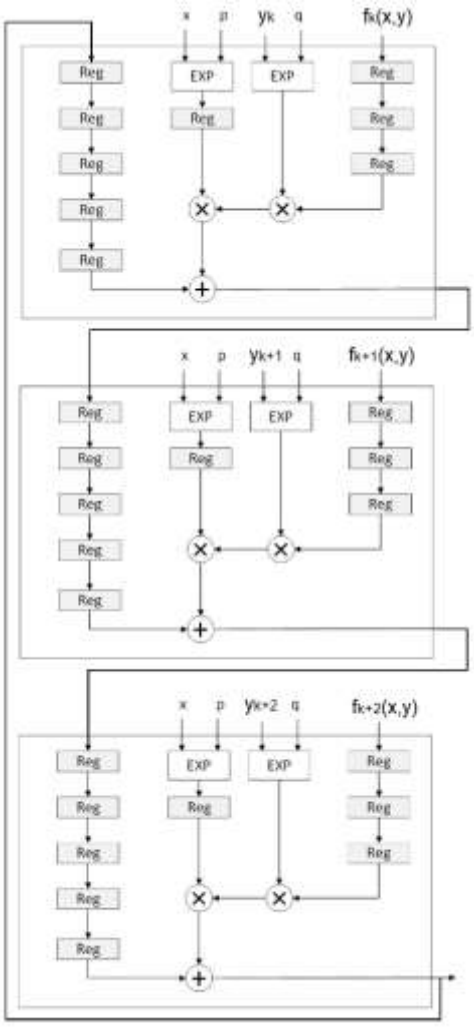


Figure 1. Systolic structure composed of three MPEs

These limitations highlight the need for novel approaches that retain the mathematical robustness of moments while addressing their shortcomings in speed, noise resilience, and discriminative capability. In particular, hardware-oriented parallelization strategies offer promising solutions by accelerating moment computation while enabling more robust handling of sonar imagery. This motivates the development of the proposed Parallel Comparator-Based Structure (PCS), introduced in the next section, which is specifically designed to optimize image moment computation for sonar image registration in underwater robotics.

3. Parallel Comparator-Based Structure (PCS)

The computational efficiency of image moment extraction is a critical determinant of performance in real-time sonar image registration. Although systolic array architectures have demonstrated significant potential in accelerating moment computation, their reliance on sequential accumulation of intermediate results inherently introduces latency that grows with the number of processing cells. To address this limitation, we propose a novel Parallel Comparator-Based Structure, which restructures the computational flow to ensure fixed latency, independent of the cell count. By relocating adders to the exterior of the

processing cells and introducing a comparator-assisted compression scheme, PCS provides a robust and scalable solution for high-speed sonar image registration.

3.1 Architectural Concept

The PCS architecture reconfigures the conventional systolic pipeline into a fully parallelized structure. Instead of chaining adders within the processing elements, each power core (PC) is responsible solely for computing terms of the form:

$$T(x, y) = x^p y^q f(x, y) \quad (2)$$

where f(x,y) represents the pixel intensity. Each PC completes its computation in five clock cycles, producing 18-bit intermediate results. With nine cells operating simultaneously, the PCS generates nine 18-bit outputs per cycle.

Figure 2 highlighting the bit-level parallelism that underpins the PCS design. To manage these results efficiently, PCS employs a compressor unit that performs multi-operand addition in parallel. Unlike traditional designs where outputs are accumulated sequentially, the PCS uses comparator-based alignment to normalize mantissas before feeding them into the compressor. This step guarantees numerical consistency and eliminates bit-width mismatch across multiple inputs.

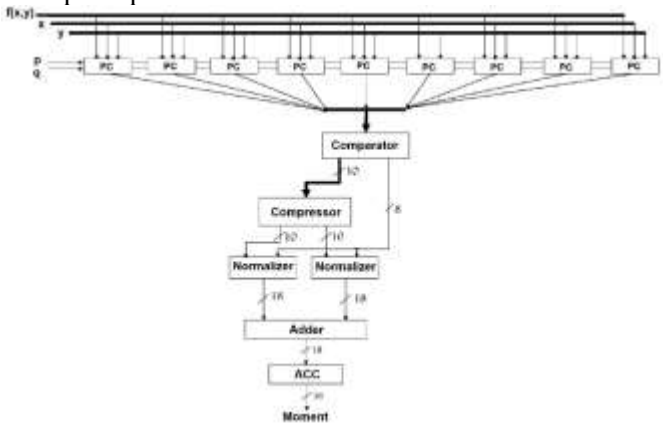


Figure 2. Parallel Comparator-Based Structure (PCS)

The aligned outputs are then routed into an 81:20 compressor (Figure 3), which consists of nine 15:2 comparators (Figure 4) and a 7:3 comparator (Figure 5). Each 15:2 comparator reduces 15 inputs into two outputs, producing seven single-bit results that are propagated into the next compression stage. The 7:3 comparator, illustrated in Fig. 5, refines the aggregation process by reducing three inputs into a compact representation suitable for final accumulation. The internal structure of the 15:2 comparator is presented in The outputs of the compressor, represented as 22-bit numbers, are paired and processed through 18-bit floating-point adders, whose results are subsequently directed into the accumulator (ACC) for final summation. This architecture ensures that the PCS achieves high throughput without sacrificing precision.

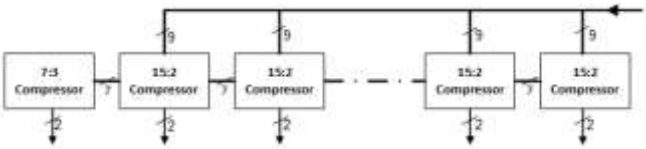


Figure 3. Architecture of 81: 20 Compressor

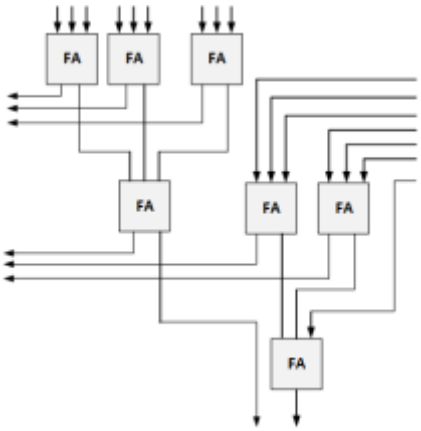


Figure 4. Design of 15:2 compressor

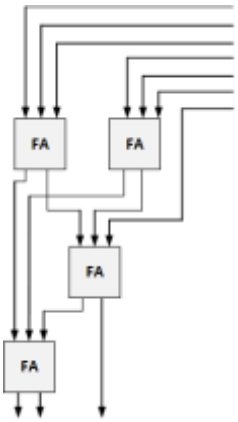


Figure 5. Structure of 7:3 compressor

3.3 Latency Analysis

A defining feature of PCS is its *fixed latency*. Regardless of the number of PCs integrated into the structure, the overall latency remains constant at 15 clock cycles. This is in stark contrast to the conventional systolic architecture, where latency is proportional to the number of cells. Specifically, systolic latency is given by:

$$L_{\text{systolic}} = T_{clk} \times (1 + 5N) \quad (3)$$

where N is the number of cells and T_{clk} is the clock cycle period. For a nine-cell systolic system, the latency is 50 clock cycles, over three times greater than PCS for the same configuration. This scalability advantage makes PCS particularly well-suited for real-time sonar applications, where latency reduction

directly translates into faster image registration and improved autonomy for AUVs.

3.4 Advantages Over Systolic Structures

The PCS framework offers several critical advantages:

1. Fixed Latency:
   Independent of the number of processing cells, ensuring predictable and stable performance across different system scales.
2. Parallelism:
   All PCs operate concurrently, producing outputs simultaneously, which dramatically reduces computation time compared to sequential systolic arrays.
3. Numerical Stability:
   Comparator-based mantissa alignment guarantees precision during compression, reducing the risk of accumulation errors that may arise in floating-point summations.
4. Scalability:
   Since latency does not increase with additional cells, PCS can accommodate larger numbers of PCs without compromising speed, enabling efficient computation of higher-order moments.
5. Hardware Efficiency:
   By relocating adders outside the PCs and employing a hierarchical comparator-compression structure, PCS minimizes redundant operations, reducing circuit complexity and power consumption relative to unoptimized systolic arrays.

3.5 Implications for Sonar Image Registration

The proposed PCS design directly addresses the computational bottlenecks of conventional systolic systems. For sonar image registration tasks that demand rapid alignment of frames in dynamic underwater environments, PCS provides a pathway to deterministic low-latency moment computation. This allows autonomous underwater vehicles to maintain real-time situational awareness, even in environments characterized by high noise, clutter, or frequent navigational updates.

Furthermore, the modularity of PCS ensures adaptability: additional PCs can be seamlessly integrated to support higher-order moment calculations without degrading system performance. Such flexibility makes PCS not only a robust replacement for existing architectures but also a scalable foundation for future generations of sonar-based navigation and inspection systems.

4. Shift Register Optimization for Parallelization

Parallelization plays a pivotal role in enhancing the computational efficiency of image moment extraction. In the PCS architecture, simultaneous data delivery to each processing cell is essential to achieve true parallelism. Without synchronized input feeding, cells may stall, leading to inconsistent performance and inefficient utilization of resources. To ensure synchronous operation, image data must first be temporarily stored and then supplied to each MPE in parallel. This buffering is typically accomplished using shift registers, which sequentially load pixel values and release them in a synchronized manner at the rising edge of the clock pulse.

4.1 Conventional Shift Register Design

In traditional parallel architectures, each cell requires a dedicated bank of shift registers proportional to the number of image rows. For an image of height mmm and a structure containing n×MPE cells, the system requires m×nMPE registers, each 18 bits wide. As both image size and the number of cells increase, the demand for shift registers grows linearly.

This scaling issue presents two major drawbacks:

1. Increased Latency:
   The time required to fill all registers with pixel data, known as incubation time, grows with image dimensions. For large sonar images, this results in significant latency before computations even begin.
2. High Power Consumption:
   A large number of registers switching simultaneously imposes considerable dynamic power requirements. This is particularly problematic in AUV systems, where power budgets are constrained.

Thus, while shift registers are essential for synchronous data feeding, the conventional design is inefficient for large-scale sonar image processing.

4.2 Proposed Optimization Method

To overcome these inefficiencies, we propose an optimized shift register design, illustrated in Figure 6. The key idea is to decouple the number of required shift registers from the image dimensions, making the system scalable and power-efficient.

Instead of assigning a large array of registers for each image row, the proposed method requires only:

$$N_{SR} = n_{MPE}^2 \tag{4}$$

where N_{SRN} denotes the number of required shift registers and n_{MPE} represents the number of Moment Processor Elements.

This quadratic dependence on n_{MPE} makes the required register count independent of image size (m). As a result, even when processing high-resolution sonar images, the hardware cost remains bounded by the number of computational cells, not the number of pixels.

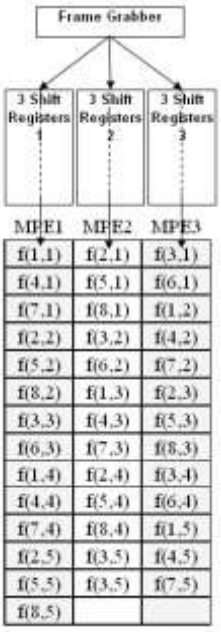


Figure 6. Proposed method for reduced shift register requirement and latency time

4.3 Latency Analysis

In the synchronous mode targeted in this design, all units calculate their outputs at the rising edge of the clock pulse. With the proposed register arrangement, each pixel of the image enters the system in one clock cycle, thereby minimizing latency.
The overall incubation time of the structure can be expressed as:

$$Latency = Tn_{MPE}^2 + 5T(n_{MPE} + 1) = 5Tn_{MPE}(n_{MPE} + 1) \quad (5)$$

where:

- Tis the clock period,
- n_{MPE} is the number of moment processor elements,
- m is the number of rows in the image.

Notably, Eq. (5) demonstrates that latency grows quadratically with n_{MPE}, but no longer depends on image size mmm. This property is critical for scaling to large sonar frames. Figure 7 illustrates the latency trends, showing that the proposed method achieves significant reductions compared to conventional architectures, particularly as m increases.

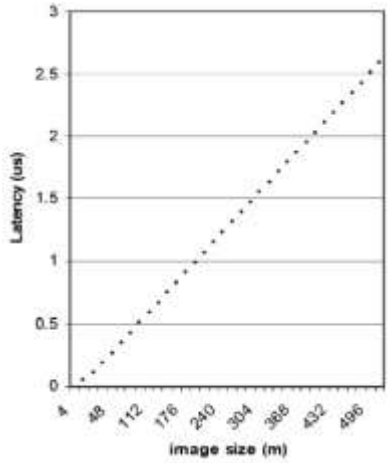


Figure 7. Effect of image size on latency reduction

4.4 Practical Advantages

1. Reduced Hardware Complexity:
   By eliminating the dependence on image dimensions, the number of required shift registers decreases drastically for large images, leading to a more compact circuit layout.
2. Lower Power Consumption:
   Fewer registers switching in parallel reduces dynamic power draw, a crucial factor for power-constrained underwater systems.
3. Scalability for High-Resolution Sonar:
   The design remains efficient even as image resolution increases, enabling real-time registration for large sonar frames without exponential hardware costs.
4. Consistent Parallelism:
   With uniform data feeding in every cycle, all MPEs operate at full utilization, avoiding idle states and maximizing throughput.

5. Simulation Results

The physical characteristics of the proposed moment computation structure were analyzed through synthesis with the Nangate 45nm open cell library using the Synopsys Design Compiler. To estimate power consumption, the Synopsys power analysis tool was employed, utilizing a VCD (Value Change Dump) file generated from post-synthesis simulations with 100,000 random input patterns. This methodology follows established ASIC design practices, where block-level characterization is performed to ensure the feasibility of integrating computational units into larger, system-level architectures.
To evaluate the performance of the proposed Parallel Comparator-Based Structure, a comparative study was conducted against four representative architectures from the literature. These included Architecture [12], Architecture [13], Architecture [14], and Architecture [15], each offering different trade-offs between computational speed, power consumption, and area

efficiency. Table 1 summarizes the results of this comparison.

Table 1. Comparative performance analysis of various structures

Architecture	[14]	[12]	[15]	[13]	PCS
Max Moment Order	16	10	18	14	14
Transistor count	43894	143253	639804	543251	1167989
Speed (Gbit/s)	86.481	32.215	92.285	618.243	1060.286
Speed (frame/s)	45.277	25.568	84.237	954.012	1623.012
Power (mw)	254.863	185.657	19.586	3.254	5.018
Area (mm^2)	0.218	0.521	0.657	0.734	2.308

5.1 Speed Performance

The PCS architecture achieved the highest speed among all compared designs, reaching a throughput of 1,060.286 Gbit/s and a frame processing rate of 1,623.012 frames/s. This represents:

- A 73% improvement in bit-level throughput compared to Architecture [13].
- Nearly a 19× increase in frame rate relative to Architecture [15].
- More than a 60× increase in frame rate compared to early designs such as Architecture [12].

This substantial speed advantage is attributed to PCS's fixed-latency parallelism, where multiple power cores operate concurrently without the sequential accumulation bottleneck of systolic architectures. For real-time sonar image registration, such high throughput translates into the ability to process large frames at mission-critical rates, even under noisy and dynamic underwater conditions.

5.2 Power Consumption

While PCS exhibits remarkable speed, its power consumption, measured at 5.018 mW, is higher than Architecture [13] (3.254 mW) but remains orders of magnitude lower than older designs such as Architecture [14] (254.863 mW). Architecture [15] shows the lowest power consumption (19.586 mW), but this comes at the expense of drastically reduced speed.

From a system integration standpoint, the modest increase in power consumption of PCS compared to [13] is justified by the more than 70% speed improvement. For battery-powered AUVs, where energy efficiency is critical, PCS offers an attractive compromise: high performance with a manageable power budget.

5.3 Area Utilization

The PCS design occupies the largest silicon footprint among the architectures evaluated, with a total area of 2.308 mm². This represents a substantial increase compared to Architecture [13] at 0.734 mm², Architecture [15] at 0.657 mm², and Architecture [14] at just 0.218 mm²—making PCS approximately three, four, and ten times larger, respectively. The expanded area stems from the inclusion of multiple comparator units, compressor logic, and a greater number of power cores necessary to support its parallel processing capabilities. Although this larger footprint introduces challenges for chip integration, it reflects a conscious design decision that favors speed and reliability over compactness. In scenarios where silicon area is less of a constraint, such as dedicated sonar processing modules in autonomous underwater vehicles (AUVs), this trade-off is both practical and justified.

5.4 Maximum Moment Order

The supported maximum moment order varies across architectures. Architecture [15] supports the highest (18), whereas PCS and Architecture [13] both achieve an order of 14, which is adequate for most sonar image registration tasks. Higher-order moments are more sensitive to noise and often provide diminishing returns in practical sonar imagery. Thus, PCS balances computational feasibility with robustness, focusing on orders that deliver meaningful shape representation without unnecessary sensitivity.

5.5 Discussion of Trade-Offs

The comparative results clearly demonstrate the performance dominance of PCS in terms of speed and frame rate. However, this comes with two trade-offs:

1. Higher Area:
   PCS requires significantly more transistors and larger silicon area, raising design complexity and fabrication cost.
2. Moderately Higher Power Consumption:
   Although PCS is less power-efficient than Architecture [13], it remains far more efficient than earlier designs ([12], [14]) and is within the acceptable range for embedded AUV hardware.

For mission-critical underwater applications, where reliable real-time image registration directly impacts navigation, localization, and obstacle avoidance, PCS provides a superior solution. The marginal increase in power and area is outweighed by the dramatic improvement in processing throughput, ensuring that AUVs can handle high-resolution sonar imagery without latency bottlenecks.

5.6 Implications for Underwater Vehicle Autonomy

The simulation results confirm that PCS is well positioned to meet the demands of next-generation underwater robotics. With frame rates exceeding 1,600 fps, PCS enables:

- Real-time sonar mosaicking for large-area seabed mapping.

- Rapid defect detection in pipeline and structural inspection.
- Dynamic navigation and localization, even in environments with high noise and clutter.

By combining fixed-latency performance with optimized shift register design (Section 4), PCS offers a scalable and future-proof architecture that can be extended to higher resolutions and larger image dimensions without compromising speed.

6. Conclusion

This paper presents the Parallel Comparator-Based Structure (PCS), a novel hardware architecture designed to enhance moment computation in sonar image registration. PCS delivers high throughput—up to 1,623 frames per second—through fixed-latency, parallel processing, outperforming traditional systolic and serial methods. Despite a larger transistor count and area, PCS maintains low power consumption (5.018 mW), making it suitable for embedded systems like AUVs.

Capable of computing up to 14th-order image moments, PCS balances accuracy with efficiency, offering a scalable solution for real-time underwater tasks. Its architectural principles—parallelism, comparator-based compression, and fixed-latency design—extend to broader domains such as medical imaging and industrial analytics.

Future research directions include optimizing power and area, scaling to higher-resolution inputs, integrating with heterogeneous platforms, embedding into full sonar pipelines, and validating in field deployments. Overall, PCS represents a transformative step in hardware-accelerated image moment computation for autonomous underwater operations.

7. References

[1] Bao, H., Zhang, Y., Song, M., Kong, Q., Hu, X., & An, X. A review of underwater vehicle motion stability. *Ocean Engineering, 287*, 115735. (2023)

[2] Eickstedt, D. P. (2006). *Adaptive sampling in autonomous marine sensor networks*. Massachusetts Institute of Technology.

[3] Zhou, Y., Zhang, Y., Gao, J., & An, X. (2021). *Visual servo control of underwater vehicles based on image moments.* Paper presented at the 2021 6th IEEE International Conference on Advanced Robotics and Mechatronics (ICARM).

[4] Bonnin-Pascual, F., & Ortiz, A. On the use of robots and vision technologies for the inspection of vessels: A survey on recent advances. *Ocean Engineering, 190*, 106420. (2019)

[5] aMandlburger, G. A review of active and passive optical methods in hydrography. *The International Hydrographic Review*(28), 8-52. (2022); bMueller, R. P., Brown, R. S., Hop, H., & Moulton, L. Video and acoustic camera techniques for studying fish under ice: a review and comparison. *Reviews in Fish Biology and Fisheries, 16*, 213-226. (2006)

[6] Huy, D. Q., Sadjoli, N., Azam, A. B., Elhadidi, B., Cai, Y., & Seet, G. Object perception in underwater environments: a survey on sensors and sensing methodologies. *Ocean Engineering, 267*, 113202. (2023)

[7] Khan, N. Y., McCane, B., & Wyvill, G. (2011). *SIFT and SURF performance evaluation against various image deformations on benchmark dataset.* Paper presented at the 2011 International Conference on Digital Image Computing: Techniques and Applications.

[8] Gabriele, K. Convolutional linear genetic programming for underwater image classification. (2020)

[9] Wang, Q., He, B., Zhang, Y., Yu, F., Huang, X., & Yang, R. An autonomous cooperative system of multi-AUV for underwater targets detection and localization. *Engineering Applications of Artificial Intelligence, 121*, 105907. (2023)

[10] Raffaitin, C., Romero, J.-S., Romero, J.-S., & Procel, L.-M. (2019). *Hardware implementation of a shape recognition algorithm based on invariant moments.* Paper presented at the Proceedings of the 32nd Symposium on Integrated Circuits and Systems Design.

[11] Watanabe, Y., Komuro, T., Kagami, S., & Ishikawa, M. (2005). *Parallel extraction architecture for image moments of numerous objects.* Paper presented at the Seventh International Workshop on Computer Architecture for Machine Perception (CAMP'05).

[12] Iwashita, A., Komuro, T., & Ishikawa, M. An image-moment sensor with variable-length pipeline structure. *IEICE transactions on electronics, 90*(10), 1876-1883. (2007)

[13] Monajati, M. Hardware-Accelerated Image Moment Computation for UUV Navigation. *International Journal of Coastal, Offshore and Enviromental Engineering*. (2023)

[14] Roma, N., & Sousa, L. (2000). *In the development and evaluation of specialized processors for computing high-order 2-D image moments in real-time.* Paper presented at the Proceedings Fifth IEEE International Workshop on Computer Architectures for Machine Perception.

[15] Di Ruberto, C., Putzu, L., & Rodriguez, G. Fast and accurate computation of orthogonal moments for texture analysis. *Pattern Recognition, 83*, 498-510. (2018)